

# Multiphysics Modeling

## *Series Editors*

**Jochen Bundschuh**

*University of Southern Queensland (USQ), Toowoomba, Australia  
Royal Institute of Technology (KTH), Stockholm, Sweden*

**Mario César Suárez Arriaga**

*Department of Applied Mathematics and Earth Sciences,  
Faculty of Physics and Mathematical Sciences, Michoacán University UMSNH,  
Morelia, Michoacán, Mexico*

ISSN: 1877-0274

## Volume 5

# Geochemical Modeling of Groundwater, Vadose and Geothermal Systems

*Editors*

Jochen Bundschuh

*University of Southern Queensland (USQ), Toowoomba, Australia  
Royal Institute of Technology (KTH), Stockholm, Sweden*

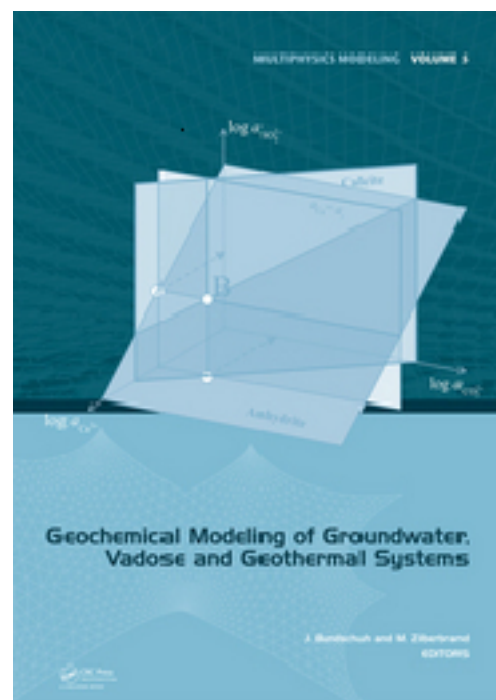
Michael Zilberbrand

*Hydrological Service of Israel, Research Division, Jerusalem, Israel*

 **CRC Press**  
Taylor & Francis Group  
Boca Raton London New York Leiden

CRC Press is an imprint of the  
Taylor & Francis Group, an **informa** business

A BALKEMA BOOK



CRC Press  
Taylor & Francis Group  
6000 Broken Sound Parkway NW, Suite 300  
Boca Raton, FL 33487-2742

© 2012 by Taylor & Francis Group, LLC  
CRC Press is an imprint of Taylor & Francis Group, an Informa business

No claim to original U.S. Government works  
Version Date: 20120117

International Standard Book Number-13: 978-0-203-12298-3 (eBook - PDF)

This book contains information obtained from authentic and highly regarded sources. Reasonable efforts have been made to publish reliable data and information, but the author and publisher cannot assume responsibility for the validity of all materials or the consequences of their use. The authors and publishers have attempted to trace the copyright holders of all material reproduced in this publication and apologize to copyright holders if permission to publish in this form has not been obtained. If any copyright material has not been acknowledged please write and let us know so we may rectify in any future reprint.

Except as permitted under U.S. Copyright Law, no part of this book may be reprinted, reproduced, transmitted, or utilized in any form by any electronic, mechanical, or other means, now known or hereafter invented, including photocopying, microfilming, and recording, or in any information storage or retrieval system, without written permission from the publishers.

For permission to photocopy or use material electronically from this work, please access [www.copyright.com](http://www.copyright.com) (<http://www.copyright.com/>) or contact the Copyright Clearance Center, Inc. (CCC), 222 Rosewood Drive, Danvers, MA 01923, 978-750-8400. CCC is a not-for-profit organization that provides licenses and registration for a variety of users. For organizations that have been granted a photocopy license by the CCC, a separate system of payment has been arranged.

**Trademark Notice:** Product or corporate names may be trademarks or registered trademarks, and are used only for identification and explanation without intent to infringe.

Visit the Taylor & Francis Web site at  
<http://www.taylorandfrancis.com>

and the CRC Press Web site at  
<http://www.crcpress.com>

## About the book series

Numerical modeling is the process of obtaining approximate solutions to complex problems of scientific and/or engineering interest. The book series addresses novel mathematical and numerical techniques with an interdisciplinary emphasis that cuts across all fields of science, engineering and technology. It focuses on breakthrough research in a richly varied range of applications in physical, chemical, biological, geoscientific, medical and other fields in response to the explosively growing interest in numerical modeling in general and its expansion to ever more sophisticated physics. The goal of this series is to bridge the knowledge gap among engineers, scientists, and software developers trained in a variety of disciplines and to improve knowledge transfer among these groups involved in research, development and/or education.

This book series offers a unique collection of worked problems in different fields of engineering and applied mathematics and science, with a welcome emphasis on coupling techniques. The book series fills a need for up-to-date information on numerical modeling. Faster computers and newly developed or improved numerical methods such as boundary element and meshless methods or genetic codes have made numerical modeling the most efficient state-of-art tool for integrating scientific and technological knowledge in the description of phenomena and processes in engineered and natural systems. In general, these challenging problems are fundamentally coupled processes that involve dynamically evolving fluid flow, mass transport, heat transfer, deformation of solids, and chemical and biological reactions.

This series provides an understanding of complicated coupled phenomena and processes, its forecasting, and approaches in problem solving for a diverse group of applications, including natural resources exploration and exploitation (e.g., water resources and geothermal and petroleum reservoirs), natural disaster risk reduction (earthquakes, volcanic eruptions, tsunamis), evaluation and mitigation of human-induced phenomena as climate change), and optimization of engineering systems (e.g., construction design, manufacturing processes).

Jochen Bundschuh  
Mario César Suárez-Arriaga  
(*Series Editors*)

## Editorial board of the book series

- Iouri Balachov  
*Advanced Power Generation, Physical Sciences Division,  
SRI International, Menlo Park, CA 94025, USA  
E-mail: [iouri.balachov@sri.com](mailto:iouri.balachov@sri.com)*
- Jacob Bear  
*Dept. of Civil and Environmental Eng., Technion,  
Israel Inst. of Technology, Haifa 32000, Israel  
E-mail: [cvrbear@techunix.technion.ac.il](mailto:cvrbear@techunix.technion.ac.il)*
- Angelika Bunse-Gerstner  
*Center of Industrial Mathematics, Faculty of  
Mathematics and Computer Science, University of Bremen,  
Bremen, Germany  
Email: [Bunse-Gerstner@math.uni-bremen.de](mailto:Bunse-Gerstner@math.uni-bremen.de)*
- Chun-Jung Chen  
*Chen Life Science Group, Research Division,  
National Synchrotron Radiation Research Center,  
and Department of Physics, National Tsing  
Hua University, Hsinchu 30076, Taiwan  
Email: [cjchen@nsrrc.org.tw](mailto:cjchen@nsrrc.org.tw)*
- Alexander H.D. Cheng  
*Department of Civil Engineering, University of  
Mississippi, MS 38677-1848  
E-mail: [acheng@olemiss.edu](mailto:acheng@olemiss.edu)*
- Martín A. Díaz Viera  
*Instituto Mexicano del Petróleo (IMP), Mexico City, Mexico  
E-mail: [mdiazv@imp.mx](mailto:mdiazv@imp.mx)*
- Hans J. Diersch  
*Groundwater Modelling Centre, DHI-WASY GmbH,  
12526 Berlin, Germany  
E-mail: [H.Diersch@dhi-wasy.de](mailto:H.Diersch@dhi-wasy.de)*
- Jesus A. Dominguez  
*ASRC Aerospace Corporation, Kennedy Space Center, FL, USA  
E-mail: [jesus.a.dominguez@nasa.gov](mailto:jesus.a.dominguez@nasa.gov)*
- Donald Estep  
*Department of Mathematics, Department of Statistics,  
Program for Interdisciplinary Mathematics,  
Ecology, & Statistics; Director, Center for  
Interdisciplinary Mathematics and Statistics,  
Colorado State University, Fort Collins, CO 80523, USA  
E-mail: [don.estep@gmail.com](mailto:don.estep@gmail.com)*
- Ed Fontes  
*COMSOL, SE-111 40, Stockholm, Sweden  
E-mail: [ed@comsol.com](mailto:ed@comsol.com)*
- Edward Furlani  
*Device Physics and Simulation, OCTO,  
Device Science & Technology Research,  
Fluidics Dept., Eastman Kodak Company,  
NY 14650-2216, USA  
E-mail: [edward.furlani@kodak.com](mailto:edward.furlani@kodak.com)*
- Pierre Glynn  
*National Research Program/Eastern Branch, U.S. Geological  
Survey, 432 National Center, Reston, VA 20192, USA  
Email: [pglynn@usgs.gov](mailto:pglynn@usgs.gov)*
- Ismael Herrera  
*Institute of Geophysics, National University  
of Mexico (UNAM), 14000, Mexico D.F., Mexico  
E-mail: [iherrera@unam.mx](mailto:iherrera@unam.mx)*

- Rafid al Khoury *Computational Mechanics, Faculty of Civil Engineering and Geosciences, Delft University of Technology, 2628 CN Delft, The Netherlands*  
*E-mail: [R.I.N.alKhoury@tudelft.nl](mailto:R.I.N.alKhoury@tudelft.nl)*
- Jim Knox *Life Support Systems Development Team, NASA Marshall Space Flight Center, Huntsville, AL 35812, USA*  
*E-mail: [Jim.Knox@nasa.gov](mailto:Jim.Knox@nasa.gov)*
- William Layton *Department of Mathematics, University of Pittsburgh, Pittsburgh, PA 15260, USA*  
*E-mail: [wjl@math.pitt.edu](mailto:wjl@math.pitt.edu)*
- Kewen Li *Stanford University, Department of Energy Resources Engineering, Stanford, CA 94305-2220, USA*  
*E-mail: [kewenli@stanford.edu](mailto:kewenli@stanford.edu)*
- Jen-Fin Lin *Center for Micro/Nano Science and Technology, National Cheng Kung University, Tainan, Taiwan*  
*E-mail: [jflin@mail.ncku.edu.tw](mailto:jflin@mail.ncku.edu.tw)*
- Rainald Löhner *School of Computational Sciences, George Mason University, MS 6A2, USA*  
*E-mail: [rlohner@gmu.edu](mailto:rlohner@gmu.edu)*
- Emily Nelson *Bio Science and Technology Branch, NASA Glenn Research Center, Cleveland, OH 44135, USA*  
*E-mail: [emily.s.nelson@nasa.gov](mailto:emily.s.nelson@nasa.gov)*
- Enrico Nobile *Department of Naval Architecture, Ocean and Environmental Engineering (DINMA), University of Trieste, Trieste, Italy*  
*E-mail: [nobile@units.it](mailto:nobile@units.it)*
- Jennifer Ryan *Delft Institute of Applied Mathematics, Delft University of Technology, 2628 CD Delft, The Netherlands*  
*E-mail: [j.k.ryan@tudelft.nl](mailto:j.k.ryan@tudelft.nl)*
- Rosalind Sadleir *Department of Biomedical Engineering, University of Florida, Gainesville, FL 32611-6131, USA*  
*E-mail: [rsadleir@bme.ufl.edu](mailto:rsadleir@bme.ufl.edu)*
- Fernando Samaniego V. *Faculty of Engineering, Institute of Geophysics, National University of Mexico (UNAM), 14000, Mexico City, Mexico*  
*E-mail: [fsamaniegov@pep.pemex.com](mailto:fsamaniegov@pep.pemex.com)*
- Peter Schätzl *Groundwater Modelling Centre, DHI-WASY GmbH, 12526 Berlin, Germany*  
*E-mail: [p.schaetzl@dhi-wasy.de](mailto:p.schaetzl@dhi-wasy.de)*
- Xinpu Shen *Landmark Graphics Corporation, Houston, TX 77042-3021, USA*  
*E-mail: [xinpushen@yahoo.com](mailto:xinpushen@yahoo.com)*
- Roger Thunvik *Dept. Land & Water Resources Engineering, Royal Institute of Technology (KTH), SE-100 44 Stockholm, Sweden*  
*E-mail: [roger@kth.se](mailto:roger@kth.se)*
- Clifford I. Voss *U.S. Geological Survey, Reston, VA 20192, USA*  
*E-mail: [cvoss@usgs.gov](mailto:cvoss@usgs.gov)*
- Thomas Westermann *Karlsruhe University of Applied Sciences, 76133 Karlsruhe, Germany*  
*E-mail: [thomas.westermann@hs-karlsruhe.de](mailto:thomas.westermann@hs-karlsruhe.de)*
- Michael Zilberbrand *Hydrological Service of Israel, Jerusalem 91360, Israel*  
*E-mail: [michaelz20@water.gov.il](mailto:michaelz20@water.gov.il)*

# Table of contents

About the book series	vii
Editorial board of the book series	ix
Contributors	xvii
Foreword	xix
Editors' preface	xxi
About the editors	xxv
Acknowledgements	xxvii

## ***Section 1: Introduction to groundwater geochemistry and fundamentals of hydrogeochemical modeling***

1 Hydrogeochemistry principles for geochemical modeling ( <i>J. Bundschuh &amp; O. Sracek</i> )	3
1.1 Sampling and analysis of water, solids and gases	3
1.1.1 Measurement of field parameters	5
1.1.2 Filtration and preservation of water samples	7
1.1.3 Sampling of solid materials	8
1.1.4 Sampling of gases	9
1.2 Introduction to thermodynamics	10
1.3 Chemical composition of precipitation	15
1.4 Hydrochemical processes	16
1.4.1 Introduction	16
1.4.2 Oxidation-reduction reactions	16
1.4.3 Organic matter decomposition, photosynthesis and aerobic respiration	17
1.4.4 Nitrification and denitrification	17
1.4.5 Sorption	18
1.5 Kinetics	22
2 Thermodynamics of gas and mineral solubility in the unsaturated-zone water ( <i>L. Mercury &amp; M. Zilberbrand</i> )	27
2.1 Introduction	27
2.2 Background	27
2.2.1 Capillary water	27
2.2.2 "Capillarizing" the water by the dryness of the soil atmosphere	30
2.2.3 Capillarity and size of pores	31
2.2.4 Capillary water: stable or metastable?	32
2.3 Capillary thermodynamics	33
2.3.1 Capillary solutions and the gas-solutions equilibria	33
2.3.2 Solids in capillary situations	34

2.3.3	Thermodynamic modeling of reactions in capillary systems	34
2.3.4	Simplified modeling of salt solubility in capillary systems	35
2.4	Illustrations in natural settings	36
2.4.1	Capillarity and mineralogy of desert roses	36
2.4.2	Capillarity and the dissolution of gases	38
2.5	Hydrogeochemical modeling in the unsaturated zone	39
2.6	Conclusions	40
3	Governing equations and solution algorithms for geochemical modeling ( <i>C. Ayora, M.W. Saaltink &amp; J. Carrera</i> )	45
3.1	The formulation of reactions	45
3.1.1	Species, reactions and stoichiometric coefficients	45
3.1.2	Equilibrium reactions in terms of the stoichiometric matrix	47
3.1.3	Primary and secondary species	49
3.1.4	Components and component matrix	52
3.1.4.1	Method 1 (aqueous components)	53
3.1.4.2	Method 2 (eliminate constant activity species)	57
3.1.4.3	Other methods	57
3.2	Homogeneous reactions	58
3.2.1	Speciation calculations	59
3.2.1.1	Algorithm 1	60
3.2.1.2	Algorithm 2	61
3.3	Heterogeneous reactions	63
3.3.1	Surface complexation reactions	63
3.3.2	Cation exchange reactions	68
3.3.3	Reactions with a solid phase	71
3.3.4	Reactions with a gas phase	71
3.4	Reaction paths	73
3.5	Formulation of kinetic reactions	76
4	Fluid flow, solute and heat transport equations ( <i>M.W. Saaltink, A. Yakirevich, J. Carrera &amp; C. Ayora</i> )	83
4.1	Introduction	83
4.2	Groundwater flow equations	83
4.2.1	Single phase flow	84
4.2.1.1	The conservation mass for the fluid	84
4.2.1.2	The momentum mass balance equations for the fluid	84
4.2.1.3	Flow equations	87
4.2.2	Multiphase flow	90
4.2.2.1	Multiphase system	90
4.3	Transport of conservative solutes	92
4.3.1	Advection, diffusion and dispersion	92
4.3.1.1	Advection	92
4.3.1.2	Diffusion	93
4.3.1.3	Dispersion	94
4.3.2	Transport equations of conservative solutes	96
4.4	Heat transport equations	97
4.4.1	Conduction and convection	97
4.4.1.1	Heat conduction	97
4.4.1.2	Heat convection	98
4.4.2	Heat transport in single fluid phase systems	98
4.4.3	Heat transport in multiple fluid phases systems	99

---

4.5	Reactive transport	99
4.5.1	The need for reactive transport: calcite dissolution in the fresh-salt water mixing zone	99
4.5.2	Mass balance equations	102
4.5.3	Constant activity species	106
4.5.4	Analytical solution for a binary system: equilibrium reaction rates	108
4.5.4.1	Problem statement	108
4.5.4.2	Methodology of solution	109
4.5.4.3	An analytical solution: pulse injection in a binary system	112
4.6	The effect of heterogeneity and non-local formulations	115
4.6.1	The limitations of traditional formulations and the need for upscaling	116
4.6.2	Solution of reactive transport in MRMT formulations	119
5	Numerical solutions of reactive transport equations ( <i>M.W. Saaltink, J. Carrera &amp; C. Ayora</i> )	127
5.1	Introduction	127
5.2	Methods for discretizing space and time	127
5.2.1	Finite differences	127
5.2.1.1	Fundamentals	127
5.2.1.2	Application to conservative transport	129
5.2.2	Finite elements	131
5.2.3	Instability and numerical dispersion	134
5.3	Methods for solving reactive transport equations	135
5.3.1	Sequential Iteration Approach (SIA)	136
5.3.2	Direct Substitution Approach (DSA)	138
5.3.3	Comparison between SIA and DSA	140
6	Elaboration of a geochemical model ( <i>M. Zilberbrand</i> )	143
6.1	Introduction	143
6.2	Model types and the most popular existing software packages	143
6.2.1	Speciation-solubility models	143
6.2.2	Reaction-path models	145
6.2.3	Inverse (mass-balance) models	145
6.2.4	Reactive transport models	145
6.3	Data required for geochemical modeling	145
6.3.1	Data for speciation-solubility models	145
6.3.2	Data for reaction-path models	147
6.3.3	Data for inverse (mass-balance) models	147
6.3.4	Data for reactive transport models	147
6.4	Schematization and choice of thermodynamic database	147
6.5	Modeling and interpretation of its results	149
6.6	Possible errors and misconceptions in model elaboration	150
7	Advances in geochemical modeling for geothermal applications ( <i>P. Birkle</i> )	153
7.1	Introduction	153
7.2	Development of geothermal reservoir tools	153
7.3	Types of geochemical models for geothermal systems	155
7.4	Requirements for geochemical simulations of geothermal reservoirs	156
7.5	Popular computer software for geothermal system modeling	156

7.6	Flow and geochemical model calibration	159
7.7	Selection of recent applications (2000–2010)—Case studies	160
7.7.1	General applications	160
7.7.2	Conceptual reservoir models	160
7.7.3	Lumped parameter models	164
7.7.4	Advanced numerical modeling	165
7.7.4.1	Reservoir design and magnitude—Reconstruction of reservoir parameters	165
7.7.4.2	Origin of acidity for reservoir fluids	165
7.7.4.3	Mineral-fluid equilibria	165
7.7.4.4	Fluid reinjection—Scaling effects	165
7.7.4.5	Hot-Dry Rock (HDR) systems (Soultz-sous-Forêts, France)	168
7.7.4.6	CO <sub>2</sub> injection into geothermal reservoirs	169
7.8	Conclusions—Future challenges	170

## Section 2: *Cases studies*

8	Integrating field observations and inverse and forward modeling: application at a site with acidic, heavy-metal-contaminated groundwater ( <i>P. Glynn &amp; J. Brown</i> )	181
8.1	Introduction	181
8.2	Geochemical modeling: computer codes, theory and assumptions	182
8.2.1	Inverse geochemical modeling	182
8.2.1.1	Principles, codes and theory	182
8.2.1.2	Assumptions used in inverse modeling	183
8.2.2	Forward geochemical modeling	186
8.2.2.1	Principles and codes	186
8.3	The Pinal Creek basin site: brief description	188
8.3.1	Geology	189
8.3.2	Hydrology and groundwater flow	190
8.4	Inverse geochemical modeling at the Pinal Creek site	190
8.4.1	Examination of end-member waters and their conservative constituents	191
8.4.2	The thermodynamic state of the end-member waters	192
8.4.3	NETPATH inverse modeling: simulation results	194
8.4.4	Inverse geochemical modeling with PHREEQC	200
8.5	Reactive-transport modeling at the Pinal Creek site	203
8.5.1	Summary of previous reactive-transport modeling	205
8.5.2	A reactive-transport sensitivity analysis on the movement of pH and pe-controlling mineral fronts	206
8.5.2.1	A simple model for advective transport of a reactive front: the MnO <sub>2</sub> dissolution front	206
8.5.2.2	Determination of the initial MnO <sub>2,s</sub> and carbonate mineral concentrations	207
8.5.2.3	Setup of the 1-D reactive-transport simulations	209
8.5.2.4	Simulation results: movement of the Fe(II)-rich waters and of the MnO <sub>2</sub> dissolution front	211
8.5.2.5	Simulation results: evolution of the low-pH waters	212
8.5.2.6	The effect of the initial carbonate to initial MnO <sub>2</sub> ratio on the evolution of the low-pH waters	213

8.5.2.7	Influence of the aluminum mineral allowed to precipitate on the evolution of the low-pH waters	215
8.5.2.8	Effects of the irreversible dissolution of Ca and Mg silicates on the evolution of low-pH Fe(II)-rich waters	217
8.5.2.9	The effect of not allowing rhodochrosite precipitation	218
8.5.2.10	The CO <sub>2</sub> open system simulations	218
8.5.2.11	The effect of longitudinal dispersion	219
8.5.2.12	The influence of cation exchange and surface-complexation sorption processes	220
8.5.2.13	Other minor effects on the evolution of the low-pH waters	221
8.5.2.14	Comparison of the reactive transport simulation results with observations at the Pinal Creek site	221
8.6	Conclusions	224
8.7	The Senior Author's fifteen year perspective on the Glynn and Brown (1996) paper	226
9	Models and measurements of porosity and permeability evolution in a sandstone formation ( <i>S. Emmanuel, J.J. Ague &amp; O. Walderhaug</i> )	235
9.1	Introduction	235
9.2	Porosity measurements in mineralized rock	236
9.3	Theory and numerical modeling of porosity evolution	238
9.3.1	Conceptual model of the porous medium	238
9.3.2	Reaction kinetics	240
9.3.3	Reactive transport equations	243
9.3.4	Numerical solution and model optimization	244
9.4	Comparison between numerical models and measurements	245
9.5	Implications for bulk reaction rates	247
9.6	Implications for permeability evolution in aquifers	248
9.7	Concluding remarks	249
10	Geochemical modeling of water chemistry evolution in the Guarani Aquifer System in São Paulo, Brazil ( <i>O. Sracek &amp; R. Hirata</i> )	253
11	Modeling of reactive transport at a site contaminated by petroleum hydrocarbons at Hnevice, Czech Republic ( <i>O. Sracek &amp; Z. Vencelides</i> )	259
11.1	Site characterization and conceptual model	259
11.2	Speciation and inverse geochemical modeling	261
11.3	Modeling of reactive transport	263
12	Numerical modeling for preliminary assessment of natural remediation of phosphorus in variably saturated soil in a peri-urban settlement in Kampala, Uganda ( <i>R.N. Kulabako, R. Thunvik, M. Nahubega &amp; L.A. Soutter</i> )	267
12.1	Introduction	267
12.2	Setting	267
12.3	Numerical model	269
12.3.1	Flow model	269
12.3.2	Solute model	274
12.3.2.1	Soil phosphorus sorption	274
12.3.2.2	Solute transport model	275

12.4 Simulations	276
12.5 Results and discussion	277
12.5.1 Field measurements	277
12.5.2 Pollution and remediation simulation scenarios	278
12.5.3 Sensitivity analyses	279
12.5.3.1 Impact of change of sorption coefficients ( $K_L$ and $K_{p,lin}$ ) on pollution time	279
12.5.3.2 Impact of change of the pore size distribution values on pollution time	279
12.5.3.3 Impact of change of the air entry values on pollution time	281
12.6 Conclusions	281
Subject index	287
Book series page	305

## Contributors

- Jay J. Ague  
(Chapter 9)  
Department of Geology and Geophysics, Yale University, New Haven, Connecticut, USA and Yale Peabody Museum of Natural History, Yale University, New Haven, CT 06511, USA
- Carlos Ayora  
(Chapters 3, 4 and 5)  
Department of Geosciences, Institute of Environmental Assessment and Water Research (IDÆA-CSIC), c/Jordi Girona, 18–26, 08034 Barcelona, Spain
- Peter Birkle  
(Chapter 7)  
Instituto de Investigaciones Eléctricas (IIE), Gerencia de Geotermia, Reforma 113, Col. Palmira, Cuernavaca, Morelos, 62490 Mexico
- Jochen Bundschuh  
(Chapter 1)  
University of Southern Queensland, Toowoomba, Queensland 4350, Australia & Department of Land and Water Resources Engineering, Royal Institute of Technology, SE-100–44 Stockholm, Sweden
- James G. Brown  
(Chapter 8)  
Formerly with the US Geological Survey in Tucson, Arizona
- Jesus Carrera Ramirez  
(Chapters 3, 4 and 5)  
Institute of Environmental Assessment and Water Research (IDAEA), Spanish Council for Scientific Research, Jordi Girona 18, 08034 Barcelona, Spain
- Simon Emmanuel  
(Chapter 9)  
Institute of Earth Sciences, The Hebrew University of Jerusalem, Givat Ram, Jerusalem, 91904, Israel
- Pierre Glynn  
(Chapter 8)  
National Research Program/Eastern Branch, U.S. Geological Survey, 432 National Center, Reston, VA 20192, USA
- Ricardo Hirata  
(Chapter 10)  
Department of Sedimentary and Environmental Geology, Institute of Geosciences, University of São Paulo, Rua do Lago 562, Cidade Universitária, CEP 05508-900, São Paulo, SP, Brazil
- Robinah Nakawunde Kulabako  
(Chapter 12)  
Department of Civil and Environmental Engineering, Makerere University, P.O.Box 7062 Kampala, Uganda
- Lionel Mercury  
(Chapter 2)  
Institut des Sciences de la Terre d'Orléans, UMR 6113 CNRS/Université d'Orléans, 1 A rue 8 de la Férolerie, 45071 Orléans Cedex, France

- Maimuna Nalubega  
(Chapter 12)  
Department of Civil and Environmental Engineering, Makerere University, P.O. Box 7062 Kampala, Uganda
- Maarten W. Saaltink  
(Chapters 3, 4 and 5)  
GHS, Department of Geotechnical Engineering and Geosciences, Universitat Politècnica de Catalunya, UPC-BarcelonaTech, Jordi Girona 1–3, 08034 Barcelona, Spain
- Ondra Sracek  
(Chapters 1, 10 and 11)  
Department of Geology, Faculty of Science, Palacký University, 17. listopadu 12, 771 46 Olomouc, Czech Republic & OPV s.r.o. (Protection of Groundwater Ltd), Bělohorská 31, 169 00 Praha 6, Czech Republic
- Leigh A. Soutter  
(Chapter 12)  
Physics Logic LLC, 6333E Mockingbird Lane, Suite 147PMB 722, Dallas, TX 75214, USA
- Roger Thunvik  
(Chapter 12)  
Department of Land and Water Resources Engineering, Royal Institute of Technology, SE-100–44 Stockholm, Sweden
- Zbynek Vencelides  
(Chapter 11)  
OPV, Bělohorská 31, 169 00 Praha 6, Czech Republic
- Olav Walderhaug  
(Chapter 9)  
Statoil ASA, N-4035 Stavanger, Norway
- Alexander Yakirevich  
(Chapter 4)  
Zuckerberg Institute for Water Research (ZIWR), The Jacob Blaustein Institute for Desert Research, Ben-Gurion University of the Negev, Sede-Boqer Campus, 84990, Israel
- Michael Zilberbrand  
(Chapters 2 and 6)  
Hydrological Service of Israel, Yaffo Str. 234, Jerusalem 91063, Israel

## Foreword

The world beneath our feet often remains unseen, and yet it provides us with water that feeds our streams, our ecosystems, and our water wells. Its shallowest parts, the soil and vadose zones, breathe gases in and out, help regulate moisture, fix nutrients, breakdown minerals, decompose and recycle organic debris and other waste, and sustain a rich microbial ecosystem that is vital to the sun-fed plants living on the surface. A bit deeper, in the saturated zone, permeable environments (aquifers) provide us with naturally filtered drinking water, and water for many other uses (e.g., irrigation). Deeper yet, permeability and storativity decrease, fluid residence times increase, dissolved salts increase, and selected groundwater environments provide an opportunity to store wastes (e.g., brines, hazardous chemicals, nuclear waste). Geochemical processes affect water quality as well as the mineral fabric and geologic framework of the subsurface, including its permeability and capacity to store water.

The subsurface also provides mineral and energy resources that are essential to human society. Water is often essential in the formation and development of those resources (e.g., hydrothermal mineral deposits, geothermal energy). Groundwater is also often affected by the presence of mineral or energy resources (e.g., oil, coal) or by their extraction (e.g., acid mine drainage). Elevated levels of toxic chemicals can occur either naturally (e.g., arsenic in shallow Bengal basin groundwaters) or as the result of human action (e.g., gasoline and oil spills). Geochemical and biogeochemical reactions drive the transformation, mobility, and often the relative toxicity of constituents of concern in groundwater environments.

Because of their large relevant volumes, relative stability, and distribution of residence times, groundwater environments also serve as an archive of climate and land-use change, including human-driven change. Dissolved gases, i.e., noble and nitrogen gas concentrations, in groundwaters around the world have recorded a shift of generally at least 4 to 5°C in recharge temperatures as the world became warmer after the last glacial maximum about 20,000 years ago. Secondary calcite precipitated in aquifers, such as found in Devil's Hole (NV, USA), has recorded the  $^{18}\text{O}$  (i.e., temperature) and  $^{13}\text{C}$  (i.e., vegetation distribution) history of recharging water over the last 500,000 years. On shorter timescales, shallow groundwaters have also recorded the history of land-use change (e.g., increased fertilizers and pesticides) as well as the diversity of anthropogenic constituents (e.g., chlorofluorocarbon compounds, methyl tert-butyl ether) introduced in the environment over the last 50 years.

Groundwater provides a ubiquitous control on water availability and water quality in ecosystems, often in more ways than the lay public realizes. The relatively stable temperatures of groundwaters and their often dominant contribution to streamflow helps moderate temperature and flow variability and helps stabilize aquatic habitats. The lagged response of groundwater systems means that human actions that affect surface conditions have a delayed effect on the water quality and availability of groundwater, and therefore on the surface waters and environment that it feeds. Conversely, the stability, lagged response and heterogeneity of groundwater systems make them difficult and time consuming to remediate, once contaminated or otherwise altered.

Pervasive heterogeneity, from the scale of pores and mineral grains to the regional scale of geologic formations and facies, is a key characteristic of groundwater environments. In turn, characterizing and modeling that physical, geochemical, and microbiological heterogeneity, and its effects on the transport and transformation of groundwater solutes, are major challenges for hydrogeologists and geochemists. The challenges are great enough to warrant the

application of a wide variety of geophysical, geochemical, and numerical modeling tools and tracers (e.g., heat and solutes).

So, why do we need geochemical and biogeochemical modeling of groundwater systems? A first answer is that geochemical and microbial processes are active processes that help trace the origin, flowpaths, residence times, and evolution of waters in the subsurface; and these processes also often affect the permeability and physical properties of geologic materials controlling flow and transport. Given the complexity of groundwater systems, their heterogeneity and inaccessibility, the path to enhanced understanding of subsurface systems lies in making use of all information and simulation tools available—not just physical flow and conservative transport models. Modeling, in all its forms, helps organize and provide a framework for the information that is available, helps recognize information that is missing and needed to answer specific questions, helps explore (and sometimes forecast) a diversity of future scenarios, and generally helps test hypotheses and gain understanding.

A second answer is that geochemical and biogeochemical processes transform not only geologic materials and their interfaces with subsurface fluids, but also affect the nature, transport, and fate of solutes, colloids, and microbes in the subsurface. Modeling and understanding these processes and their temperature dependence can potentially result in better management and regulatory decisions regarding (i) human activities on the land surface, (ii) appropriate extraction and use of subsurface resources (water, energy, minerals), (iii) suitable practices for waste disposal, and (iv) cost-effective contaminant remediation. Additionally, modeling and understanding these processes can help explore and document the archive of climate, environmental, and land-surface changes recorded in groundwater systems—from the distant past when human activities were not a major influence, to the present when they often are.

The twelve chapters in this handbook provide an excellent introduction and a highly useful reference on the methods and challenges of groundwater modeling, with an emphasis on the modeling of geochemical and biogeochemical processes. The principles of aqueous chemistry and the basic theories describing chemical reactions and the physics of fluid, solute, and heat transport are discussed, together with the algorithms used in numerical simulations of groundwater geochemical modeling. Practical issues, such as useful sampling methods and analytical characterization techniques, are covered. A broad array of applications and case studies of geochemical modeling are also discussed, including geochemical evolution in the Guarani regional aquifer (in Brazil), porosity development, geothermal applications, and a diversity of modeling approaches and studies relating to reactive transport at sites contaminated by petroleum hydrocarbons, excess phosphorus, and acidic heavy-metal-contaminated waters.

The diversity of relevant topics, and the basic and advanced methods and approaches to geochemical and biogeochemical modeling covered in this handbook, make it a useful reference for practicing hydrogeologists and geochemists around the world. The importance of discovering, studying, utilizing, preserving, and/or remediating the world beneath our feet has never been greater for society's welfare.

Pierre Glynn  
*Chief, National Research Program/Eastern Branch*  
*U.S. Geological Survey, Reston, VA*

## Editors' preface

*"The grand aim of all science is to cover the greatest number of empirical facts by logical deduction from the smallest number of hypotheses or axioms."*

Albert Einstein

*"The purpose of science is not to analyze or describe but to make useful models of the world. A model is useful if it allows us to get use out of it."*

Edward de Bono

Geochemical modeling is an important tool in environmental studies, and in the areas of subsurface and surface hydrology, pedology, water resources management, mining geology, geothermics, hydrocarbon geology, and related areas dealing with the exploration and extraction of natural resources. Geochemical modeling simulates the chemical and physical processes affecting the distribution of chemical species in liquid, gas, and solid phases. The reactions and processes, and their coupled interactions, are dependent on a number of environmental variables (e.g., temperature, pressure, ionic strength), and are also affected by the dynamics of matter and energy flows, including fluid, solute and heat flow.

This book seeks to make easily available to a broad readership some basic knowledge and fundamental concepts regarding the mathematical modeling of geochemical and groundwater processes, from the shallow vadose zone to deep geothermal systems. Since it is impossible to cover this subject given the space limitations, a selection of essential topics and case studies has been made. However, almost all the developments described herein are discussed in detail. Fundamental concepts, and the physical laws and equations needed to model different processes are described and presented in a simple and logical manner.

The book explains in a didactic manner the different applications of geochemical modeling, the existing conceptual methods, and the mathematical and numerical tools that can provide useful solutions. The reader will also receive a thorough understanding of (i) the physical laws describing the flow of mass and energy and the transport of solutes, (ii) the partial differential or algebraic equations representing these laws, and (iii) the principal numerical methods that allow approximate solutions of these equations and their corresponding mathematical models.

In the last 20 years, significant progress has been made in the use of different computational methods for geochemical and groundwater modeling. New concepts, methods and important findings have been presented in numerous publications. However, these often cover either specific issues or are restricted to specific systems or applications. Other publications related to the topics presented in this book may be restricted to describing some modeling software, or alternatively, the knowledge contained may not be applicable or transferable to groundwater and geochemical modeling without major modifications. Many of the publications do not necessarily describe the basic physical, chemical, mathematical and numerical theories and principles used. We saw a need for a synoptic compendium on the fundamentals of groundwater and geochemical modeling that would also have broad applicability to a diversity of environments. Our compendium clearly reveals the need for further research and development, that to be most useful, should be informed by additional field studies and practical applications of numerical modeling. Hopefully, this handbook will stimulate its readership to address some of these needs.

This book is meant to help overcome some of the barriers that hinder the use (or the correct use) of geochemical modeling. It presents applications of geochemical modeling in real case studies. Additionally, we emphasize the need for critical consideration and review of geochemical modeling and simulation results. A well-designed application will (i) start with a judicious examination of all available primary information, including the methods and techniques used for extraction and analysis of water, gas and solid samples, (ii) will carefully consider the applicable processes and domain boundaries of the simulations, and (iii) will test the simulation results using sensitivity analyses and a variety of validation/verification techniques. The reader will learn that the quality of the simulation results depends on the preparation of the model, the quality of the input data, the knowledge of the geological or pedological situation, the knowledge of the hydrogeochemical parameters and data, and the knowledge of the initial values and boundary conditions for the given subsurface system.

Our handbook provides a review of physical, chemical, mathematical, and numerical theory, and describes the correct use of computational methods in simulating chemical reaction processes in low- and high-temperature aqueous systems such as groundwater, petroleum and geothermal systems. The book also presents new and stimulating ideas for other possible simulations and applications.

Chapter 1 gives an introduction to the best practices in sampling and sample preservation, which together with accurate analyses play a vital role and are a precondition for geochemical modeling. The chapter also provides a summary of the basic principles of aqueous geochemistry and thermodynamics; this section is kept purposely short since more detailed information is given in several excellent text books to which we refer. In Chapter 2, the thermodynamics of gas and mineral solubility in the unsaturated-zone are treated in more detail since these aspects are not fully dealt with in the previously mentioned textbooks. Chapter 3 describes the governing equations and solution algorithms for geochemical modeling; it contains the basic concepts for the mathematical formulation of homogeneous and heterogeneous chemical reactions, including their kinetic simulation, and for the calculation of species concentrations. Chapter 4 provides the physical laws and mathematical equations describing fluid heat, and reactive solute transport, and presents the relevant computational solution algorithms for geochemical modeling; the numerical solution methods for the reactive transport equations are separately discussed in Chapter 5. Chapter 6 discusses how a conceptual model is implemented into a mathematical/numerical model, and indicates the processes, model parameters and data needs relevant for individual field scenarios and modeling tasks. Limitations and problems of existing thermodynamic databases are discussed. The principle types of geochemical models (speciation, reaction-path or forward, inverse- and reactive-transport models) are described together with examples of the most common codes. Chapter 7 deals with the advances in geochemical modeling for geothermal applications. The second part of the book (Chapters 8–12) discusses the application of geochemical models in different scientific areas and environmental settings. The focus is on the practical aspects of modeling, by the use of case studies of real-world environmental problems, including (i) inverse and forward modeling of heavy metal transport in an aquifer under acidic conditions, (ii) modeling and measurements of porosity and permeability evolution in a sandstone aquifer, (iii) geochemical modeling of water chemistry evolution along groundwater flow paths, (iv) modeling of reactive solute transport at a site contaminated by petroleum hydrocarbons, and (v) modeling for preliminary assessment of natural remediation of phosphorus in variably saturated soil.

This book is addressed to students, teachers, other professionals, and to the institutions involved in water resources and environmental management. We hope that it will give them an introduction on the practical use of geochemical modeling in their fields, and that it will beneficially contribute to policy-making. We also hope that this book will provide a reference used by educational and scientific institutions. The book should prove useful to senior undergraduate and graduate students, postgraduates, professional geologists and geophysicists,

engineers, environmental scientists, soil scientists, hydrochemists, and others interested in groundwater and geochemistry.

The book fills a gap in the literature through its presentation of insights in geochemical modeling as applied to a diversity of subsurface systems from close to the Earth's surface, down to deep-seated geothermal reservoirs. It also encourages a broad community of environmental scientists, geologists, chemists, pedologists, hydrologists, engineers and applied mathematicians to join together to help better protect and manage our freshwaters and our environment.

Finally, through its 2012 publication date, this book reminds us of the 50<sup>th</sup> anniversary of a key milestone in geochemical modeling. In 1962, R.M. Garrels and M.E. Thompson of Harvard University published the first paper that used thermodynamic modeling to predict the speciation of seawater.

Jochen Bundschuh  
Michael Zilberbrand  
*January 2012*

## About the editors



Jochen Bundschuh (1960, Germany) received his PhD from the University of Tübingen in 1990 after completing a thesis on the numerical modeling of heat transport in aquifers in 1990. He works in the areas of geothermics, subsurface and surface hydrology, integrated water resources management, and associated disciplines. From 1993 to 1999 he served as an expert for the German Agency of Technical Cooperation (GTZ), and as a long-term professor for the DAAD (German Academic Exchange Service) in Argentine. From 2001 to 2008, he served as an adviser to the Costa Rican government at the Instituto Costarricense de Electricidad (ICE) within the framework of the German governmental cooperation program (Integrated Expert Program of CIM; GTZ/BA). He assisted Costa Rica in the evaluation and development of its huge low-enthalpy geothermal resources for power generation. Starting in 2005, he was appointed Affiliate Professor at the Royal Institute of Technology, Stockholm, Sweden. In 2006, he was elected Vice-President of the International Society of Groundwater for Sustainable Development ISGSD. From 2009 through 2011, he was Visiting Professor at the Department of Earth Sciences at the National Cheng Kung University, Tainan, Taiwan. At the end of 2011, he was appointed as Professor of Hydrogeology at the University of Southern Queensland, Toowoomba, Australia.

Dr. Bundschuh has authored the books “Low-Enthalpy Geothermal Resources for Power Generation” (2008) and “Introduction to the Numerical Modeling of Groundwater and Geothermal Systems: Fundamentals of Mass, Energy and Solute Transport in Poroelastic Rocks” (2010) (both CRC Press/Balkema). He also edited the books “Geothermal Energy Resources for Developing Countries” (2002), “Natural Arsenic in Groundwater” (2005), and the two-volume monograph “Central America: Geology, Resources and Hazards” (2007), “Groundwater for Sustainable Development” (2008), “Natural Arsenic in Groundwater of Latin America (2008). Dr. Bundschuh also serves as an editor for several book series: “Multi-physics Modeling”, “Arsenic in the Environment”, and “Sustainable Energy Developments” (all CRC Press/Balkema).



Michael Zilberbrand was born in 1949 in the Ukraine. He received his PhD in 1987 from the Institute of Geological Sciences of the Academy of Sciences of the Ukraine. His thesis focused on physical and numerical modeling of water and salt transport in the unsaturated zone. He has taught a course on unsaturated zone processes at the Hebrew University of Jerusalem. Since 1996, he has worked as a research scientist in the Hydrological Service of Israel, applying his knowledge of hydrogeological and hydrogeochemical modeling. He is a member of the Israeli Geological Society.

Dr. Zilberbrand is a co-author of an approved patent on a device for estimating the rate and parameters of phase transition and vapor transfer in the air. He has conducted numerous field and laboratory studies and modeling of geochemical processes in the vadose zone and in groundwater systems, and has also conducted fundamental research of aqueous speciation in the vadose zone.

Dr. Zilberbrand has published 17 papers and 6 book chapters, including a publication in the *Encyclopaedia of Surface and Colloid Science*. He has reviewed numerous manuscripts for the United State–Israel Binational Science Foundation (BSF), *Geochimica et Cosmochimica Acta*, *Journal of Hydrology*, *Chemical Geology* and other international scientific journals.

## Acknowledgements

This book would be incomplete without an expression of our sincere and deep sense of gratitude to Pierre Glynn at US Geological Survey (Reston, VA), for his careful reading; his valuable comments and suggestions greatly improved chapters 1, 3, 4 and 5.

We thank David Parkhurst of the USGS (U.S. Geological Survey, Denver Federal Center, Denver, CO, USA) for his valuable remarks on Chapter 2. We express our gratitude to Mario César Arriaga Suarez (Dept. of Applied Mathematics and Earth Sciences, Michoacán University UMSNH, Morelia, Mexico) who provided important inputs to improve the mathematical descriptions in Chapters 3 to 5.

We thank the following scientists who reviewed the other chapters and made a number of very useful suggestions for its improvement: Nicolas F. Spycher (Earth Sciences Division, Lawrence Berkeley National Laboratory, Berkeley, CA; Chapter 7); David Parkhurst (U.S. Geological Survey, Denver, CO; Chapter 8); Mark Fuhrman (Office of Nuclear Regulatory Research, U.S. Nuclear Regulatory Commission, Rockville, MD; Chapters 8 and 9); Alexander Yakirevich (Jacob Blaustein Institute for Desert Research, Ben-Gurion University of the Negev, Sede-Boqer Campus, Israel; Chapters 10 and 11); Simon Emmanuel (Institute of Earth Sciences, The Hebrew University of Jerusalem, Jerusalem, Israel; Chapters 10 and 11); Maarten W. Saaltink (Dept. Geotechnical Engineering and Geosciences, Universitat Politècnica de Catalunya, Barcelona, Spain; Chapter 12); and Micòl Mastrocicco (Earth Sciences Department, University of Ferrara, Ferrara, Italy). We wish to express our sincere thanks to them, whose efforts contributed to the high quality of the book.

The editors thank also the technical people of Taylor & Francis Group, for the excellent typesetting of the manuscript. Finally, we thank the board members of the book series Multiphysics Modeling for their editorial suggestions.

Jochen Bundschuh  
Michael Zilberbrand  
*January, 2012*

## CHAPTER 8

# Integrating field observations and inverse and forward modeling: application at a site with acidic, heavy-metal-contaminated groundwater

Pierre Glynn & James Brown

*“I had,’ said he, ‘come to an entirely erroneous conclusion which shows, my dear Watson, how dangerous it always is to reason from insufficient data.”*

Sir Arthur Conan Doyle (1891)

*“Remember that all models are wrong; the practical question is how wrong do they have to be to not be useful.”*

George Edward Pelham Box (1987)

### 8.1 INTRODUCTION

*Historical note:* This chapter presents a revised version of Glynn and Brown (1996), a study that discussed in detail the theory and application of inverse and forward geochemical modeling with the computer codes PHREEQC, PHREEQM, and NETPATH, and the application of these codes in modeling contaminated groundwaters in the Pinal Creek basin (Arizona, USA). The modeling study focuses on the evolution and transport of acidic, reducing, waters because those conditions control the transport of metal contaminants in the groundwaters of the Pinal Creek basin. In addition to presenting the essential results and conclusions of Glynn and Brown (1996), this chapter provides a 15-year perspective on the original study. It discusses follow-up work done in the Pinal Creek basin, comments on lessons learned from investigations at the site, and provides suggestions that may be useful to geochemical and modeling investigations at other sites.

The construction of a multispecies reactive transport model used to predict the future evolution and movement of groundwater contaminants requires, at a minimum, three separate but related elements: (i) an understanding of the groundwater flow system and its possible transients, (ii) an understanding of dispersion and other processes causing observed dilution or “mixing” of different water types, and (iii) an understanding of the primary reactions controlling the distribution of various contaminants, not only among solid and phases, but also within the groundwater itself. The degree of understanding of all three of these elements, and perhaps more importantly an appreciation for the remaining knowledge gaps, will be essential in determining the usefulness of the constructed model. Indeed, even though a groundwater model may not adequately predict the future evolution of a contaminant plume, the process of constructing and using a model often results in an improved understanding of contaminant transport at the site.

---

Sources: \*Sir Arthur Conan Doyle: The Adventure of the Speckled Band’, The Adventures of Sherlock Holmes, 1891; \*George Edward Pelham Box; In: George E.P. Box and Norman R. Draper: Empirical Model-Building and Response Surfaces, 1987.

Most groundwater contamination sites have less geochemical and hydrogeologic information known about them than is desirable for predictive modeling of reactive contaminant transport. Detailed hydrogeologic and geochemical studies are usually much too expensive to consider.<sup>1</sup> The resulting lack of knowledge on the operative chemical and hydrologic processes at a given site means that investigators should try to use, as efficiently as possible, all tools and knowledge available. We believe that a combination of inverse and forward modeling of groundwater flow, contaminant transport, and geochemical evolution, may often provide the greatest knowledge gains for the least amount of money and time. In particular, geochemical inverse modeling should be used first, prior to forward geochemical modeling, both to explain the currently observed groundwater chemistry in the aquifer system, and to make predictions on the future chemical evolution of the groundwaters.

This chapter focuses on geochemical modeling and will show how both inverse and forward geochemical modeling approaches were used to better understand the evolution of acidic, heavy-metal-contaminated groundwaters in the Pinal Creek basin, near Globe, Arizona. The Pinal Creek basin is a site with sparse spatial information (30 wells distributed in a 15 km long and  $10^2$  to  $10^3$  m wide sulfate plume) and with significant temporal variations in both chemical and hydrological characteristics (water-table movements of more than 15 m during a three month period, groundwater velocities on the order of 3 to 5 m day<sup>-1</sup>; Brown and Harvey, 1994). The Pinal Creek site is well suited to test our modeling philosophy.

## 8.2 GEOCHEMICAL MODELING: COMPUTER CODES, THEORY AND ASSUMPTIONS

### 8.2.1 *Inverse geochemical modeling*

#### 8.2.1.1 *Principles, codes and theory*

Inverse geochemical modeling uses existing groundwater chemical and isotopic analyses, which are assumed to be representative of the groundwater along a given groundwater flowpath, and attempts to identify and quantify the reactions that are responsible for the chemical and isotopic evolution of the groundwater. Although an aqueous speciation code may be used to identify thermodynamically possible (or impossible) reactions and to determine the dissolved inorganic carbon content and the redox state (RS) of the groundwaters, the inverse modeling approach does not require that reactions proceed to thermodynamic equilibrium. Indeed, mass-balance constraints and the judgment of the user concerning the possible reactions are the only constraints posed in the inverse modeling approach.

Inverse geochemical modeling codes (BALANCE, Parkhurst *et al.*, 1982; NETPATH, Plummer *et al.*, 1991, 1994; PHREEQC,<sup>2</sup> Parkhurst, 1995, 1997, Parkhurst and Appelo, 1999; PHREEQCi,<sup>3</sup> Charlton *et al.*, 1997 and Charlton and Parkhurst, 1999) essentially solve a system of algebraic mass-balance equations. These relate the masses of elements, isotopes, redox oxidation states, and water found in a “final” sampled water along a flowpath to the masses found in contributing “initial” waters along the same flowpath, and to the

<sup>1</sup>Studies at the Cape Cod (LeBlanc, 1984) and Borden sites (Mackay *et al.*, 1986) are examples of what we would consider detailed studies. On the order of  $10^3$  to  $10^4$  sampling points were installed to study plumes on the order of  $10^2$  meters to a few kilometers long. However, even at these sites, after three decades, many questions remain regarding the operative geochemical and hydrogeologic processes, and studies continue to refine and improve existing knowledge.

<sup>2</sup>The PHREEQC series of numerical codes (PHREEQCi, PHREEQC versions 1 and 2) have both inverse and forward geochemical modeling capabilities.

<sup>3</sup>PHREEQCi is an interactive version of PHREEQC with a windows-based graphical user interface.

masses lost or gained through heterogeneous reactions between the aqueous phase and other phases (solid, gaseous, exchange or surface sorption phases). Each “inverse model” calculated by an inverse geochemical modeling code consists of a set of reaction mass transfers and “initial” solution fractions that satisfies the algebraic mass balance constraints for the observed “initial” and “final” solution compositions. The list of possible reactions and contributing “initial” solutions is postulated by the user. Usually, more than one model, or set of mass transfers, can be calculated for a given problem, and the user then tries to add additional constraints, for example additional information regarding the chemical and/or isotopic compositions of the initial and final solutions, to limit the number of models.

Mass-action equations and thermodynamic equilibrium speciation of the “initial” and “final” aqueous solutions are also solved in the NETPATH and PHREEQC codes (but not in the earlier BALANCE code). These speciation calculations primarily serve to inform the user as to the reactions that might be thermodynamically feasible. The calculations are also used to establish the redox and charge balance states and to determine the total dissolved inorganic carbon balance for the various aqueous solutions. Significant differences exist between the NETPATH and the PHREEQC inverse modeling capabilities, for example in the treatment of redox balances and solution charge balances. Perhaps, the most important difference between NETPATH and PHREEQC is that PHREEQC allows each analytical input datum for each of the aqueous solutions to be adjusted within an uncertainty range specified by the user. PHREEQC then calculates sets of phase mass transfers, solution mixing fractions, and adjustments to the analytical data that satisfy the mass-balance constraints, are consistent with the specified uncertainty ranges, and minimize the sum of the adjustments to the analytical data. The mathematical descriptions of the NETPATH and PHREEQC (and PHREEQCi) codes will not be discussed here. The reader is referred to Glynn and Brown (1996), Parkhurst (1995, 1997), Parkhurst and Appelo (1999), and Plummer *et al.* (1994) for further information. More recently, in their guide on radiocarbon dating of groundwater systems, Plummer and Glynn (in press) review the unique capabilities of the NETPATH code to simulate Rayleigh fractionation processes and assess groundwater residence times through inverse geochemical modeling.

#### 8.2.1.2 Assumptions used in inverse modeling

By definition, a model is a construct of assumptions that is meant to help understand some facet(s) of reality. Inverse geochemical modeling of groundwaters requires the user to make assumptions concerning (i) the types of geochemical reactions postulated to be present, (ii) the rates of reaction relative to the movement of the water and its mobile constituents, and (iii) the present distribution of chemical constituents in the aquifer system studied and the prior evolution of this distribution. The last 2 sets of assumptions require that the user have some presumptive knowledge of the groundwater flow and transport system and of its prior evolution.

##### *Knowledge of flowpaths and the assumption of a steady-state groundwater flow field*

These are the most important and possibly the most tenuous assumptions used in inverse modeling of the chemical and isotopic evolution in a groundwater system. The user often does not have enough hydrologic knowledge to precisely determine the flowpaths in a groundwater system. Furthermore, even if there is sufficient knowledge of the hydrogeologic system, existing wells must often be used. One rarely has the luxury of emplacing new sampling wells. However, when analyses are available from several wells, the spatial array of chemical and isotopic information may itself be used to decide the most likely flowpath. In most cases, the user will pick a direction that shows the least amount of dilution for the most conservative solutes to deduce the direction of flow.

Most groundwater systems are likely to experience some seasonal and interannual fluctuations in hydraulic heads. Therefore, flowlines and groundwater velocities are likely to change at least seasonally, and steady-state conditions may not apply during the time scale

of interest. The time scale of interest will normally be the time required for groundwater flow between the wells used in the inverse modeling simulation. The user typically assumes a steady-state groundwater flow field over the time scale of interest, or at the least assumes that the groundwater flow field observed at the time of sampling represents the long-term average velocity field.

*The assumption of chemical steady-state*

The groundwater analyses used in an inverse model usually represent samples taken concurrently or near-concurrently. The inverse modeling approach generally assumes that the parcel of water sampled from a “final”, downgradient, well (well B in Fig. 8.1) used to have the same composition as that of the water sampled concurrently at an “initial”, upgradient, well (well A in Fig. 8.1). This assumption will certainly be reasonable if the groundwater system has remained in chemical (and isotopic) steady-state at least during the travel time required for the water to move from the initial well to the final well. The assumption of chemical and isotopic steady-state simply states that although chemical and isotopic compositions may vary spatially, they do not vary in time at any given point in the groundwater system. In groundwater systems with spatially varying chemical and isotopic compositions, the assumption of chemical steady state implies a steady-state groundwater flow field (i.e., hydrologic steady-state), that is, flow lines and groundwater velocities that have not varied in time.

Most groundwater contamination cases involve dynamically evolving contaminant plumes, for which there can be no assumption of chemical steady-state. (Steady-state plumes, in which the rate of diffusive/dispersive and reactive loss of solutes balances the rate of their influx and/or production are uncommon). Fortunately, the assumption of chemical and

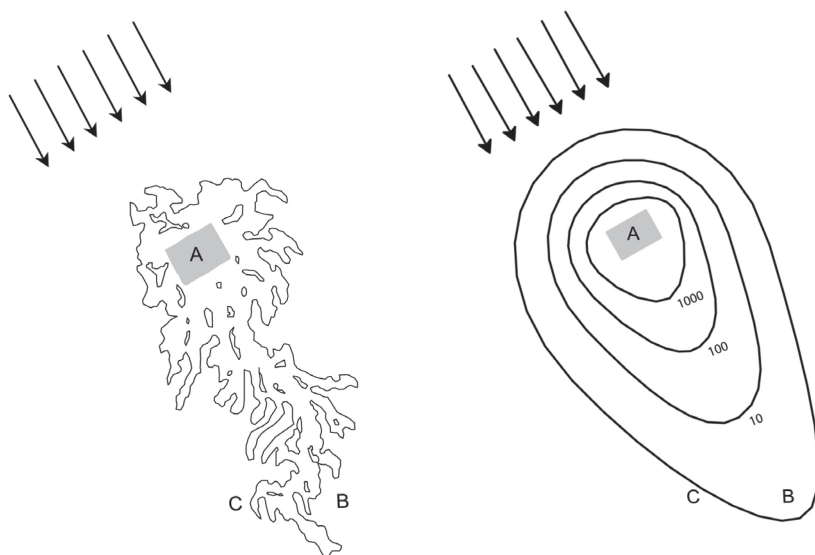


Figure 8.1. Two map views of a groundwater contaminant plume. Left: actual layout of the plume, drawn with a single concentration contour of concern. A is a well emplaced near or in the source of the contamination (stippled) and B and C are wells further downgradient. Right: results of a transport model for the same groundwater contaminant plume based on a fit of concentration data obtained from several observation wells. Additional concentration contours are drawn. The large transverse and longitudinal dispersion of the modeled plume results not only from the mixing that actually occurs in the ground but also from mixing that occurs during pumping at the observation wells. Uncertainty in simulation results is also caused by the inability to obtain a sufficiently detailed time-dependent representation of the contaminant plume and of the transient groundwater velocity field.

isotopic steady-state is not required for inverse geochemical modeling to be meaningful. The less stringent constraint required for inverse modeling is that the “initial”, upgradient, water composition used in inverse modeling (well A, sampled ideally at time  $t_0$ , or more commonly at time  $t_1$ ) should be representative of the composition that the “final” water sampled down-gradient at well B (at time  $t_2$ ) used to have, prior to its chemical evolution and movement from A to B. This less stringent constraint allows the groundwater compositions at points *in between* the “initial” and “final” wells (A and B) to have varied with time, as long as the chemical composition of waters from the “initial” well (A) has remained invariant, or the appropriate sample from well A at time  $t_0$  can be obtained. Strictly from a mass-balance point of view, it could be argued that the constraint could be reduced further to require only that the *changes* in composition between waters from well A (at time  $t_0$ ) and B (at time  $t_2$ ), rather than the *actual* compositions of waters from wells A (at time  $t_0$ ) and B (at time  $t_2$ ) should have remained constant. (A uniform dilution, or concentration, of the waters sampled at the “initial” and “final” wells, however, could lead the user to conclude from his inspection of the mineral saturation indices and general speciation of the waters that some other set of reactions was responsible for the evolution of water A into water B.) Finally, although the locations of the “initial” and “final” waters used in inverse geochemical modeling do not enter in the calculation of the reaction sets and reaction extents responsible for the overall evolution of water A into B, location information is important in assessing whether the reactions are reasonable from a kinetic, mineralogic and hydrologic perspective.

*How does “mixing” occur in groundwater systems?*

The U.S. Geological Survey inverse geochemical modeling codes (BALANCE, NETPATH, and the general geochemical code PHREEQC) calculate “mixing” fractions of initial waters and extent of reactions with solid and gas phases that account for the chemical composition of the final water. Clearly in most groundwater environments, “mixing” of groundwaters should be modeled as a continuous process rather than as a discrete process where a small number of specified water compositions are mixed together. Unfortunately, the inverse geochemical codes presented here cannot replicate a “continuous” mixing process. Forward transport modeling codes can replicate a continuous mixing process such as dispersion, but even then, their results and the very basis of their conceptual models are usually fraught with uncertainty. In using a set of discrete “initial” water compositions, inverse geochemical models inherently assume that the “initial” waters chosen encompass the range of intermediate waters that are actually involved in the real, continuous mixing process.

Although the location, timing, and sequence of the mixing and reaction processes is of no mathematical significance in the solution of the mass-balance equations, the user should try to determine where, when, and why such mixing processes have occurred in the groundwater environment. The “mixing” of initial waters by dispersion, for example, may well have led to heterogeneous mass transfers in areas that are not directly on the flowpath between a principal “initial” water and the “final” water. The inverse models will, nevertheless, implicitly incorporate those mass transfers in their solution of *net* mass transfer amounts.

The premise of inverse geochemical modeling is that the “final” and “initial” groundwaters used in a model should be related to each other. Ideally, they represent very small volumes of water sampled from a unique flowline or pathline. If it were indeed possible to do so (it is not), then the “final” groundwater sampled could only have experienced “mixing” as the result of the following processes:

1. Diffusion of chemical and isotopic constituents (and possibly of water) to or from the flowline (or pathline) to neighboring flow lines or to stagnant water zones.
2. Sampling from the pathline for more than an infinitesimally small amount of time, in the case of a system not in chemical steady-state. (Although most groundwater analyses do not require large samples, and the samples are therefore typically collected over small time periods, the length of sampling time may be an important consideration for some analytes.) If the system is not in chemical steady-state, the concentration of various constituents

- may be changing as a function of time at the final well and therefore a sample may in fact represent some groundwater composition averaged out in time and therefore in space.
3. The sampling of multiple flow lines that have undergone different chemical and isotopic evolution. Sampling-induced mixing of a diversity of solution chemistries may occur particularly in regions of converging flow, and may also occur when sampling from wells screened across large or multiple intervals. Flow convergence may occur naturally or may be the direct result of pumping.

Using the “mixing” option in an inverse geochemical model may also be needed because the “initial” and “final” groundwaters may not be chemically related despite the best efforts of the user. Just as excessively high values of dispersivity are often used in groundwater transport modeling because of a lack of precise spatial and temporal information (see Fig. 8.1), the use of the “mixing” option in NETPATH or in PHREEQC can often be the result of insufficient information on a groundwater system. For example, in Figure 8.1, if the “final” well used in the inverse model was off to the side of the path line of heaviest contamination (well C for example) and if well A was used as the “initial” well, the inverse model defined by the user would probably require a significant contribution of “background” water to explain the extent of “dilution” between well A and the “final” well. Similarly pumping a large amount of water from the “final” well chosen (well B or C) and using the average composition of this water as the “final” water composition in the inverse model could also lead to a serious misrepresentation of the amount of mixing. An error in the mixing fractions of “initial” waters could result in significant errors in the reaction mass transfers calculated by the inverse model. Furthermore, using water compositions averaged over a large volume by the sampling process could mislead the modeler into thinking that certain reactions were thermodynamically impossible, when in fact proper sampling, and location, of the “initial” and “final” waters would have indicated that these reactions were in fact possible.

## 8.2.2 *Forward geochemical modeling*

### 8.2.2.1 *Principles and codes*

Unlike inverse geochemical modeling, which attempts to explain observations and quantify the reactive mass transfers and mixing processes responsible for the observed chemical evolution along a flowpath in a groundwater system, forward modeling and reactive-transport modeling attempt to predict the evolution of a groundwater given certain postulated reactions and hydrodynamic processes. In their study, Glynn and Brown (1996) used the PHREEQM (Appelo and Willemsen, 1987) code for their reactive-transport simulations, rather than PHREEQC, because version 1 of PHREEQC (Parkhurst, 1995), the version that was available at the time, only simulated advective transport and reactions. PHREEQC version 2 (Parkhurst and Appelo, 1999) implemented advective-dispersive transport, by using an algorithm similar to the one used in PHREEQM. Because the concepts of forward geochemical modeling and reactive-transport modeling are widely known, this discussion will be limited to a brief description of the reactive transport capabilities of the PHREEQM and PHREEQC geochemical codes.

The PHREEQM code, and later the PHREEQC code, added significant capabilities to earlier geochemical speciation and mass-transfer codes, such as the U.S Geological Survey code PHREEQE (Parkhurst *et al.*, 1980). PHREEQM and PHREEQC simulated the transport of aqueous solutions by advection, dispersion, and diffusion in a 1-dimensional column (made up of a series of “cells”) and simulated the reaction of those solutions with minerals and surfaces inside the column. The codes also allowed simulation of cation-exchange processes. PHREEQM typically used the local equilibrium assumption in its modeling of reactive transport. PHREEQC, starting with its second version (Parkhurst and Appelo, 1999), implemented a wide range of capabilities that were not available in PHREEQM. These included modeling of kinetically limited reactions, modeling of additional surface speciation and

sorption reactions, modeling of solid-solution aqueous-solution reactions as presented in Glynn (1991a, 2000), transverse diffusion, and many other capabilities.

The transport algorithms in PHREEQM and PHREEQC use an operator splitting technique, where advection is modeled by shifting cell contents from one cell to the next at every time step or “shift”. Dispersion and/or diffusion is simulated by mixing the aqueous contents of each cell with that of adjacent cells. This algorithm gives the codes the advantage (over most typical finite-difference and finite-element codes) of being able to simulate not only an advective-dispersive transport process or a diffusive transport process, but also a purely advective, albeit one-dimensional, transport process. The mixing factors  $f$  calculated are a function of the aquifer dispersivity  $\alpha$  and the molecular diffusivity  $D^*$ :

$$f_i = \frac{\alpha_i + \alpha_{i+1}}{l_i + l_{i+1}} + 4D^* \frac{\Delta t}{(l_i + l_{i+1})^2} \quad (8.1)$$

where  $i$  is the cell number,  $l$  is the cell length, and  $\Delta t$  is the time step.

The above equation can be derived from a finite difference approximation (ignoring advection) centered in space and forward in time. Because the simulation of dispersion is centered in space, PHREEQM and PHREEQC show no numerical dispersion error for conservative constituents when simulating advection-dispersion processes. Numerical dispersion does occur, however, in dispersion of non-conservative constituents and is dependent on the amount of retardation experienced by each constituent and the cell lengths (the maximum numerical dispersivity equals 1/2 the cell length; *cf.* Herzer and Kinzelbach, 1989). The codes do not show any numerical dispersion in simulations with only diffusion as a transport process. The lack of sequential iterations between the solution of the chemical equilibrium equations and the simulation of the transport processes at every time step can theoretically generate errors, although comparisons (Glynn *et al.*, 1991; or Figs. 9 and 10 in Glynn and Brown, 1996) of PHREEQM with the sequential iteration finite difference code MSTID (Engesgaard and Kipp, 1992) suggest that the error is typically small as long as an appropriate discretization is used. Operator splitting can also generate error, although, again, comparisons of PHREEQM with the MSTID code and results by Steefel and MacQuarrie (1996) suggest that this error is usually minor. A much more complete description of the PHREEQM and PHREEQC codes and their capabilities can be found in Appelo and Postma (1993 and 2005, respectively). Unless mentioned otherwise, all PHREEQC simulations referred to in this chapter were performed with the first version of the code (Parkhurst, 1995).

Forward geochemical modeling is conceptually different from inverse geochemical modeling. Indeed, forward modeling seeks to *predict* the chemical composition of an aqueous solution, given the composition of an initial solution and given certain specified reactions, some of which are usually considered to reach thermodynamic equilibrium (or have a prescribed kinetic progression). Forward modeling is most suitable and most useful, when the amount of chemical and isotopic data available for a given groundwater system is limited, and when the objective is to predict the future evolution of the system. In contrast, inverse modeling is most useful when abundant chemical, isotopic, hydrologic and mineralogic data are present and all that is desired is an explanation of the past chemical evolution of the groundwater system. Of course, just as understanding the past is a key to understanding the future, inverse modeling can provide insight regarding the reactions that control the future chemical evolution of a groundwater system.

Forward modeling codes can also be used for the purpose of inverse modeling. A series of trial and error simulations or automated parameter estimation can be used to adjust reaction extents or reaction rates to align forward simulation results with actual observations (VanCappellen and Gaillard, 1996; Steefel and MacQuarrie, 1996). Although this latest approach can be time consuming, it does have the advantage over simpler inverse geochemical codes of a more accurate representation of groundwater mixing as a continuous, rather than discrete, process. This parameter-estimation approach does not necessarily require the

assumption of chemical steady-state, although it is subject to the same constraints as simpler inverse geochemical codes in choosing initial and final water compositions (see discussion in previous section), their location and time of sampling. The disadvantages of this approach, relative to non-transport-oriented inverse geochemical modeling, are the computer time requirements, the significantly greater number of adjustable parameters, including flow and transport parameters, and the consequently greater number of solutions that may explain the observations. Further references in this chapter to inverse modeling will generally not refer to the use of forward codes as part of an inverse modeling approach, although many of the statements made may apply equally well to this latter more sophisticated approach.

The Pinal Creek Toxics Program investigation site, a site of groundwater contamination by acidic, metal-laden, and sulfate-rich wastewater near Globe, Arizona provides a good example of the improved understanding of the chemical reaction and transport processes that may be gained through the combined use of both inverse modeling and forward modeling approaches. The primary purpose of this chapter is to describe some of the insights that can be gained through this combined approach, and through the examination of available field observations. A brief description of the site is first needed.

### 8.3 THE PINAL CREEK BASIN SITE: BRIEF DESCRIPTION

The Pinal Creek basin is located in central Arizona, about 100 km east of Phoenix (Fig. 8.2). The surface drainage area of the basin occupies 516 km<sup>2</sup>, of which 170 km<sup>2</sup> is covered by alluvium and basin fill, which form the regional aquifer; 27 km<sup>2</sup> of the basin's area is covered by mine

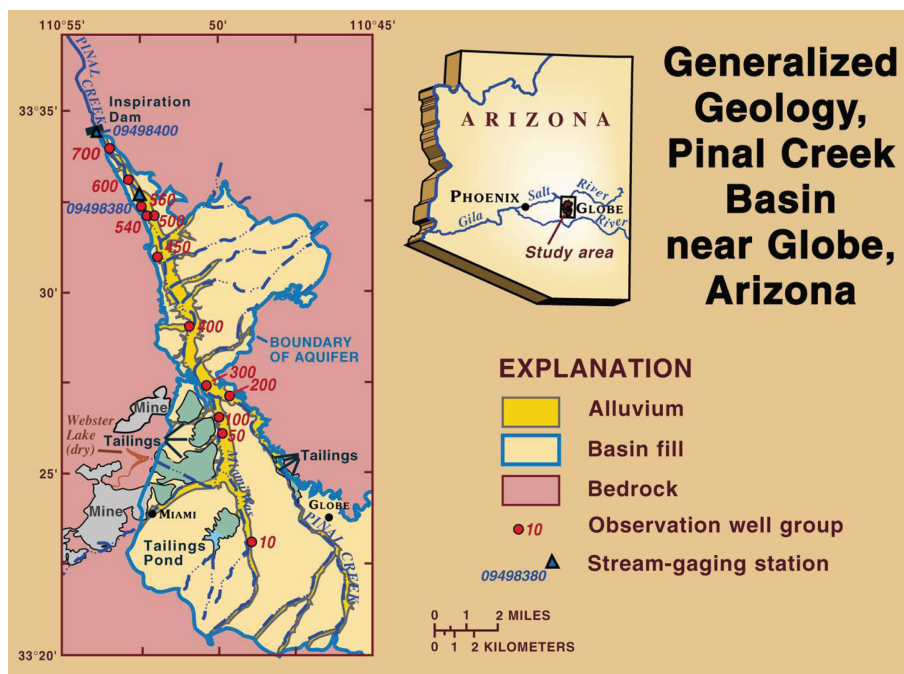


Figure 8.2. Location and generalized geology of the Pinal Creek basin study area. Several wells screened at different depths exist at each well group site. Well names are related to site names by their first, or first and second, digits. For example: site 400 includes well 402; site 500 includes wells 503 and 504; site 50 includes well 51; site 450 includes wells 451 and 452. Dashed dotted stream lines represent intermittent streams. All stream reaches are intermittent, except Pinal Creek itself to the north of well group 500.

tailings. Mining, mainly for copper, began in the late 1870s and has been the largest economic activity in the basin. Because of the long history of mining, there are several potential sources of contamination to the regional aquifer (Eychaner, 1991; Brown and Harvey, 1994). For example, pyrite is thought to be the most abundant sulfide mineral in the tailings. Following significant rainfall, oxidation of pyrite in the tailings and subsequent transport of this contaminated water into the alluvial aquifer could represent a significant source of acidity, iron, and sulfate in the aquifer. A similar phenomenon could also occur in the relatively undisturbed naturally mineralized areas in the basin, although the amount of this flow is expected to be small in relation to flow from the disturbed mining areas and tailings. Finally, the unlined water impoundments that were used during copper refining and mineral processing operations are also a likely source of groundwater contamination in the basin. The water in the impoundments is rich in sulfuric acid (used in copper refining) and heavy metals. The largest suspected single source of contamination in the basin was Webster Lake, an unlined surface-water impoundment that existed from 1940 to 1988. In 1988 it was drained at the order of the U.S. Environmental Protection Agency (Tolle and Arthur, 1991). Maximum volume of the lake was more than 7 million m<sup>3</sup>. In 1988, a sample of water from the lake had a *pH* of 2.7; concentrations of iron and sulfate were 6 g L<sup>-1</sup> and 20 g L<sup>-1</sup>, respectively; and aluminum, copper, cobalt, nickel, and zinc were present at concentrations greater than 20 mg L<sup>-1</sup>.

### 8.3.1 Geology

Peterson (1962) describes the complex and highly diverse geology and mineral deposits of the Pinal Creek basin area. Older Precambrian age rocks in the basin include schist, diorite, granite, conglomerate, quartzite, limestone, and basalt. Paleozoic age rocks include quartzite, limestone and shale. Younger Mesozoic- and Cenozoic-age rocks are mainly intrusive and include granite, granodiorite, diabase, and monzonite. These are exposed in the hills north of Globe and Miami. Finally and most importantly from an economic perspective, the igneous and metamorphic rocks include a major body of copper porphyry ore. Chalcocite, chalcopyrite, and pyrite predominate in the deeper parts of the ore body, while chrysocolla, malachite, and azurite predominate in its upper, oxidized zone.

The Pinal Creek basin's configuration was created by high-angle block faulting associated with basin subsidence that began 19 to 15 million years ago and continued until about 8 million years ago. The basin fill, which is derived from rocks of the surrounding mountains and forms the deeper aquifer in the basin, has a highly variable lithology, ranging "from completely unsorted and unconsolidated rubble of angular blocks as much as 4.5 m in diameter, to well-stratified deposits of firmly cemented sand, silt, and gravel containing well-rounded pebbles and cobbles" (Peterson, 1962). Carbonate content of the basin fill is about 1.5% (Eychaner, 1989).

Unconsolidated stream alluvium overlies the basin fill along Miami Wash, Pinal Creek, and other drainages. The alluvium is from 300 to 800 m wide and is less than 50 m thick. The alluvium contains cobble- to clay-sized material, although sand- to gravel-sized material is most abundant. Sand-sized particles contain quartz, feldspar, and lesser amounts of mica and a variety of rock fragments. Gravel-sized materials consist mainly of rock fragments of granite, volcanic rocks, and schist. The alluvium also contains interbedded clays and lenticular clay layers that were found to be as much as 12 m thick at Nugget Wash (Hydro Geo Chem, Inc., 1989). A sample of alluvium collected in 1985 (Eychaner and Stollenwerk, 1985) contained 0.34 percent calcite by weight. This concentration is equivalent to 0.18 moles of carbonate material per liter of water, using the bulk density of 1.65 g cm<sup>-3</sup> and porosity of 0.316 determined for alluvium used in a column experiment (Stollenwerk, 1994).

Manganese cycling and transport is of interest in our study. Indeed, secondary manganese oxide deposits are highly visible in the perennial Pinal Creek streambed, frequently forming a black hardpan layer. Estimates of the concentration of primary manganese oxide minerals were based on samples of alluvium not affected by acidic contamination. At well site 500, in the neutralized part of the plume, the depth-averaged content of manganese oxides

was  $0.079 \text{ mol L}^{-1}$ , based on sequential extractions done by Ficklin *et al.* (1991). Stollenwerk (1994) estimated that  $0.0449 \text{ mol L}^{-1}$  of manganese could be available for reaction in a sample of alluvium obtained from a gravel quarry just east of well site 200.

### 8.3.2 *Hydrology and groundwater flow*

Groundwater flow in the Pinal Creek basin is the result of past geologic events, the past and present climate, and human activities. Because the area climate is semiarid, most of the drainages in the basin are usually dry but convey large amounts of runoff during and after severe storms. Streams that drain the Pinal Mountains also flow during and following snowmelt in late winter and early spring. Most of the groundwater recharge in the basin occurs in the winter and spring, with lesser recharge events during the summer monsoonal period. The amount and the distribution of precipitation controls the size, frequency, and duration of streamflow, and therefore controls the quantity and distribution of water that infiltrates the permeable stream beds and recharges the unconsolidated alluvial and consolidated basin-fill aquifers.

Groundwater in the basin fill flows generally northward from the flanks of the Pinal Mountains, and westward from the Apache Peak alluvial fan. Most groundwater in the basin fill eventually flows upward into the alluvium and then flows generally north to the perennial reach of Pinal Creek. A greater quantity of water, however, recharges the alluvium directly and flows north, mixing with the water from the basin fill. In the northern part of the basin, the aquifer is constricted by the impermeable basement rocks. This constriction forces groundwater to the land surface, generating perennial flow from about 6 km above Inspiration Dam to the Salt River, which is a major source of drinking water for the Phoenix Metropolitan area.

## 8.4 INVERSE GEOCHEMICAL MODELING AT THE PINAL CREEK SITE

Like most sites with point-source groundwater contamination, the chemistry of groundwaters in the Pinal Creek basin exhibits both spatial and temporal variation. The most heavily contaminated groundwaters are typically found near the base of the unconsolidated alluvial aquifer, where a zone of coarser (and possibly less carbonate-rich) material is suspected to be present. The wells with the most contaminated waters at each well site are 51, 101, 302, 402, 503, 601 and 702 in a down-gradient direction (Fig. 8.2). Although other wells at each site also show the presence of contaminated water, wells with the most contaminated waters (as measured by total dissolved solids, chloride, or any other relatively conservative constituent) present the most logical choice for inverse modeling. To further narrow the scope of the inverse-modeling study, we focus on the significant changes in the chemical characteristics between samples from well 402 and 503. The two water samples chosen represent an acidic contaminated water sampled from well 402 in January 1989 and a neutralized contaminated water sampled from well 503 in November 1991. The two wells are 5.6 kilometers apart. From the difference in sampling times and the distance between wells, we calculate that a parcel of water leaving well 402 would have to travel at a linear groundwater velocity of about  $5.2 \text{ m day}^{-1}$ . This velocity is in the range of  $4.2$  to  $5.6 \text{ m day}^{-1}$  estimated by using Darcy's law, assuming an effective porosity of 0.3 and a hydraulic conductivity of  $200 \text{ m day}^{-1}$  (Brown *et al.*, 1995; Brown, 1996).

Glynn and Brown (1996) initially used the NETPATH inverse modeling code. Unlike the first version of PHREEQC, the only one available at the time, the NETPATH code was interactive and allowed the authors to quickly determine primary sources and sinks in their inverse simulations. The NETPATH code (i) helped identify some of the possible reaction mechanisms responsible for the chemical evolution of the groundwaters between wells 402 and 503, and (ii) quantified some of the reaction mass-transfers involved.

## 8.4.1 Examination of end-member waters and their conservative constituents

The first step in an inverse modeling study is to examine the chemical composition and thermodynamic state of the waters that will be used in the model. The chemical analyses for the waters chosen for the inverse modeling study are given below in Table 8.1. The charge imbalances calculated by the speciation code WATEQFP (embedded in NETPATH) for the well 402, 504 and 503 samples were -3.1, 1.5 and 4.4%, respectively.

As can be seen, the most significant differences in groundwater chemistry between the well 402 and 503 samples are the increase in *pH* from 3.9 to 5.6, the 25% increase in calcium and magnesium, the complete removal of 590 mg L<sup>-1</sup> of dissolved iron, the 90% removal of 18.4 mg L<sup>-1</sup> of dissolved aluminum, the 60% increase in manganese, and the 30% decrease in sulfate. Silica concentrations are nearly constant. As is the case in any geochemical modeling analysis, however, conservative (i.e., nonreactive) constituents are perhaps the most important constituents to examine because they give information on physical flow and transport processes. Any groundwater sampling and analysis program should ensure measurement of at least one, but preferably two or more, relatively non-reactive tracers, such as chloride, bromide, <sup>18</sup>O and <sup>2</sup>H. Sodium may also be relatively conservative although it may increase in solution due to cation exchange, feldspar dissolution, or evaporite dissolution processes. Sodium is rarely taken out of solution by reaction processes other than cation exchange. In the case of the Pinal Creek groundwaters, the high Ca/Na ratio in the acidic waters (Ca/Na = 2.4 mol/mol in well 402) and the even higher ratio in the neutralized waters (Ca/Na = 4.2 mol/mol in well 503) suggest that removal of sodium by cation exchange is not likely.

Table 8.1. Chemical composition of three groundwaters from the Pinal Creek basin: an acidic contaminated water (well 402), a background uncontaminated water (well 504), and a neutralized contaminated water (well 503). Concentrations in mg L<sup>-1</sup>. Concentration changes are expressed relative to well 402. ND: not determined. *TDIC*: total dissolved inorganic carbon.

Concentration or value	Well 402 1989/1/12	Well 504 1991/11/22	Well 503 1991/11/22	Change: 402 to 503	Change: Reaction only <sup>1</sup>
pH	4.13	7.05	5.59		
<i>Eh</i> (in mV)	420 est. <sup>2</sup>	350	410		
Temperature	18°C	20.5°C	18.2°C	1.1%	
Dissolved oxygen	0.3	6.64	<0.1		
Calcium	502	44.6 <sup>3</sup>	634	26%	57%
Magnesium	161	15.6 <sup>3</sup>	200	24%	54%
Sodium	121	19.8 <sup>3</sup>	86	-29%	-13%
Potassium	7 est. <sup>2</sup>	2.1	5 est. <sup>2</sup>	-29%	-16%
Iron	591	0.004	<0.1	-100%	-100%
Manganese	71.6	<0.001	116	62%	106%
Aluminum	18.4	<0.01	2.3 est. <sup>2</sup>	-88%	-84%
Strontium	2.29	0.335	2.7	18%	44%
Silica (as SiO <sub>2</sub> )	85.6	27 <sup>3</sup>	91.8	7.2%	26%
Chloride	140	9.7 <sup>3</sup>	112	-20%	0%
<i>TDIC</i> (as C)	50	ND	ND	ND	ND
Alkalinity (as HCO <sub>3</sub> )	ND	227	66	ND	ND
Sulfate	3260	14.2 <sup>3</sup>	2350	-28%	-8%
Fluoride	10 est. <sup>2</sup>	0.3	1.5 est. <sup>2</sup>	-85%	-81%

<sup>1</sup> Assumes chloride is conservative. The relative change expressed represents the relative difference in concentration between a mixture of waters from wells 402 and 504, determined on the basis of chloride concentrations, and well 503 water. <sup>2</sup> Values were estimated by inspecting earlier and later analyses.

<sup>3</sup> Average of two analyses.

The decrease in both Cl and Na between wells 402 and 503 suggests that dilution is occurring. This dilution may be caused either by longitudinal and transverse dispersion along the flowpath or by the well-sampling process. It is also important to recognize that the groundwater sample taken from well 503 in November 1991 was probably not exactly on the pathline originating from well 402 in January 1989. Well 503 may be “off” (to the side or above) the most contaminated pathline, and the well 503 sample might therefore be more diluted than a hypothetical sample taken from the pathline. In recognition of the difficulty in determining the causes and the exact proportions of the various groundwaters responsible for the dilution of the well 503 water relative to the well 402 water, an uncontaminated water sampled in November 1991 from below the plume at well 504 was used as the source of diluting water in our inverse geochemical model.

Although chloride undergoes a 20% decrease between wells 402 and 503, sodium undergoes an even greater decrease of about 29%. If the decrease in chloride is used to calculate the fraction (0.21) of water from well 504 diluting the water from well 402, the observed sodium concentration in well 503 is still 13% lower than the calculated diluted sodium concentration (Table 8.1, last column). This greater observed decrease in sodium may be at least partly due to a greater Cl/Na ratio in the average diluting water relative to that of the background water (well 504) used in the calculation. Indeed, although the average Cl/Na ratio in the uncontaminated waters below the plume (wells 404, 504) or upgradient (well 010) from the plume is 0.44 mg/mg ( $\pm 0.10$ ), the average Cl/Na ratio for the most contaminated waters along the flowpath is close to three times higher (well 51:  $1.48 \pm 0.74$ , well 101:  $1.35 \pm 0.44$ , well 302:  $1.32 \pm 0.36$ , well 402:  $1.29 \pm 0.44$ , well 503:  $1.17 \pm 0.43$ ; all ratios in mg/mg). [Note the decreasing Cl/Na ratio with distance downgradient, i.e., with increasing neutralization and dilution of the contaminated waters.] Dilute (only slightly contaminated) groundwaters sampled from wells on the side of the plume (wells 201, 202) also have a much higher average Cl/Na ratio ( $0.91 \pm 0.30$ ) than that of the uncontaminated groundwaters. An argument can therefore be made that these slightly contaminated waters should have been used as diluting waters in the NETPATH modeling, instead of (or in addition to) the uncontaminated water chosen here. The discrepancy in the chloride and sodium dilution factors is, however, a measure of the uncertainty inherent in trying to model the groundwater mixing process with a simple inverse geochemical model.

#### 8.4.2 *The thermodynamic state of the end-member waters*

After examining the conservative constituent concentrations of the groundwaters, the next step is to examine the aqueous-speciation results, in particular the mineral saturation indices (Table 8.2) calculated for the three end-member waters chosen in our model. The speciation calculations were performed with the WATEQFP code incorporated in the database management code DB distributed with the NETPATH code. The thermodynamic database used in WATEQFP is a subset of the database described for WATEQ4F (Nordstrom *et al.*, 1990), and is also the basis for the phreeqc.dat and wateq4f.dat databases included with the PHREEQC code (Parkhurst and Appelo, 1999).

The background water (well 504) is predominantly rich in  $\text{CaHCO}_3$ , and is typical of the uncontaminated groundwaters in the Pinal Creek basin. These waters are usually near saturation with calcite, dolomite and chalcedony, have near to slightly above neutral *pH* values, and have equilibrium  $\text{CO}_2$  partial pressures between  $10^{-1.5}$  and  $10^{-2.0}$ . The uncontaminated groundwaters are typically rich in dissolved oxygen and other dissolved atmospheric gases (Glynn and Busenberg, 1994a; Robertson, 1991, Winograd and Robertson, 1982).

In comparison, the acidic water from well 402 is highly undersaturated with respect to calcite, dolomite, siderite ( $\text{FeCO}_3$ , *SI*: -2.6) and rhodochrosite ( $\text{MnCO}_3$ , *SI*: -3.3) and is near saturation with amorphous silica, kaolinite, and gypsum. The water is undersaturated

Table 8.2. Saturation indices and carbon dioxide equilibrium partial pressures for an acidic groundwater (well 402), an uncontaminated groundwater (well 504) and a neutralized contaminated groundwater (well 503) from the Pinal Creek basin alluvial and basin-fill aquifers. NC: could not be calculated.

Mineral	Well 402 (acidic) 1989/1/12	Well 504 (background) 1991/11/22	Well 503 (neutralized) 1991/11/22
Calcite	-5.0	-0.5	-1.8
Dolomite	-10.2	-1.1	-3.9
Siderite	-2.6	-11.5	NC
Rhodochrosite	-3.3	NC	-0.0
Gypsum	0.0	-2.6	0.1
Fluorite	-3.2	-2.2	-2.5
SiO <sub>2</sub> (am)	-0.1	-0.6	-0.0
Chalcedony	0.8	0.3	0.8
Al(OH) <sub>3</sub> (am)	-4.0	NC	-0.8
Gibbsite	-1.3	NC	1.9
Kaolinite	0.7	NC	7.2
Alunite	1.8	NC	6.6
Fe(OH) <sub>3</sub> (am)	-1.0	0.5	NC
Goethite	4.9	6.4	NC
K-Jarosite	0.0	-8.5	NC(<-3)
Log $p_{\text{CO}_2}$ (in atm)	-1.0	-1.7	-0.9

with respect to amorphous Fe(OH)<sub>3</sub> but supersaturated with respect to goethite, and highly undersaturated with respect to all manganese oxides in the thermodynamic database used by NETPATH: pyrolusite (MnO<sub>2</sub>), hausmanite (Mn<sub>3</sub>O<sub>4</sub>), manganite (MnOOH) and pyrochroite (Mn(OH)<sub>2</sub>). These speciation results, based on the relatively high measured  $Eh$  (420 mV), are consistent with the high Fe and Mn contents of the water and the lack of any evidence of sulfate reduction. Surprisingly, the calculated equilibrium CO<sub>2</sub> partial pressure, 10<sup>-1.0</sup> for well 402, is close to that of the neutralized water (well 503).

In comparison to the acidic water from well 402, the partially neutralized water from well 503 is not as highly undersaturated with respect to calcite and dolomite, and remains close to saturation with respect to both gypsum and amorphous silica. Unlike its more acidic precursor, the water is highly supersaturated with respect to kaolinite and is likely near saturation with respect to some Al(OH)<sub>3</sub> phase: it is undersaturated with respect to amorphous Al(OH)<sub>3</sub> but supersaturated with respect to the more stable form of Al(OH)<sub>3</sub>, gibbsite. Although most of the dissolved iron has been removed, manganese has increased, and the water is at saturation with rhodochrosite. The water is still undersaturated with respect to several manganese oxides (pyrolusite  $SI$ : -9.1, hausmanite  $SI$ : -13.4, manganite  $SI$ : -4.7, pyrochroite  $SI$ : -7.2), although the uncertainty in these saturation indices is high, given the poor knowledge of manganese oxide thermodynamics and the dependence of the calculated saturation indices on the measured  $Eh$ . Indeed, lack of data on the vanishingly small dissolved Mn(IV) and Mn(III) concentrations makes any saturation index calculations for the Mn(IV) and Mn(III) minerals (pyrolusite, hausmanite, manganite) almost meaningless, because the calculations assume that the measured  $Eh$  values are representative of the Mn(IV)/Mn(II) and Mn(III)/Mn(II) aqueous activity ratios. Finally, the equilibrium CO<sub>2</sub> partial pressure (10<sup>-0.9</sup>) is close to that of the acidic water from well 402, and is more than an order of magnitude higher than are expected from equilibrium with unsaturated zone CO<sub>2</sub> partial pressures (Glynn and Busenberg, 1994b).

8.4.3 *NETPATH inverse modeling: simulation results*

The first NETPATH inverse modeling simulation considered the following 11 mass balance constraints: Cl, Ca, Mg, Na, Al, Si, RS (redox state), Fe, Mn, C, and S. The simulation also considered 14 phases for possible reactions. In addition, some phases were “forced” to be included (NETPATH model results without the phase were excluded from consideration), and some phase reactions were specified either as dissolution only, or as precipitation/exsolution only. The phases specified are listed below along with any associated constraints:

Calcite (forced inclusion; dissolution only),  
 Goethite (forced inclusion; precipitation only),  
 Gypsum (forced inclusion; precipitation only),  
 Kaolinite (precipitation only),  
 SiO<sub>2</sub>,  
 Dolomite (dissolution only),  
 MnO<sub>2</sub> (dissolution only),  
 Rhodochrosite (MnCO<sub>3</sub>),  
 Anorthite (CaAl<sub>2</sub>Si<sub>2</sub>O<sub>8</sub>; dissolution only),  
 Gibbsite,  
 Mn(OH)<sub>3</sub> (precipitation only),  
 O<sub>2</sub> gas (dissolution only),  
 CO<sub>2</sub> gas (exsolution only),  
 Pure Na phase.

The last phase in the list was added to keep track of the Na imbalance. In the first NETPATH simulation, the mixing fractions of well 402 and well 504 waters were determined through the chloride concentrations because no Cl phases were specified. The 11 element mass-balance constraints allow one mixing fraction and 10 phase mole transfers to be calculated. Because of the many models that include 10 of the 14 possible phases, additional mass-transfer limitations were necessary to minimize the number of possible models. NETPATH checked 330 models or possible solutions and found 12 that did not violate the limitations placed (i.e., whether a phase was forced to be included in all models, and whether it was allowed to dissolve only, precipitate/exsolve only, or both). Of the 12 models, 6 are given here (Table 8.3). They adequately represent the range of possible solutions given by the NETPATH code and will be further discussed. It is noted that linear combinations of models also form possible models.

The phases in the simulation were chosen, based on knowledge of the mineralogy of the basin-fill and alluvial aquifer materials, and the examination of saturation indices of the well 402 and well 503 water. In addition to selecting plausible phases, the saturation indices were used to determine which reactions might be thermodynamically feasible (dissolution-only and precipitation-only constraints). Although gypsum is not present in the uncontaminated aquifer, the contaminated waters are consistently slightly supersaturated with respect to gypsum. In fact, samples brought back from the field precipitate gypsum over the course of several months. Calcite and dolomite are known to be present in the aquifer materials and were therefore included in the model. Similarly, there is no lack of manganese oxides in the alluvial materials. Manganese oxides form at the contact between the Mn(II) rich-groundwaters and oxygenated groundwaters, and are also widely disseminated in the uncontaminated sand and gravel (Ficklin *et al.*, 1991). Lind and Stollenwerk (1994) conducted an elution experiment reacting acidic iron- and manganese-rich groundwater from well 101 with alluvial material from well 601, which is downgradient from the manganese-contaminated groundwaters. Based on X-ray diffraction results, Lind and Stollenwerk (1994) found that pyrolusite ( $\beta$ -MnO<sub>2</sub>) and a solid resembling kutnahorite (CaMn(CO<sub>3</sub>)<sub>2</sub>) were present before, but not after the elution of the alluvial materials.

Although goethite was the Fe(III) phase chosen (for precipitation only), choosing any other Fe(III) oxide would have resulted in the same Fe mass-transfer values. Similarly, we could

Table 8.3. Models from the first NETPATH simulation. Results in millimoles per kilogram of H<sub>2</sub>O. Positive numbers indicate dissolution, negative numbers precipitation or degassing.

Reaction or addition	Model 1 anorthite gibbsite	Model 2 gibbsite SiO <sub>2</sub>	Model 3 kaolinite SiO <sub>2</sub>	Model 4 electron transfer	Model 5 O <sub>2</sub> gas	Model 6 O <sub>2</sub> gas rhodo. diss.
Well 504	0.216	0.216	0.216	0.216	0.216	0.216
Pure Na	-0.579	-0.579	-0.579	-0.579	-0.579	-0.579
Dolomite +	2.899	2.899	2.899	2.899	2.899	2.899
Gypsum -F	-2.219	-2.219	-2.219	-2.219	-2.219	-2.219
Goethite -F	-8.339	-8.339	-8.339	-8.339	-8.339	-8.339
Calcite +F	4.929	5.086	5.086	4.929	4.929	4.929
Anorthite	0.157			0.157	0.157	0.157
Kaolinite			-0.226			
Gibbsite	-0.766	-0.452		-0.766	-0.766	-0.766
SiO <sub>2</sub>		0.314	0.766			
Rhodochrosite	-2.972	-2.972	-2.972			1.092
MnO <sub>2</sub> +	4.064	4.064	4.064	7.036	1.092	
Mn(OH) <sub>3</sub> -				-5.944		
O <sub>2</sub> gas +					1.486	2.032
CO <sub>2</sub> gas -	-6.033	-6.190	-6.190	-9.005	-9.005	-10.097
Net protons consumed	5.707	5.707	5.707	5.707	5.707	5.707

Notes: In the first column, F indicates a forced phase, + a dissolution only phase, - a precipitation only or an exsolution only phase.

have picked amorphous Al(OH)<sub>3</sub> instead of gibbsite. Whereas thermodynamic stability might distinguish among the potential iron phases, thermodynamic stability is not incorporated explicitly into NETPATH calculations. In fact, Fe and Al are most likely precipitating as fairly amorphous precipitates, that may recrystallize to more stable crystalline forms with time. The WATEQFP speciation results suggest that the waters near well 503 may be precipitating some Al(OH)<sub>3</sub> phase. The speciation results also suggest that kaolinite may be forming near well 402, but probably is not forming quickly near well 503 (as evidenced by the very high supersaturation with respect to kaolinite). The precipitation of amorphous forms of Al and Fe(III) minerals upon reaction of the alluvial sediments with acidic waters is also suggested by the elution experiments of Lind and Stollenwerk (1994) and by the selective extractions performed by Ficklin *et al.* (1991) on core materials from wells 107 (acidic), 451 (partially neutralized) and 505 (neutralized). Ficklin *et al.* (1991) also report no visible association between Al and SO<sub>4</sub> and argue against the formation of an AlOHSO<sub>4</sub> phase. Stollenwerk and Eychaner (1987) had earlier argued that this phase controlled aluminum concentrations in the acidic groundwaters. Furthermore, in his column elution studies, Stollenwerk (1994) found that he could best simulate the behavior of dissolved aluminum by using amorphous Al(OH)<sub>3</sub> as the solubility-limiting phase at *pH* values above 4.7 and AlOHSO<sub>4</sub> at lower *pH* values. Stollenwerk, however, changed the solubility product of the AlOHSO<sub>4</sub> phase to best fit his experimental results (from log *K* = -3.23 to log *K* = -2.2).

Considering the available evidence, Glynn and Brown (1996) considered that the issue of AlOHSO<sub>4</sub> precipitation was not resolved and required further research. More recently, Kirk Nordstrom (U.S. Geological Survey, personal communication, 2011), and a review by Bigham and Nordstrom (2000), have provided good arguments suggesting that an AlOHSO<sub>4</sub> phase probably did not occur in groundwaters at the Pinal Creek site. Because the water from well 402 is close to saturation with kaolinite, and because kaolinite is known to form

in acidic waters with high dissolved silica (Blair Jones, U.S. Geological Survey, personal communication, 1996), Glynn and Brown (1996) preferred the hypothesis of Al control by kaolinite in the more acidic waters from the site. However, these authors also investigated the effect of possible  $\text{AlOHSO}_4$  reactions in their inverse and forward geochemical modeling for the site. The results were interesting and therefore will be presented here, despite the recent knowledge arguing further against  $\text{AlOHSO}_4$  reaction control at the Pinal Creek site.

Because well 503 water is close to saturation with respect to rhodochrosite, we chose this mineral as a possible Mn sink. We believe that reductive dissolution of  $\text{MnO}_2$  is the primary process causing dissolved Fe(II) to oxidize and precipitate from solution. The only problem with this reaction mechanism is that the increase in dissolved Mn(II) is too small relative to the decrease in Fe(II). Several other possible reactions could explain the missing dissolved manganese:

1. Mn(II) may be precipitating out as rhodochrosite;
2. An electron transfer process may be taking place during which the oxidation state of the Mn oxide simply decreases while only partially releasing Mn into the solution.
3. Mn(II) may be sorbing onto the freshly precipitated Fe-oxyhydroxides.
4. Oxygen is known to be diffusing through the unsaturated zone into the groundwaters near the water table. However, because the sampling depths for wells 402 and 503 are substantially below the water table, the addition of significant amounts of oxygen is considered unlikely.

Although  $\text{O}_2$  ingassing was considered in the first NETPATH simulation, this reaction will be discarded in the second simulation. For similar reasons, the possibility of  $\text{CO}_2$  exsolution from a deep flowpath is unlikely. Glynn and Busenberg (1994b) estimated, based on their measurements of dissolved gases in the Pinal Creek basin groundwaters, that only groundwaters within 2 m of the water table could be exsolving dissolved gases and  $\text{CO}_2$ . Significant  $\text{CO}_2$  exsolution would also cause exsolution of other dissolved gases such as  $\text{N}_2$  and Ar. For example, exsolution of  $\text{CH}_4$  and  $\text{CO}_2$  from an hydrocarbon contaminant plume has been held responsible for the low dissolved Ar and  $\text{N}_2$  concentrations measured in groundwaters from the U.S. Geological Survey Bemidji Toxics site (Revesz *et al.*, 1995). Instead, groundwaters from the Pinal Creek site show high concentrations of both dissolved  $\text{N}_2$  and Ar because of the large amounts (often above  $20 \text{ mL L}^{-1}$ ) of excess air entrained during groundwater recharge (Glynn and Busenberg, 1994b).

Interestingly, the results of the first NETPATH simulation suggest that other Ca and Mg sources (in addition to calcite and dolomite) are needed if  $\text{CO}_2$  is disallowed as a sink for the excess carbon provided by the dissolution of the carbonates. We initially thought that rhodochrosite ( $\text{MnCO}_3$ ) would provide an additional carbon sink, but found that, given the Mn mass-balance constraints, the rhodochrosite sink would not be sufficient to account for the excess carbon. The presence of another Mn sink (such as Mn(II) sorption) instead or in addition to rhodochrosite precipitation would only exacerbate this problem. Therefore, because no other carbon sinks are likely to be present (the waters are undersaturated with respect to siderite), the next approach was to incorporate another Ca source, specifically a Ca silicate, so as to reduce the amount of carbon coming into solution from calcite. Although anorthite was chosen, it is likely that any silicate mineral dissolution accelerated by the acidic groundwaters would also act as a source of Mg, Na, and K (and probably Fe and Mn) to the solution. However, the dissolution of Ca-rich silicates (and perhaps Mg-rich silicates) is expected to be faster than that of Na- and K-rich silicates. On the basis of their observations and elution experiments, Lind and Stollenwerk (1994) suggest that tremolite ( $\text{Ca}_2\text{Mg}_5\text{Si}_8\text{O}_{22}(\text{OH})_2$ ) dissolution may be a source of both Ca and Mg to the Pinal Creek groundwaters. Indeed, amphiboles, such as tremolite, and pyroxenes are expected to have faster reaction rates than feldspar minerals, although their abundance in the alluvial materials is minor compared to that of the feldspar minerals. The presence of  $\text{CO}_2$  degassing in all the models found by the first NETPATH simulation suggests that some Mg-silicate phase (such as tremolite) must be included if models without  $\text{CO}_2$  degassing are to be found.

The last row in Table 8.3 gives an estimate of the net number of millimoles of protons consumed by the various reaction models. The number of protons consumed in each reaction model was calculated by estimating the number of protons consumed by the *dissolution* of one millimole of each solid or gaseous phase multiplied by the mole transfer in the reaction model. The number of protons consumed is dependent on the degree of protonation or hydroxylation of the various aqueous species produced by the dissolution reactions. For example, a calcite dissolution reaction will show consumption of two protons per mole of calcite dissolved if the reaction is written to produce  $\text{H}_2\text{CO}_3^0$  (or equivalently aqueous  $\text{CO}_2$ ; henceforth,  $\text{H}_2\text{CO}_3^0$  refers to the sum of the  $\text{H}_2\text{CO}_3^0$  and the much more dominant aqueous  $\text{CO}_2$  species), but will show consumption of only one proton if the reaction is written to produce  $\text{HCO}_3^-$ . The proton consumption calculations shown here assume that the reaction byproducts are the dominant aqueous species determined from the speciation of the well 402 water, such as:  $\text{AlF}^{2+}$ ,  $\text{AlF}_2^+$ ,  $\text{AlSO}_4^+$ ,  $\text{Al}(\text{SO}_4)_2^-$  and  $\text{Al}^{+3}$  for Al;  $\text{Mn}^{2+}$  and  $\text{MnSO}_4^0$  for Mn;  $\text{Fe}^{2+}$  and  $\text{FeSO}_4^0$  for Fe;  $\text{H}_2\text{CO}_3^0$  for *TDIC* (species listed in order of decreasing predominance). Using this assumption, the number of moles of protons consumed per mole of phase dissolved are: 14 for tremolite; 8 for anorthite; 6 for kaolinite; 4 for dolomite,  $\text{MnO}_2$  and  $\text{O}_2$  gas; 3 for goethite (or  $\text{Fe}(\text{OH})_3$ ), gibbsite (or  $\text{Al}(\text{OH})_3$ ) and  $\text{Mn}(\text{OH})_3$ ; 2 for calcite and rhodochrosite; 1 for  $\text{AlOHSO}_4$ . All other phases mentioned in Tables 8.3 and 8.4 are assumed not to consume protons upon dissolution. The consumption of protons by the heterogeneous mass-transfer reactions must necessarily be matched by an increase in solution *pH* and also by the release of protons from homogeneous deprotonation reactions (e.g.,  $\text{H}_2\text{CO}_3^0 \rightleftharpoons \text{HCO}_3^- + \text{H}^+$ ;  $\text{HSO}_4^- \rightleftharpoons \text{SO}_4^{2-} + \text{H}^+$ ). Given (i) that the increase in *pH* between wells 402 and 503 corresponds to approximately a 0.1 millimole decrease in  $\text{H}^+$  concentration, (ii) that the difference in  $\text{H}_2\text{CO}_3^0$  concentrations in well 402 and 503 waters is less than 1 millimolal (and  $\text{HCO}_3^-$  is always at least 5 times lower than the  $\text{H}_2\text{CO}_3^0$  concentration), (iii) that the concentration of  $\text{HSO}_4^-$  in well 402 water is close to 0.1 millimolal, and (iv) that there are no other major homogeneous deprotonation reactions, it appears that the 5.7 millimoles of proton consumption calculated for the various reaction models presented in Table 8.3 are at least 5 times too high. Unaccounted surface deprotonation or proton exchange reactions offer one possible reason for this discrepancy. Erroneous reaction models and analytical uncertainty in the basic data collected are other possible reasons.

The most interesting results of the first NETPATH inverse modeling simulation are the following. Gas exsolution or dissolution were found necessary in all models, even though anorthite dissolution and rhodochrosite precipitation were included. Of all the models found by the first NETPATH simulation, we prefer the 3 models that considered  $\text{MnO}_2$  dissolution and rhodochrosite precipitation, rather than an electron-transfer mechanism ( $\text{MnO}_2 \rightleftharpoons \text{Mn}(\text{OH})_3$ ) or  $\text{O}_2$  ingassing (with or without accompanying rhodochrosite dissolution). Of those three models, we also prefer the two models (models 1 and 2 in Table 8.3) that did not involve kaolinite precipitation. Although possible, the very high supersaturation of well 503 water with respect to kaolinite suggests that the mineral does not undergo fast precipitation, at least at *pH* values > 4. Instead, we favor aluminum control by  $\text{Al}(\text{OH})_3$  precipitation (with possible recrystallization to gibbsite).

#### *The second and third NETPATH simulations*

A second NETPATH simulation used Na as the conservative constituent, instead of chloride, and resulted only in "invalid" models that required the dissolution, rather than the precipitation, of 2.22 millimoles of gypsum per kg of water. Because both the acidic and neutralized groundwaters at Pinal Creek are supersaturated with respect to gypsum, slightly but consistently, a model with gypsum dissolution was not plausible. A pure chloride source (0.484 millimoles) was used in this second simulation. The calculated mixing fraction of background water from well 504 was 0.347 (instead of 0.216). A third NETPATH simulation used an intermediate mixing fraction of 0.281 (instead of 0.216 or 0.347) and resulted in 12 models that were similar to those of the first NETPATH simulation, but had different mass-transfer amounts. Gypsum precipitation was small (−0.003 millimoles). All models

required CO<sub>2</sub> mass transfer, but in somewhat smaller amounts (e.g., -5.4 instead of -6.0 millimoles for Model 1, Table 8.3).

*The fourth NETPATH simulation*

A fourth NETPATH simulation was used to explore the effects of including tremolite [Ca<sub>2</sub>Mg<sub>5</sub>Si<sub>8</sub>O<sub>22</sub>(OH)<sub>2</sub>], biotite [KMg<sub>1.5</sub>Fe<sub>1.5</sub>AlSi<sub>3</sub>O<sub>10</sub>(OH)<sub>2</sub>], forsterite [Mg<sub>2</sub>SiO<sub>4</sub>], a pure Mn sink (to simulate Mn(II) sorption) and AlOH<sub>4</sub>SO<sub>4</sub>, while excluding some of the reactions considered unrealistic in the previous simulations, namely CO<sub>2</sub> exsolution, O<sub>2</sub> dissolution, and kaolinite precipitation. Forsterite was included for numerical exploration because it is a pure Mg-silicate with a high Mg/Si ratio. Tremolite and biotite were included because those minerals are commonly found in the Pinal Creek basin sediments. Although K is present in biotite, no mass-balance for K was included in the NETPATH simulations because of the large uncertainties in our estimated K data. The fourth NETPATH simulation resulted in 19 possible models. Of the 19 models, 6 included more than 1 Mg-silicate phase and are not presented here (Table 8.4) for reasons of space and simplicity. Five models included tremolite as the only Mg-silicate phase, and differed from each other in their treatment of the Mn and Al mass-balances (Models 7 and 10 through 13 in Table 8.4). Five other similar models included biotite instead of tremolite (Model 8 in Table 8.4) and 3 remaining models included forsterite but did not include AlOH<sub>4</sub>SO<sub>4</sub>.

Table 8.4. Models from the fourth NETPATH simulation. Same phases included as in first three simulations, except for the following changes: (i) tremolite, biotite, forsterite, AlOH<sub>4</sub>SO<sub>4</sub>, and a pure Mn sink included as possible phases; (ii) kaolinite and gases excluded.

Reaction or addition	Model 7 tremolite	Model 8 biotite	Model 9 forsterite	Model 10 tremolite electron transfer	Model 11 tremolite Mn sink	Model 12 tremolite AlOH <sub>4</sub> SO <sub>4</sub>	Model 13 tremolite no anorth. AlOH <sub>4</sub> SO <sub>4</sub>
Well 504	0.216	0.216	0.216	0.216	0.216	0.216	0.216
Pure Na	-0.579	-0.579	-0.579	-0.579	-0.579	-0.579	-0.579
Dolomite +							
Gypsum -F	-2.219	-2.219	-2.219	-2.219	-2.219	-0.648	-0.089
Goethite -F	-8.339	-11.238	-8.339	-8.339	-8.339	-8.339	-8.339
Calcite +F	4.696	6.146	4.696	1.724	1.724	4.696	4.696
Anorthite	2.130	1.840	3.290	5.102	5.102	0.559	
AlOH <sub>4</sub> SO <sub>4</sub> -						-1.571	-2.130
Gibbsite	-4.712	-6.066	-7.032	-10.656	-10.656		1.678
SiO <sub>2</sub>	-8.587	-9.166	-7.717	-14.530	-14.530	-5.445	-4.326
Rhodochrosite	-2.972	-4.422	-2.972			-2.972	-2.972
MnO <sub>2</sub> +	4.064	5.514	4.064	7.036	4.064	4.064	4.064
Mn(OH) <sub>3</sub> -				-5.944			
Mn sink -					-2.972		
Tremolite	0.580			0.580	0.580	0.580	0.580
Biotite		1.933					
Forsterite			1.450				
Net protons consumed	5.711	7.642	5.711	5.711	11.655	5.708	5.711

Notes: Results in millimoles per kilogram of H<sub>2</sub>O. Positive numbers indicate dissolution, negative numbers precipitation or degassing. In the first column, F indicates a forced phase, + a dissolution only phase, - a precipitation/exsolution only phase.

None of the models found included dolomite, a mineral present in the alluvium as rock fragments and in dolomite formations in the surrounding hills. Dolomite should certainly be as reactive with the acidic waters as some of the silicate minerals. The problem appears to be that dolomite dissolution requires a carbon sink in addition to rhodochrosite. This carbon sink has not yet been identified. Of all the models presented in Table 8.4, we prefer the models (Models 7 through 9) that considered  $\text{MnO}_2$  dissolution and rhodochrosite precipitation and that did not include  $\text{AlOH}\text{SO}_4$ . The models with electron transfer combined with any of the Mg-silicate phases are also plausible. In reality, the reactions occurring and responsible for the evolution of well 402 water to well 503 water are likely to be some linear combination that may include, but will not be restricted to, the mass-transfer models that we found using the NETPATH code. Many more models could have been found had we included other phases (silicates in particular), but their description and classification would not add substantive insight into the predominant reactions occurring in the basin. Table 8.4 also gives the millimoles of protons consumed for each reaction, using the assumptions discussed earlier (see discussion of Table 8.3). Once again it appears that the millimoles of proton consumption calculated for the various reaction models presented in Table 8.4 are about 3 to 10 times too high. Unaccounted surface deprotonation and proton-exchange reactions and uncertainty in the analytical data offer possible reasons for the discrepancy. This problem will be circumvented in the PHREEQC inverse modeling demonstration discussed later, because PHREEQC always includes alkalinity mass-balance and charge-balance equations and also considers possible uncertainties in the analytical data.

Fifth and sixth NETPATH simulations used the phases considered in the fourth simulation, but explored the effects of using either (i) Na (instead of Cl) as the conservative constituent to determine the mixing fractions of the waters from wells 402 and 504, or (ii) an average mixing fraction of well 504 water (similar to the third NETPATH simulation). The results of these simulations are discussed in Glynn and Brown (1996), but the main results of the simulations are that they either produce unrealistic models (e.g., requiring gypsum dissolution rather than precipitation), or they require a Na sink. Loss of Na to an ion-exchange mechanism is unlikely given the relatively high and increasing Ca/Na ratio along the flowpath. It is possible that accelerated weathering of silicate minerals by the acidic waters may be causing a significant increase in the cation exchange capacity of minerals exposed to the groundwaters and could thereby be responsible for a net removal of Na (and other cations) from solution (Blair Jones, U.S. Geological Survey, verbal communication). However, it is more likely that analytical error or unrepresentative concentrations in the background water chosen to simulate the downgradient dilution process are responsible for the inconsistency in the Cl and Na dilution results.

#### *Conclusions from the NETPATH inverse modeling simulations*

The most important conclusion provided by the NETPATH simulations is that Ca- and Mg-silicate mineral dissolution must be a significant process. Many researchers at the Pinal Creek site originally believed that calcite and dolomite dissolution was responsible for the most of the acid neutralization. However, Glynn (1991b) demonstrated that the increase in Sr concentrations between wells 51 and 402 must have been caused by silicate mineral dissolution—the amount of Sr present in limestone and dolomite formations contributing to the carbonate content of the alluvial materials is too small relative to the amount of Sr that precipitates as an impurity in gypsum. Sr is a significant impurity in Ca-silicate minerals and is released to the solution during their dissolution. Similarly, dissolved inorganic carbon  $\delta^{13}\text{C}$  data (Glynn, Busenberg and Brown, unpublished data collected in June 1993) ranges from  $-9.15$  to  $-12.90$  per mil for the acidic or neutralized contaminated groundwaters, and from  $-10.95$  to  $-14.00$  per mil for the uncontaminated waters, suggesting that neutralization of the acidic plume by silicate minerals must indeed be important. [All  $\delta^{13}\text{C}$  values are expressed relative to the Vienna PDB standard.] If the calcite and dolomite  $\delta^{13}\text{C}$  values are near 0 per mil,

as is reasonable for marine carbonates, closed system dissolution of those carbonates caused by acid neutralization reactions deep within the aquifer should result in higher  $\delta^{13}\text{C}$  values.

#### 8.4.4 *Inverse geochemical modeling with PHREEQC*

PHREEQC provides additional capabilities for modeling the chemical evolution between the well 402 and well 503 waters because it considers uncertainties associated with individual element analyses and also solves alkalinity-balance, water mass-balance, and charge-balance equations. PHREEQC allows each analytical datum for each aqueous solution to be adjusted within an uncertainty range that is specified by the user. PHREEQC determines sets of phase mass transfers, solution mixing fractions, and adjustments to the analytical data that satisfy mass-balance constraints and are consistent with the specified uncertainties. As an option, PHREEQC will also determine mass-transfer models (later referred to as “minimal” models) that minimize the number of phases involved. Most constraints used by PHREEQC inverse modeling are automatically specified by providing a list of potentially reactive phases. For example, if tremolite is identified as a potential reactant, PHREEQC will automatically include mass-balance constraints on Ca, Mg, and Si (NETPATH does not do this). In addition to the mass-balance constraints defined by specifying a list of potential reactants, PHREEQC also lets the user specify additional mass-balance constraints that may be used in determining the mixing fractions for two or more solutions that mix to form a final solution.

Unlike NETPATH, PHREEQC includes a charge-balance constraint, which specifies that the sum of the deviations from the analytical data for a given solution must equal the charge imbalance present in that solution. PHREEQC also uses a water mass-balance constraint to account for mixing, water derived from mineral reactions, and water evaporation or dilution (PHREEQC and NETPATH are not limited to groundwater problems). The charge-balance and water mass-balance constraints used by PHREEQC are equivalent to including a mass balance on hydrogen or oxygen. During the inverse modeling simulation, PHREEQC will adjust not only the analytical element concentrations, it will also adjust the *pH* of the waters. The adjustment to total dissolved inorganic carbon is constrained to be consistent with the adjustments to *pH* and alkalinity. Finally, in addition to including a general electron balance constraint (such as is done in NETPATH), PHREEQC also includes mole-balance equations for individual valence states of redox-active elements.

A PHREEQC inverse-modeling simulation was constructed by including all the phases used in the NETPATH simulations, except for kaolinite and  $\text{CO}_2$  and  $\text{O}_2$  gases, which were excluded. Including biotite [ $\text{KMg}_{1.5}\text{Fe}_{1.5}\text{AlSi}_3\text{O}_{10}(\text{OH})_2$ ] in PHREEQC forced the code to account for the K mass-balance. However, K is not expected to accumulate in the Pinal Creek basin groundwaters and should also not be used to determine the mixing fractions of well 402 and well 504 waters. Therefore, a pure potassium-montmorillonite [ $\text{K}_{0.33}\text{Al}_{2.33}\text{Si}_{3.67}\text{O}_{10}(\text{OH})_2$ ] was also included in the simulations with biotite and was only allowed to precipitate. Both sodium and chloride were specified as mass-balance constraints. Pure Na, pure Cl and pure Mn sinks were not specified, because PHREEQC requires charge-balanced phases. Adding charge imbalance would prevent PHREEQC from correctly adjusting the analytical data within the user-specified uncertainties. A  $\pm 5\%$  relative uncertainty was chosen for all elements, except for K ( $\pm 20\%$ ) and for Cl for which an uncertainty of  $\pm 10\%$  was initially chosen but later was reduced to  $\pm 5\%$ . The lower uncertainty for Cl did not affect the number of mass transfer models calculated by PHREEQC, minimal or otherwise, did not significantly affect the calculated mixing fractions of well 504 water, and did not result in any changes in the phases included in the mass-transfer models. The uncertainty in the *pH* of the three waters from wells 402, 504 and 503 was  $\pm 0.05$  *pH* units. The “minimal” option was initially chosen to reduce the number of possible models to those minimizing the number of phases involved. Some additional precipitation-only and dissolution-only constraints were added for the phases. The models shown in Table 8.5 are a representative selection of all the models found by PHREEQC. Table 8.5 shows most of the tremolite-containing models, but other

Table 8.5. PHREEQC inverse modeling simulation results. Amounts of mass transfer and net proton consumption are reported in millimoles per kilogram of H<sub>2</sub>O. Only mass-transfer sets (models) with the minimum significant number of phases are shown.

Reaction or addition	Model 1 tremolite non-min.	Model 2 tremolite	Model 3 tremolite no calcite	Model 4 tremolite e <sup>-</sup> transf.	Model 5 tremolite AlOHSO <sub>4</sub>	Model 6 tremolite AlOHSO <sub>4</sub> e <sup>-</sup> transf.	Model 7 biotite
504mf.	0.258	0.258	0.258	0.258	0.258	0.258	0.258
504 mf. min.	0.258	0.258	0.258	0.258	0.258	0.258	0.258
504 mf. max.	0.277	0.277	0.277	0.277	0.264	0.264	0.263
Dolomite +	0.398		2.191		0.290		2.291
Gypsum -							
Goethite -	-8.292	-8.292	-8.292	-8.291	-8.292	-8.292	-9.074
Calcite +	3.588	4.383		1.626	3.817	3.991	
Anorthite +			2.512	2.202			2.691
AlOHSO <sub>4</sub> -					-0.423	-0.423	
Gibbsite-	-0.423	-0.423	-5.448	-4.827			-2.167
SiO <sub>2</sub> -	-3.649	-3.649	-5.803	-8.687	-3.165	-3.629	
Rhodochrosite	-2.757	-2.757	-2.756		-2.769	-2.364	-3.253
MnO <sub>2</sub> +	3.903	3.903	3.903	6.659	3.903	4.309	4.294
Mn(OH) <sub>3</sub> -				-5.512		-0.811	
Tremolite +	0.500	0.500	0.142	0.580	0.440	0.498	
Biotite +							0.521
K-mont.-							-1.796
Net protons consumed	-0.279	-0.281	-0.272	-0.266	-0.271	-0.270	-0.298
Alk. change	0.214	0.213	0.213	0.213	0.213	0.213	0.190
Difference	0.493	0.494	0.485	0.479	0.484	0.483	0.487

Abbreviations: 504mf., well 504 mixing fraction; +, dissolution only; -, precipitation only; Alk., alkalinity change; non-min., not a "minimal" model; K-mont., K-montmorillonite; e<sup>-</sup> transf., electron transfer.

models found (with biotite/K-montmorillonite, forsterite or tremolite) were essentially variations on the combination of reactions shown in Table 8.5. It should be remembered that, similar to the NETPATH models, linear combinations of PHREEQC inverse models also represent possible models. With the exception of Model 1<sup>4</sup>, all models reported in Table 8.5 are "minimal" models, i.e., had the minimum number of phases.

PHREEQC calculates, as an option, the minimum and maximum mass transfers associated with any given phase in any given model. These minimum and maximum mass transfers are constrained by the uncertainty ranges specified for the various element and *pH* analyses. Only the minimum and maximum mixing fractions of well 504 water are given in Table 8.5. The optimal mixing fractions of well 504 water reported by PHREEQC are close to the minimum possible values and do not change significantly between the various models. The mixing fraction of 0.258 reported in Table 8.5 is between the values of 0.216 and 0.347 determined by NETPATH respectively assuming conservative dissolved Cl or conservative dissolved Na.

The absence of gypsum precipitation in all of the minimal or non-minimal models is one of the most important results of the PHREEQC inverse modeling. PHREEQC revealed that SO<sub>4</sub> could be considered a conservative entity given the ±5% uncertainty associated with the analyses. Although most of the reasonable NETPATH mass-transfer models

<sup>4</sup>Model 1 can be compared with its equivalent "minimal" model, Model 2.

based on chloride conservation precipitated 2 millimoles of gypsum, this mass-transfer was insignificant given the  $\pm 5\%$  relative uncertainty on the  $\text{SO}_4$  concentrations and the high  $\text{SO}_4$  concentrations in the well 402 and 503 waters. All of the mass-transfer models reported by NETPATH included 10 phases. In contrast, given the uncertainties in the analytical data, inverse modeling with PHREEQC showed that only 7 or 8 phases were required.

The second major conclusion, which confirmed the earlier NETPATH simulation results, is that Ca- and Mg-silicate phases are needed in addition to calcite and dolomite to explain the Ca, Mg and C mass balances. Another conclusion, not revealed by the previous NETPATH simulations, was the presence of dolomite dissolution in some of the minimal models. This conclusion was satisfying, because dolomite is present in the aquifer and should react in acidic environments. The PHREEQC results presented in Table 8.5 show a net production of close to 0.3 millimoles of protons. This proton balance was calculated, as previously done for the NETPATH model results (see discussion of Table 8.3), from the mass transfers in the PHREEQC models. The net proton consumption calculated for the PHREEQC models is an order of magnitude smaller than calculated for the NETPATH models. Because of alkalinity-balance and charge-balance equations are included in PHREEQC calculations, the net amount of protons released and consumed by heterogeneous and homogeneous reactions is consistent with the *pH* values of the initial and final waters, given the uncertainties specified by the user. The proton consumption can be checked against the change in alkalinity between the final well 503 water and the mixture of the well 402 and 504 waters. The alkalinity changes reported in Table 8.5 use the adjusted alkalinities calculated by PHREEQC for each inverse model. The difference between the net proton consumption and the net alkalinity change is caused by the lack of accounting for the consumption of dissolved oxygen ( $6.64 \text{ mg L}^{-1}$  in well 504) in our proton consumption calculations. The difference of 0.49 millimoles is close to 4 times the difference between the oxygen content of the well 503 water and a mixture of the well 504 and well 402 waters ( $4 \times 0.121 = 0.484$  millimoles). The reaction of the dissolved  $\text{O}_2$  present in well 504 water reduces the amount of  $\text{MnO}_2$  that undergoes reductive dissolution. The fact that 4 protons are consumed rather than 2 for each mole of oxygen consumed appears to be an error in the PHREEQC version 1 code (David Parkhurst, personal communication). Because the  $\text{MnO}_2$  mass transfer is 30 times greater than the oxygen mass-transfer, this error does not significantly affect our results.

Out of the 6 minimal models presented in Table 8.5, our favorite models are Models 7, 2, 4, and 3. These models do not involve  $\text{AlOHSO}_4$  precipitation. As previously mentioned, Glynn and Brown's (1996) view that the evidence for possible Al control by  $\text{AlOHSO}_4$  precipitation during the evolution from well 402 water to well 503 water was weak is supported by Bigham and Nordstrom's (2000) review of the environmental conditions needed for  $\text{AlOHSO}_4$  occurrence. Consequently, our preference for amorphous  $\text{Al}(\text{OH})_3$  as the controlling Al phase is stronger than it was in 1996. Tremolite is present in the alluvial materials and its reaction with acidic water from the Pinal Creek site has been documented by Lind and Stollenwerk (1994). Nevertheless, tremolite dissolution probably contributes much less Ca than dissolution of Ca-rich plagioclase feldspars (such as anorthite and labradorite) during the neutralization of the acidic groundwaters. The accompanying release of Na during feldspar dissolution could be a problem, however, because the PHREEQC models consider Na as a conservative constituent, within the uncertainty of the analytical data. Too much Na dissolution would require a Na sink, which remains elusive. As mentioned earlier, additional cation exchange capacity resulting from the transformation of the feldspars and other aluminosilicates into secondary clay minerals is the only plausible Na sink. Sorption on freshly precipitated iron oxyhydroxides could represent another Na sink, but the affinity of Na for these precipitates is considerably weaker than the affinity of the other cations in the solution.

Two additional PHREEQC inverse modeling simulations were conducted allowing cation exchange of Na for Ca in one simulation and exchange of Na for H in another. The results are discussed in some detail in Glynn and Brown (1996). The cation exchange capacity of the Pinal Creek alluvial sediments is generally low, probably less than 1 meq/100 g, given

the coarseness of the sediment and the low organic carbon content (less than 1%). Lacking further information regarding ion-exchange reactions at the Pinal Creek site, Models 7, 4, 2 and 3 from the earlier PHREEQC inverse modeling simulation, which do not include cation exchange (Table 8.5), remain our preferred models. Simulating cation exchange in an inverse geochemical model presumes that the user has knowledge of the thermodynamically preferred directions of exchange. Although we feel that Na replacement for Ca on exchange sites should generally not occur given the preferential dissolution of Ca relative to Na in the mineral dissolution reactions, and the greater charge density (and sorption affinity) of Ca over Na, the direction of exchange for other ion-exchange reactions has much greater uncertainty. Proton release from exchange sites during the neutralization of well 402 water is possible. Our inverse geochemical modeling simulations point out the need for further experiments to determine cation exchange capacities and directions of exchange. The ability of inverse modeling to highlight knowledge gaps is perhaps one of its greatest benefits. As will be demonstrated in the next section, forward geochemical modeling may also provide insight into cation exchange reactions.

Although some mass-transfer processes are likely to occur continuously throughout the flowpath used in inverse modeling, some mass-transfer processes (such as cation exchange reactions) will affect the groundwater chemistry only in narrow portions of the flow system. In the case of continuous processes, an overall rate of reaction (expressed for example in moles per kg of H<sub>2</sub>O per travel time or per travelled volume of aquifer) may be provided by the inverse modeling results. In the case of a non-continuous process, however, such rates will have little meaning. Unfortunately, inverse geochemical modeling cannot provide information on the heterogeneous mass-transfer reactions occurring at specific points along a flowpath, but provides, instead, only the *net* amounts of mass transfer between an initial and a final endpoint. Forward geochemical modeling can, however, provide insight on the evolution through time of chemical compositions at specific points along a postulated flowpath. *Field corroboration or confirmation* of forward modeling simulations, however, may require significantly more spatial (and temporal) information than may be available.

## 8.5 REACTIVE-TRANSPORT MODELING AT THE PINAL CREEK SITE

Inverse modeling is a valuable tool that can be used to gain an improved understanding of the geochemical processes that occur, or have previously occurred, in an aquifer. By itself however, inverse modeling cannot be used to make predictions on the future chemical evolution of a groundwater system, or in the case of a contaminated groundwater, on the movement of contaminants. Forward reactive-transport modeling is needed to make such predictions. Inverse modeling results, nevertheless, can be used to identify potential reactions that should be considered by a reactive transport model.

In metal-contaminated acidic groundwaters, such as those present at the Pinal Creek site, *pH* and *Eh* conditions are the primary chemical variables controlling the transport of metals and determining the quality of the groundwaters. The partially-neutralized, Fe(II)-poor groundwaters (such as the well 503 water used in our inverse modeling exercise) have significantly lower metal concentrations than the more acidic Fe(II)-rich waters (such as the well 402 water). The partially neutralized waters are still contaminated and have high SO<sub>4</sub>, Ca, and Mn concentrations that make them unsuitable for most beneficial uses, but nevertheless offer a significant improvement in water quality. Therefore, the ability to predict the movement and reaction of the low-*pH* and Fe(II)-rich groundwater zones is desirable.

Inverse modeling can help identify the possible reactions affecting the neutralization and oxidation of the low-*pH* and Fe(II)-rich groundwaters. Generally however, the movement of the low-*pH* and Fe(II)-rich waters will be controlled by the following factors:

1. the groundwater velocity field,
2. the dilution of the contaminated groundwaters by longitudinal and transverse dispersion,

3. the extents of heterogeneous mass-transfer reactions affecting the *pH* and Fe(II) concentrations in the groundwaters (causing the low-*pH* Fe(II)-rich waters to evolve into higher-*pH* Fe(II)-poor waters), and
4. the initial concentration and composition of mineral and gas phases contacting the groundwaters and responsible for their chemical evolution.

The following sections briefly discuss ongoing research efforts aimed at a better understanding of the movement and chemical evolution of acidic, metal-laden groundwaters at the Pinal Creek site. The research findings from the Pinal Creek site will hopefully provide information, not only on the processes affecting acidic, metal-laden groundwaters in semi-arid alluvial basins, but also on the most efficient techniques to characterize and model the spread of contaminated waters at sites with similarly sparse spatial information.

#### *The groundwater velocity field*

Groundwater velocities can be estimated through the construction of a groundwater flow model. Calculations using Darcy's law on observed heads and estimated hydraulic conductivities have provided estimates of groundwater velocities in the Pinal Creek basin (Brown, 1996; Neaville and Brown, 1993). However, USGS efforts (in the mid to late 1990s) to construct a general flow model for both the alluvial and basin-fill aquifers were not successful, in part because of a limited number of piezometric observations, but mainly because the high hydraulic conductivity of the unconsolidated alluvium and its focused distribution along stream channels resulted in wetting and drying oscillations that caused numerical convergence problems. However, geochemical tracers ( $^{18}\text{O}$ ,  $^2\text{H}$ ,  $^{13}\text{C}$ , Cl, Ar,  $\text{N}_2$ ) were used successfully by Glynn *et al.* (1999) to understand many characteristics of the origin of groundwaters in the alluvial and basin fill aquifers, including recharge temperature, recharge elevation, the amount of excess air entrained during recharge, and the extent of evaporative losses. Additionally, repeated measurements, from field campaigns in 1991, 1993, 1996, and 1998, of chlorofluorocarbon tracers CFC-11, CFC-12, and CFC-113, and to a lesser extent of  $\text{SF}_6$  and  $^3\text{H}/^3\text{He}$  concentrations, provided estimates of travel times for waters in both the alluvial and basin-fill aquifers. Despite extreme fluctuations in the water table during that period, the independent travel-time estimates obtained from different tracers were generally consistent; and furthermore, the travel times obtained for the deeper waters in both the alluvial and basin-fill aquifers were found to be nearly invariant with time (Glynn *et al.*, 1999). Because of difficulties in the construction of a MODFLOW groundwater-flow model for the Pinal Creek aquifers, a plan to use all the available hydrologic, chemical and isotopic data to calibrate a three-dimensional reactive-transport model for the basin was never achieved. Such a model, and its supporting flow model, would have been useful in refining the understanding the movement of contaminated waters and the impact of anthropogenic or natural remediation processes at the Pinal Creek site, and should generally be considered essential in the investigation of highly dynamic contaminated groundwater systems.

#### *Transport processes and contaminant dilution*

The dilution of the acidic metal-contaminated groundwaters is certainly one of the most important processes responsible for the downgradient decrease in dissolved-metal concentrations in the Pinal Creek basin. Although this dilution process was already evident in the dry to normal recharge years (1984–1991), further dilution occurred as a result of the greater than normal recharge events that started in the spring of 1991, continued in 1992, and culminated in a 100-year-magnitude flooding event in spring 1993 (groundwater levels rose as much as 16 meters). Advanced modeling techniques are not needed to demonstrate dilution as a result of these events: plots of metal concentrations as a function of chloride clearly illustrate the process (e.g., Fig. 8.3). However, a 2- or 3-dimensional transient transport model would clearly be useful in determining the relative contributions of transverse dispersion, longitudinal dispersion, flow convergence, and transient high-intensity

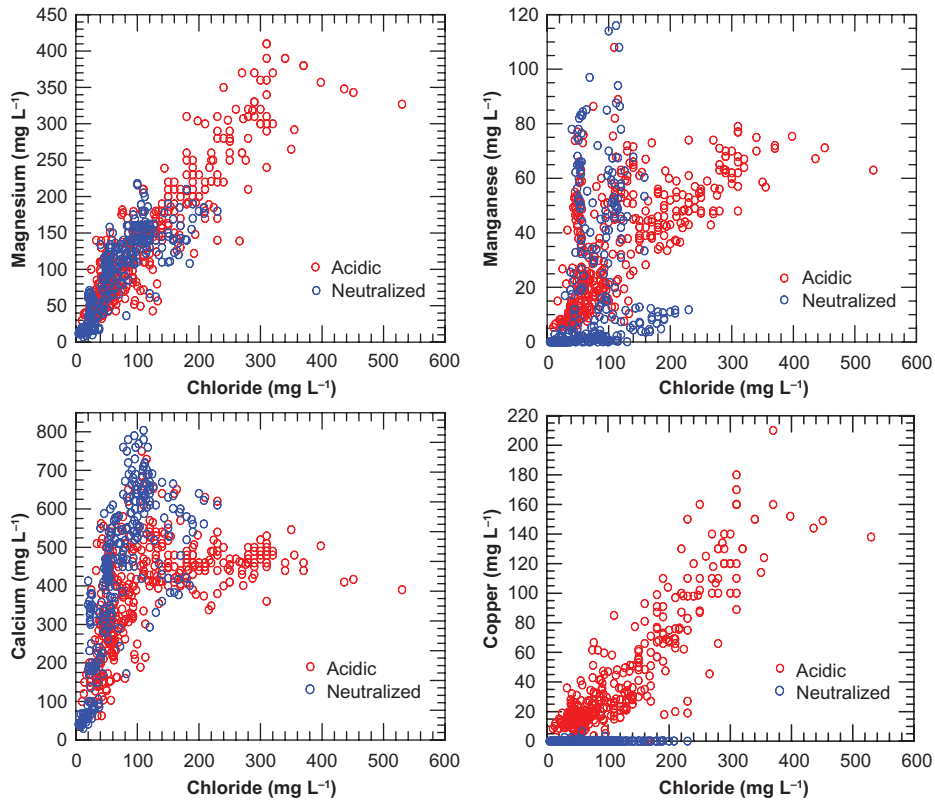


Figure 8.3. Magnesium, manganese, calcium and copper concentrations plotted against chloride concentration in acidic (upgradient) and neutralized (downgradient) groundwaters from the Pinal Creek basin.

recharge in the dilution process. Figure 8.3 also shows the relative importance, for different elements, of dilution and reaction (oxidation, neutralization, precipitation/sorption) processes in controlling groundwater chemical evolution.

### 8.5.1 Summary of previous reactive-transport modeling

Previous reactive-transport modeling conducted for the Pinal Creek site (see, Glynn and Brown, 1996, for more information) is briefly discussed here. Brown (1996) used the PHREEQC (version 1) code to construct a 1-D reactive transport model of the site based on the groundwater chemical data collected by the USGS between 1984 and 1994. The author used the 1984 chloride concentrations to back-fit the observed dilution processes as a function of time and distance along a flowpath that extended from the most acidic waters (well 51) to the most down-gradient waters (well 702). Remarkably, given the dynamic hydrology of the site, only a few adjustments were needed to fit the Cl concentration profiles for subsequent years. Adjustments were made to fit observed concentrations in 1985, 1988 and more importantly in 1993, when the equivalent of a “hundred-year” magnitude flood occurred in the valley. The results of the modeling investigation showed that dilution, rather than sorption or other reaction processes, could account for the decrease of Cu, Zn, Ni, and Co in the acidic ground-water as water flowed from well 51 to well 451. Generally, the simulated Fe(II) and

Mn(II) concentrations did not match the observed concentrations, especially downgradient from well 451. This mismatch was partly caused by a lack of knowledge at the time regarding the reactions controlling Mn and Fe; for example, rhodochrosite precipitation was not considered, and the decrease in Mn(II) concentrations was ascribed to oxidation by in gassing O<sub>2</sub> downgradient from well 503. The mismatch was also partly caused by lack of knowledge on rates of reactions, not only for redox processes, but also for carbonate and silicate mineral reactions and other reactions.

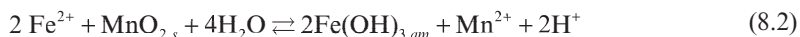
Glynn and Brown (1996) summarized the results of Glynn *et al.* (1991), who simulated the 1-dimensional transport and reactions of a highly acidic water sampled in 1987 from well 51 with a mineral assemblage thought to be reasonable for the Pinal Creek alluvial aquifer. One of the primary purposes of the simulation was to compare the results obtained from two different codes: PHREEQM and MST1D. Despite significant differences in their algorithms, the two codes gave almost identical results. The well 51 water used in the simulations was significantly more contaminated than the well 402 water that was used in the inverse modeling example presented here and in reactive-transport simulations described in this chapter. Relative to the well 51 water, conservative constituents (Cl, SO<sub>4</sub>, and Mg) in the well 402 water were diluted by a factor of approximately 2.4; Na decreased only by about 1.7, suggesting the existence of a Na source between wells 51 and 402; Fe and Al decreased significantly more than could be explained by dilution (by factors of 4.7 and 13.5 respectively); SiO<sub>2</sub>, *TDIC* and Mn did not change significantly, and Ca and Sr concentrations actually increased by 1.15 and 1.79 times, respectively. The acidity represented by the potential oxidation and precipitation of the dissolved Fe(II), Mn(II) and Al in the water from well 51 was  $1.31 \times 10^{-1}$  moles of protons compared to  $2.60 \times 10^{-2}$  for the well 402 water, or about 5 times greater. Adding the acidity represented by *TDIC* does not significantly change the potential acidity of well 51 water, but does increase the potential acidity of well 402 water to a proton molality of  $3.01 \times 10^{-2}$ , a value still 4.5 times lower than that of well 51 water. [The calculation of potential acidity assumes that (i) each mole of Fe<sup>2+</sup> oxidation and precipitation (by reductive dissolution of MnO<sub>2</sub>, or by reduction of dissolved O<sub>2</sub>) produces 2 moles of H<sup>+</sup>, (ii) oxidation of dissolved Mn<sup>2+</sup> and precipitation as MnO<sub>2</sub> (or precipitation of MnCO<sub>3</sub>) produces 2 moles of H<sup>+</sup>, (iii) precipitation of Al<sup>3+</sup> produces 3 moles of protons, and (iv) each mole of H<sub>2</sub>CO<sub>3</sub> produces 1 mole of H<sup>+</sup>.] The Glynn *et al.* (1991) simulations for the reactive transport evolution of the well 51 highly acidic water provide an interesting comparison for the reactive-transport simulations presented in the next section.

### 8.5.2 *A reactive-transport sensitivity analysis on the movement of pH and pe-controlling mineral fronts*

Some of the reactions identified by inverse modeling of the chemical evolution of groundwaters between wells 402 and 503 were used in 1-D PHREEQM and PHREEQC reactive-transport simulations to determine their effect on the movement of the low-*pH* and high-Fe(II) groundwaters in the Pinal Creek basin. Many results of this study will also be applicable to other sites where groundwater is contaminated by sulfuric acid and heavy metals. Before discussing the results of the PHREEQM and PHREEQC transport simulations, however, we will show how the movement of a single mineral dissolution front, critical in controlling the redox state of the Pinal Creek groundwaters, can be modeled without the use of a computer code.

#### 8.5.2.1 *A simple model for advective transport of a reactive front: the MnO<sub>2</sub> dissolution front*

If O<sub>2</sub> ingassing is assumed not to affect the concentrations of Fe(II) at significant depths below the water table (11 m for well 402, 21 m for well 503), the movement of dissolved Fe(II) will probably be determined by the reduction of manganese oxides, as exemplified by the following reaction:



The free energy change associated with this reaction is highly negative, and the reaction can be considered irreversible, regardless of which crystal structure is used for  $\text{MnO}_{2,s}$  (birnessite, pyrolusite) or for the precipitated iron oxyhydroxide. As a result, if the kinetics of the reductive dissolution reaction are fast relative to the movement of the water ( $5 \text{ m day}^{-1}$ ), the velocity of the dissolved Fe(II) front,  $V_{\text{Fe}}$  can be related to the velocity,  $V_{\text{H}_2\text{O}}$  of the water through an apparent retardation factor  $R$ ,

$$V_{\text{Fe}} = V_{\text{H}_2\text{O}} / R \quad (8.3)$$

where  $R$  is related to the amount,  $M_{\text{ini}}$ , of  $\text{MnO}_{2,s}$  initially present in the aquifer (expressed in moles  $\text{kg}^{-1} \text{H}_2\text{O}$ ) and to the amount,  $\Delta M$ , of  $\text{MnO}_{2,s}$  dissolved by a unit mass (1 kg of  $\text{H}_2\text{O}$ ) of Fe(II)-rich water:

$$R = 1 + \frac{M_{\text{ini}}}{\Delta M} \quad (8.4)$$

Equation (8.4) can be related to the more general equation describing the retardation of sharp reaction fronts in systems with advective, but no dispersive, transport (Dria *et al.*, 1987; similar expressions for the “traveling wave” approximation can also be found in Lichtner, 1988, 1985; Ortoleva *et al.*, 1986):

$$R = 1 + \frac{\sum_{k=1}^K g_{ik} (m_k^D - m_k^U)}{\sum_{j=1}^J h_{ij} (c_j^D - c_j^U)} \quad (8.5)$$

where  $g_{ik}$  and  $h_{ij}$  are the stoichiometric coefficients of element  $i$  in mineral  $k$  and aqueous species  $j$ ,  $m_k$  and  $c_j$  are the mineral and aqueous-species concentrations, respectively. Superscripts  $D$  and  $U$  indicate downstream and upstream concentrations, respectively.

#### 8.5.2.2 Determination of the initial $\text{MnO}_{2,s}$ and carbonate mineral concentrations

Although inverse modeling can be used to determine the mass-transfer amounts ( $\Delta M$ ) for various heterogeneous reactions, inverse modeling cannot usually reveal the initial amounts ( $M_{\text{ini}}$ ) of minerals present in an aquifer. Estimates of average initial mineral contents must be made on the basis of: batch or column experiments on unaffected aquifer materials, selective mineral extraction analyses, X-ray evidence, or observation of retardation of reactive fronts in the field.

By determining the net mineral mass transfer ( $\Delta M$ ) experienced by a packet of water between two points along a flowpath, an inverse model may be used to set a lower bound on the initial concentration of that mineral ( $M_{\text{ini}} \geq \Delta M$ ), but only if the mineral mass transfer occurs in a unique and localized part of the flowpath, such as a single reaction front. Indeed, although expressed in  $\text{mol kg}^{-1}$  of  $\text{H}_2\text{O}$ , the mineral mass transfer determined by an inverse model integrates reactions occurring in the volume of aquifer traversed by a packet of water. In the case of a slow mass-transfer reaction (relative to the movement of the water), the value of  $\Delta M$  determined by an inverse model will change with increasing flowpath length until some equilibrium or steady state is reached. The initial mineral concentration,  $M_{\text{ini}}$ , in equation (8.4) is also expressed in terms of  $\text{mol kg}^{-1} \text{H}_2\text{O}$ , but refers to a static mass of water and therefore a localized aquifer volume. In contrast, the value of  $\Delta M$  determined by inverse modeling has a Lagrangian frame of reference and its units refer to a dynamic mass of  $\text{H}_2\text{O}$  that has travelled along a specific flowpath length. In the case where the entire mass transfer occurs at a sharp reaction front, the difference in units may be moot, at least if the mineral concentration  $M_{\text{ini}}$  was initially uniform between the initial and final end points of the

flowpath. In any case, equations (8.4) and (8.5) will be of limited use for a slow reaction, one that does not result in the development of a sharp reaction front.<sup>5</sup>

Glynn and Brown (1996) used a value of  $2 \times 10^{-2}$  mol MnO<sub>2</sub> per kg H<sub>2</sub>O in their PHREEQC and PHREEQM transport simulations, primarily to stay consistent with the simulations conducted by Glynn *et al.* (1991). A higher value may be more appropriate. Indeed, on the basis of his column elution experiments, Stollenwerk (1994) suggested a value of 7.1 millimoles of MnO<sub>2</sub> per kg of sediment. Depending on values of porosity and bulk density assumed, this solid concentration is equivalent to a value between  $3.2 \times 10^{-2}$  (our estimate) and  $4.49 \times 10^{-2}$  mol kg<sup>-1</sup> of H<sub>2</sub>O (estimate based on Brown, 1996). Based on the selective extraction results of Ficklin *et al.* (1991), Brown (1996) used a value of  $7.9 \times 10^{-2}$  mol kg<sup>-1</sup> H<sub>2</sub>O in his 1-D simulation. The maximum and minimum amounts of MnO<sub>2</sub>, dissolved between wells 402 and 503 in inverse modeling simulations were  $9.2 \times 10^{-3}$  (Table 6 in Glynn and Brown, 1996) and  $3.9 \times 10^{-3}$  mol kg<sup>-1</sup> H<sub>2</sub>O (Table 8.5), respectively. These values may be considered lower bounds for the initial amount of MnO<sub>2</sub> present in the aquifer, if it is assumed that the reductive dissolution of MnO<sub>2</sub> is fast relative to the movement of the water; this assumption is used in all the PHREEQM and PHREEQC forward simulations presented in this paper. The lack of accurate groundwater flow and transport models, the large distances between the well sites, and the suggestion that the reductive dissolution of MnO<sub>2</sub> may be slow compared to the groundwater velocities make it difficult to calculate accurately the Fe(II) retardation factor, and therefore the appropriate initial MnO<sub>2</sub> content. In any case, the results of our simulations, and in particular the MnO<sub>2</sub> dissolution front retardation factors that we determine, can easily be extrapolated to other initial MnO<sub>2</sub> concentrations.

Determining appropriate initial carbonate (calcite and dolomite) concentrations for the reactive-transport simulations was also a problem. Brown (1996) used a concentration of 0.18 mol kg<sup>-1</sup> H<sub>2</sub>O in his simulation, a value consistent with the carbonate content determined by Eychaner and Stollenwerk (1985) for a sample of alluvium collected in 1985. Brown (1996) noted that the buffering capacity measurements conducted by Hydro Geo Chem, Inc. (1989) on alluvial samples collected from three different locations in the Pinal Creek basin could be translated into equivalent carbonate concentrations of 0.12 mol L<sup>-1</sup> for sand and gravel and 0.76 mol L<sup>-1</sup> for calcareous clay. These measurements, however, did not correct for possible proton adsorption and silicate dissolution reactions. Based on a description of the Pinal Creek site by Eychaner (1989, and pers. comm.), Glynn *et al.* (1991) used an initial carbonate concentration of 0.084 mol kg<sup>-1</sup> H<sub>2</sub>O (0.042 mol kg<sup>-1</sup> H<sub>2</sub>O calcite and 0.021 mol kg<sup>-1</sup> H<sub>2</sub>O dolomite). The resulting *pH* front retardation factor of 5, for the acidic well 51 water used in the simulation, approximately matched the relative rate of advance of the low-*pH* waters at the Pinal Creek site over the last 50 years. The inverse modeling results discussed in the present paper generally show a net dissolution between wells 402 and 503 of  $1.5 \times 10^{-3}$  to  $4.6 \times 10^{-3}$  mol kg<sup>-1</sup> H<sub>2</sub>O of primary carbonate minerals (Table 8.5). If the questionable assumption is made that the carbonate mineral dissolution rates are relatively fast, resulting in localized dissolution, a value of  $5 \times 10^{-3}$  mol kg<sup>-1</sup> H<sub>2</sub>O may be considered a reasonable lower bound on the initial carbonate concentration representative for the Pinal Creek alluvial sediments. In any case, because the initial carbonate mineral concentration chosen for the simulations was the most important adjustable parameter determining movement of the low-*pH* waters in our simulations (and is also the most important factor in the chemical evolution of Pinal Creek groundwaters), a set of 8 different initial carbonate concentrations ranging from  $5.25 \times 10^{-3}$  to  $3.32 \times 10^{-1}$  mol kg<sup>-1</sup> H<sub>2</sub>O were used to test each reaction-model modification.

<sup>5</sup>Lichtner (1988) and Ortoleva *et al.* (1986) have shown that reaction kinetics will not affect the rate of front propagation given enough time and distance. The front may not be as sharp but it will still propagate at the same rate as a front resulting from a simulation that uses the Local Equilibrium Assumption.

### 8.5.2.3 Setup of the 1-D reactive-transport simulations

Unless specified otherwise, most of our simulations were conducted with the local equilibrium advective transport code PHREEQC. Dispersion was not usually simulated. The reactive-transport simulations investigated the effect of the following model variations on the retardation of the low- $pH$  and high Fe(II) fronts:

1. Changing solid-carbonate concentrations. The initial concentrations chosen were:  $5.25 \times 10^{-3}$ ,  $1.05 \times 10^{-2}$ ,  $2.1 \times 10^{-2}$ ,  $3.05 \times 10^{-2}$ ,  $4.2 \times 10^{-2}$ ,  $8.4 \times 10^{-2}$ ,  $1.68 \times 10^{-1}$ , and  $3.32 \times 10^{-1}$  mol kg<sup>-1</sup> H<sub>2</sub>O.
2. Using a longitudinal dispersivity of 560 m, or no dispersivity. The dispersivity of 560 m represented 10% of the total simulation length, a rule of thumb often applied in groundwater transport modeling. Most simulations, however, used a dispersivity of 0 m, primarily to limit execution times. The PHREEQM and PHREEQC v. 2 (1996 beta version) geochemical transport codes were used for all simulations with a dispersivity of 560 m.
3. Including or excluding dolomite. Most simulations did not include dolomite.
4. Including or excluding rhodochrosite precipitation.
5. Including or excluding Al(OH)<sub>3</sub>, kaolinite, or AlOHSO<sub>4</sub> precipitation. Two different solubility products were used for AlOHSO<sub>4</sub> ( $10^{-3.2}$  and  $10^{-2.2}$ ). The higher solubility product is the value adopted by Stollenwerk (1994) in fitting the results of laboratory column experiments that reacted Pinal Creek acidic groundwater with Pinal Creek sediments.
6. Including or excluding equilibrium with an infinite reservoir of CO<sub>2</sub> at partial pressures of either  $10^{-0.9865}$ , a value based on unsaturated zone CO<sub>2</sub> gas measurements at the Pinal Creek site (Glynn and Busenberg, 1994b), or  $10^{-1.33}$ , the value used in Brown (1996). This latter value was based on the dissolved CO<sub>2</sub> concentration at well 503 (November 1991) reported by Glynn and Busenberg (1994a).
7. Including or excluding cation exchange. Two different cation exchange capacities, 1 meq/100 g and 10 meq/100 g, were tested.
8. Including or excluding diffuse double-layer surface-complexation sorption, which was based on thermodynamic data compiled in Dzombak and Morel (1990) for sorption onto hydrous ferric oxide.
9. Including or excluding the irreversible dissolution of Ca and Mg silicates to match the amounts calculated by two of our inverse modeling simulations (PHREEQC Models 2 and 7 in Table 8.5). These simulations assumed a zero-order kinetic dissolution process for the silicate minerals with an inexhaustible supply of silicate minerals. Two of the simulations were also conducted assuming a zero-order kinetic dissolution process for MnO<sub>2</sub>. In all cases, the zero-order kinetic dissolution processes were specified so that the acidic water would receive, during the course of its evolution through the transport column, exactly the silicate mineral mass transfers (and the MnO<sub>2</sub> mass-transfer when applicable) determined by inverse Models 2 and 7 in Table 8.5. The dissolution/precipitation of all other minerals was allowed to proceed to thermodynamic equilibrium at each time step and in each cell.

More than 160 reactive-transport simulations were conducted. All simulations used the water from well 402 (89/1/12) as the infilling solution. The water from well 504 (91/11/22) was used as the background water initially present in the 1-dimensional column. The 5.6 km-long column was subdivided into 10 cells of equal length and with initially homogenous mineral, surface, and aqueous concentrations. (Because mineral concentrations in PHREEQC and PHREEQM are expressed in terms of mol kg<sup>-1</sup> H<sub>2</sub>O, the porosity and bulk density of the sediments are not defined for the programs). A time step of 112 days was used, thereby simulating an average linear groundwater velocity of 5 m day<sup>-1</sup> (representative of the average groundwater velocity between wells 402 and 503). Up to a maximum of 5000 time steps (1534 years) were simulated.

Numerical dispersion affected the transport of non-conservative constituents in the simulations, and depended on the cell-length discretization,  $\Delta x$ , and on the extent of

retardation,  $R$ . The corresponding numerical dispersivity,  $\alpha_{num}$  can be calculated as follows (Herzer and Kinzelbach, 1989):

$$\alpha_{num} = \left( \frac{\Delta x}{2} - \frac{v\Delta t}{2R} \right) \quad (8.6)$$

or, in the case of our simulations with uniform time and space discretization:

$$\alpha_{num} = \frac{\Delta x}{2} \left( 1 - \frac{1}{R} \right) \quad (8.7)$$

The maximum numerical dispersivity is half the cell length or 280 m. Retardation factors of 1, 2, 5 and 10 result in numerical dispersivities of 0, 140, 224 and 252 m, respectively. Ideally, the simulations would have been run with a greater number of cells (and consequently a greater number of time steps and a smaller cell length). Execution times and the number of simulation runs, however, made this impractical. In any case, the effects of numerical dispersion on calculated front retardation factors was small (less than 5%), and decreased as the retardation (and the number of pore volumes needed to observe that retardation) increased: the uncertainty in the exact position of a sharp front within the last cell of a column matters less and less in calculating the retardation factor for a moving front as the number of pore volumes needed to observe the passing of the front increases. The effects of numerical dispersion were also tested in the simulations that assigned a longitudinal dispersivity of 560 m to simulate hydrodynamic dispersion. Hydrodynamic dispersion affects the transport of all constituents, conservative or non-conservative (and therefore retarded). Numerical dispersion has similar characteristics to hydrodynamic dispersion but, in the case of the 1D PHREEQC and PHREEQM transport simulations, it only affects the transport of non-conservative constituents. The results of these simulations are discussed later in this chapter, but support our conclusions regarding the minor effects of numerical dispersion in the Pinal Creek analysis.

Amorphous  $\text{Fe}(\text{OH})_3$ , and one aluminum phase (amorphous  $\text{Al}(\text{OH})_3$ , kaolinite, or  $\text{AlOHSO}_4$ ) were allowed to precipitate in all the simulations. Gypsum was allowed to precipitate in all the simulations except when irreversible zero-order kinetic dissolution of Ca and Mg-silicate minerals was included (following Models 2 and 7 in Table 8.5). Rhodochrosite was allowed to precipitate in all sets of simulations, except one. An essentially infinite amount of chalcedony was present in all cells. An initial concentration of  $2 \times 10^{-2} \text{ mol kg}^{-1} \text{ H}_2\text{O}$  of  $\text{MnO}_2$  was specified in all the simulations (except for the simulations that allowed irreversible dissolution of Ca and Mg silicates). Differing initial concentrations of carbonate minerals (calcite and/or dolomite) were specified in all simulations, but dolomite was included together with calcite in only a few of those simulations. Dolomite, however, was the only carbonate mineral present in simulations that attempted to emulate Model 7 in Table 8.5.

A subset of the simulations presented here are referred to as the “Basic Reaction Model” (BRM). The BRM allows one of four possible Al-bearing phases to precipitate, along with secondary gypsum and amorphous  $\text{Fe}(\text{OH})_3$  precipitation. The BRM specifies an essentially infinite amount of chalcedony, an initial  $\text{MnO}_2$  concentration of  $2 \times 10^{-2} \text{ mol kg}^{-1} \text{ H}_2\text{O}$ , and one of eight fixed initial concentrations of carbonate minerals. Additionally the BRM assumes local equilibrium, no sorption or cation exchange reactions, no  $\text{CO}_2$  gas exchange, and zero longitudinal dispersivity.

Graphical presentation of the complete suite of results is limited to a few representative  $pH$ -breakthrough curves shown in Figures 8.4 and 8.5 for the midpoint of the last cell (cell 10). The “fronts” shown in Figures 8.4 and 8.5 are generally sharp and correspond to spatial transitions between the absence and presence of given minerals. The essential findings of the study are summarized in the sections below.

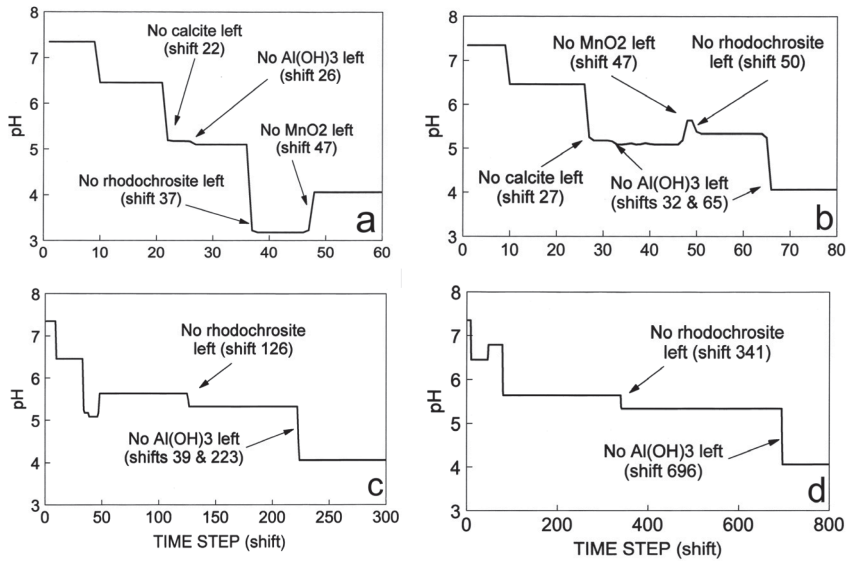


Figure 8.4. *pH* breakthrough curves for four PHREEQC advection-reaction simulations that use the “Basic Reaction Model” (BRM) with amorphous  $\text{Al}(\text{OH})_3$  as the Al-bearing phase allowed to precipitate. No dolomite was included. Initial calcite concentrations for each of the simulations shown are: a)  $2.1 \times 10^{-2} \text{ mol kg}^{-1} \text{ H}_2\text{O}$ , b)  $3.0 \times 10^{-2} \text{ mol kg}^{-1} \text{ H}_2\text{O}$ , c)  $4.2 \times 10^{-2} \text{ mol kg}^{-1} \text{ H}_2\text{O}$ , d)  $8.4 \times 10^{-2} \text{ mol kg}^{-1} \text{ H}_2\text{O}$ .

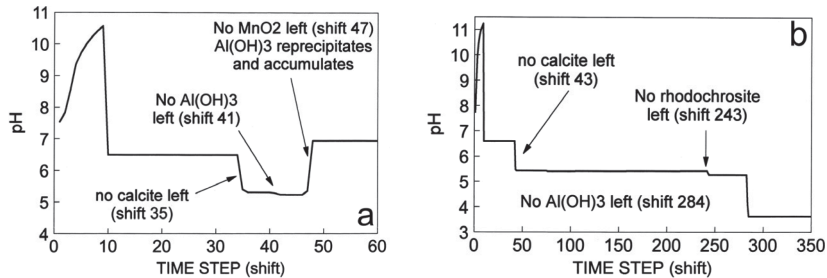


Figure 8.5. *pH* breakthrough curves for two PHREEQC advection-reaction simulations including tremolite and excluding gypsum as determined by inverse Model 2 in Table 8.5. The irreversible dissolution of tremolite ( $5.00 \times 10^{-5}$  moles per cell per time step) was simulated as a continuous zero-order reaction process matching over the length of the simulation column the amount of tremolite mass-transfer specified in inverse Model 2. The two simulations shown differed in their consideration of  $\text{MnO}_2$ : (a) an initial concentration of  $\text{MnO}_2$  of  $2 \times 10^{-2} \text{ mol kg}^{-1} \text{ H}_2\text{O}$  was specified and allowed to react to equilibrium at each time step; (b)  $\text{MnO}_2$  was added as a continuous irreversible dissolution process at the rate of  $3.903 \times 10^{-4}$  moles per cell per time step, so as to match over the length of the simulation column the amount of  $\text{MnO}_2$  mass transfer specified in inverse Model 2.

#### 8.5.2.4 Simulation results: movement of the $\text{Fe}(\text{II})$ -rich waters and of the $\text{MnO}_2$ dissolution front

As can be seen from Figures 8.4 and 8.5, the presence, extent, and movement of *pH* fronts in the simulations conducted is dependent on a number of reaction processes, including redox processes and the presence or complete dissolution of primary  $\text{MnO}_2$  and secondary rhodochrosite. The movement of the redox front is significantly easier to understand. Indeed, the

movement of the low-*pe* Fe(II)-rich groundwater zone was primarily dependent on the initial amount of MnO<sub>2</sub> specified for each simulation and was usually little affected by any other factors. A retardation factor (*R*) of 4.74 was determined for the BRM simulations containing  $2 \times 10^{-2}$  mol MnO<sub>2</sub> per kg of H<sub>2</sub>O. As mentioned earlier, the movement of the MnO<sub>2</sub> dissolution front, and of the attendant Fe(II) and low-*pe* fronts, can easily be calculated using equation (8.4). Indeed, given the Fe(II) concentration of the infilling solution (591 mg L<sup>-1</sup>, Table 8.1 or 10.58 millimolar) and the stoichiometry (2 moles of Fe(II) to reduce 1 mole of MnO<sub>2</sub>),  $\Delta M$  is  $5.29 \times 10^{-3}$  mol L<sup>-1</sup> and *R* is 4.78. The slight difference between this calculated value of *R* and the value of 4.74 determined from the PHREEQM simulations results from the use of molar concentration units for  $\Delta M$  in our calculation instead of the molal units used in PHREEQM. Apart from the initial concentration of MnO<sub>2</sub> specified, the retardation of the MnO<sub>2</sub> dissolution front is only affected by processes that affect the concentration of the reductant [dissolved Fe(II)] in the infilling water: namely, dispersion and cation exchange in our simulations. Indeed, the simulations that included dispersion showed a slight decrease in the retardation factor of the MnO<sub>2</sub> dissolution front (an *R* value of 4.6 for an MnO<sub>2</sub> concentration of  $2 \times 10^{-2}$ ); the simulations that included cation exchange, however, resulted in substantially greater MnO<sub>2</sub> retardation factors: 5.2 for the simulations with a cation-exchange capacity (*CEC*) of 1 meq/100 g and 9.2 for the simulations with *CEC* of 10 meq/100 g. (The lower *CEC* is more realistic for the Pinal Creek alluvial sediments). The increase in retardation factor is due to cation-exchange reactions that decrease the dissolved Fe(II) concentrations by, for example, Fe/Ca exchange:



Because Fe(II) surface complexation on hydrous ferric oxide was not simulated, the simulations that included surface-complexation sorption reactions did not result in increased retardation factors for the MnO<sub>2</sub> dissolution front.

#### 8.5.2.5 *Simulation results: evolution of the low-pH waters*

Unlike the movement of the low-*pe* Fe(II)-rich front, the movement of the low-*pH* groundwaters is much more difficult to predict and it is not controlled by a unique mineral dissolution/precipitation reaction. Indeed, the PHREEQM and PHREEQC simulation results show the development of several step changes in *pH* that are controlled by mineral dissolution and precipitation fronts. The consumption of the initial calcite (and dolomite, if present) in the column is typically followed by the complete dissolution of secondary rhodochrosite and, usually much later (if at all) by the dissolution of the secondary Al-bearing phase included in the simulation (Al(OH)<sub>3</sub>, AlOHSO<sub>4</sub> or kaolinite). The complete dissolution of these minerals and the loss of their proton-consuming capacity leads to abrupt *pH* decreases. In contrast, the disappearance of MnO<sub>2</sub> and the cessation of Fe(II) oxidation and Fe(OH)<sub>3</sub> precipitation results in a sharp *pH* increase.

The *pH* breakthrough curves shown in Figure 8.4 for the last cell in the column are typical of the *pH* breakthrough curves for simulations without silicate dissolution: *pH* remains high at 7.34, until the first pore volume (at shift 10) flushes through the column, and neutralized infilling water with a *pH* of about 6.5 reaches the last cell. If MnO<sub>2</sub> is the first mineral consumed and Al(OH)<sub>3</sub> is allowed to precipitate, the *pH* will increase from 6.5 to 6.8 as the MnO<sub>2</sub> is completely consumed. Later, the complete consumption of calcite will result in a *pH* decrease from about 6.8 to about 5.6, and the ensuing consumption of rhodochrosite will result in another *pH* drop to near 5.3. Finally, the disappearance of the secondary aluminum phase will result in yet another *pH* drop to about 4.06 (given a sufficiently long simulation time), which is close to the initial infilling water *pH* of 4.13. Although the final *pH* values in simulations with silicate mineral dissolution differ somewhat from the *pH* values mentioned above, the general pattern of *pH* evolution in those simulations is also strongly dependent on the disappearance of calcite (or calcite and dolomite), MnO<sub>2</sub>, secondary rhodochrosite, and the secondary aluminum phase (Fig. 8.5).

Table 8.6. *pH* values computed with the PHREEQC geochemical code (version 1; Parkhurst, 1995) by equilibrating well 402 water with various mineral phases, including chalcedony, gypsum and amorphous  $\text{Fe}(\text{OH})_3$ , and one of four possible Al bearing phases (cf. table note). The last *pH* column indicates the *pH* value in the absence of any aluminum phase.

Presence of additional minerals?			Computed equilibrium <i>pH</i> as a function of the presence of an Al phase				
$\text{MnO}_2$	Calcite	Rhodochrosite	1	2	3	4	no Al phase
Yes	Yes	Yes	6.453	6.442	6.462	6.467	
Yes	No	Yes	5.174	5.071	5.095	5.090	
Yes	No	No	<b>5.011</b>	<b>3.810</b>	<b>3.364</b>	<b>3.186</b>	<b>3.175</b>
No	Yes	Yes	6.788	6.772	6.748	6.818	
No	No	Yes	5.633	5.576	5.666	5.659	
No	No	No	5.330	4.190	4.554	3.946	4.056

Note: The identity of the Al bearing phase is indexed as follows: (1)  $\text{Al}(\text{OH})_3$ , (2) kaolinite, (3)  $\text{AlOHSO}_4$  with  $\log K_{sp} = -2.2$ , (4)  $\text{AlOHSO}_4$  with  $\log K_{sp} = -3.23$ .

Many of the *pH* values that are plateaus in Figures 8.4 and 8.5 can be simulated by equilibrating the infilling solution (well 402 water) with various assemblages of coexisting mineral phases found during the transport simulations. *pH* values resulting from PHREEQC equilibrations of well 402 water with several mineral assemblages are given in Table 8.6. The resulting *pH* values usually closely agree with the *pH* values obtained during the transport simulations (and are even within half a *pH* unit of the values reached in the simulations that incorporated  $\text{CO}_2$  exsolution and surface-complexation). The PHREEQC equilibration results clearly indicate that, although the loss of calcite results in a *pH* decrease to the range of 5.1 to 5.7, the subsequent loss of rhodochrosite results in a further *pH* decrease to values well below 5 if  $\text{Al}(\text{OH})_3$  is not present. Table 8.6 indicates that the lowest *pH* value reached during a simulation, after the complete dissolution of rhodochrosite, depends on the aluminum phase included in the simulation. Invariably, simulations that allowed amorphous  $\text{Al}(\text{OH})_3$  precipitation resulted in higher *pH* values than those simulations that allowed kaolinite, or especially,  $\text{AlOHSO}_4$  precipitation. In the presence of rhodochrosite (and possibly calcite), however, the choice of aluminum phase allowed to precipitate had little effect on the resulting *pH* values. Finally, Table 8.6 confirms the finding that the lowest *pH* values (near 3.1) were invariably attained when  $\text{MnO}_2$  was still present but all other carbonate and Al-phases were absent.

#### 8.5.2.6 The effect of the initial carbonate to initial $\text{MnO}_2$ ratio on the evolution of the low-*pH* waters

The initial carbonate mineral concentration specified in each simulation was the most important control on the movement of the calcite, rhodochrosite, and Al-phase dissolution fronts, and of the associated *pH* fronts (Tables 8.7, 8.8 and 8.9). The initial carbonate to  $\text{MnO}_2$  ratio (*CMR*) was the second most important factor affecting the retardation of dissolution fronts for rhodochrosite and the Al-bearing phase (the rhodochrosite dissolution front is important because of the decrease in *pH* associated with the front, particularly in the absence of an  $\text{Al}(\text{OH})_3$  phase). The set of simulations that allowed irreversible dissolution of Ca- and Mg-silicate minerals gave very different results from the set of simulations that did not allow Ca- and Mg-silicate dissolution. Unless mentioned otherwise, the following discussions apply only to the set of simulations that did not allow silicate mineral dissolution, although many of our conclusions will also be relevant to the simulations with Ca- and Mg-silicate dissolution.

The *CMR* ratio specified in a given simulation determines the timing of the complete dissolution of  $\text{MnO}_2$  in relation to the complete dissolution of the carbonate phases. The lowest *pH* values in the transport simulations usually occurred when  $\text{MnO}_2$  remained in a

Table 8.7. Rhodochrosite dissolution-front retardation factors for different reaction models and initial carbonate concentrations (in mol kg<sup>-1</sup> H<sub>2</sub>O). All models except one used a dispersivity of 0 meters. All models allowed precipitation of rhodochrosite and of one of four Al-bearing phases. The specified reaction models have an index that refers to the allowed Al-bearing phase. These indices and the meanings of the various reaction models are discussed in the table notes and in the text.

Reaction model	Initial carbonate mineral concentrations ( $\times 10^{-2}$ )							
	0.525	1.05	2.1	3.0	4.2	8.4	16.8	33.2
Basic Reaction Model, (1)	1.6	2.3	3.7	5.0	12.6	34.1	65.6	128.9
Dispersivity, (1), PHREEQM	1.5	2.3	3.7	4.5	12.7	35.1	67.7	133.0
Dispersivity, (1), PHREEQC	1.5	2.2	3.6	4.5	12.5			
Low CEC, (1)	1.6	2.3	3.8	5.1	11.8	33.7	65.4	128.6
High CEC, (1)	0.0	3.5	5.1	6.5	8.8	31.3	63.0	126.3
CO <sub>2</sub> , log $p_{\text{CO}_2} = -0.9865$ , (1)	1.4	2.1	3.5	5.0	12.2	32.5	56.5	104.5
CO <sub>2</sub> , log $p_{\text{CO}_2} = -1.33$ , (1)	1.5	2.2	3.7	5.9	15.2	37.5	68.8	131.4
Basic Reaction Model, (3)	1.6	2.3	3.6	4.9	14.7	42.3	81.4	159.4
Basic Reaction Model, (4)	1.6	2.3	3.6	4.8	14.5	41.3	80.9	160.2
Low CEC, (3)	1.6	2.3	3.7	5.0	13.6	41.8	80.9	158.9
High CEC, (3)	0.0	3.5	5.0	6.4	8.6	38.0	77.2	155.4
Surf. Comp., (3), no Cu, Zn, Co, Ni		3.4	4.7	12.3	22.5	47.4	86.8	165.4
Surf. Comp., (3), with Cu, Zn, Co, Ni	2.7	3.4	4.6	7.8	19.8	46.4	79.5	140.8
Tremolite, Model 2, (1)	RA	RA	RA	RA	RA	RA	RA	RA
Tremolite, MnO <sub>2</sub> , Model 2, (1)	7.3	10.9	18.2	24.3	32.6	61.6	119.4	235.3
Biotite/K-mont/An, Model 7, (1)	RA	RA	RA	RA	RA	RA	RA	RA
Biotite/K-mont/An, MnO <sub>2</sub> , Model 7, (1)	12.1	17.9	29.8	40.1	53.6	101.7	197.5	388.9
Biotite/K-mont/An, Model 7, (3)	RA	RA	RA	RA	RA	RA	RA	RA

Note: The identity of the Al bearing phase is indexed as follows: (1) Al(OH)<sub>3</sub>, (2) kaolinite, (3) AlOHSO<sub>4</sub> with log  $K_{sp} = -2.2$ , (4) AlOHSO<sub>4</sub> with log  $K_{sp} = -3.23$ .

Reaction model abbreviations and meanings:

RA:	rhodochrosite accumulates.
Dispersivity:	basic reaction model with dispersivity of 560 m;
CO <sub>2</sub> :	column open to a specified fixed $p_{\text{CO}_2}$ ;
Low CEC:	low cation exchange capacity (1 meq/100 g);
High CEC:	high cation exchange capacity (10 meq/100 g);
Surf. Comp.:	surface complexation model;
Tremolite, Model 2:	irreversible tremolite dissolution (Model 2 in Table 8.5);
Tremolite, MnO <sub>2</sub> , Model 2:	as above but with zero-order MnO <sub>2</sub> dissolution;
Biotite/K-mont/An, Model 7:	irreversible biotite and anorthite dissolution and K-montmorillonite precipitation (Model 7 in Table 8.5);
Biotite/K-mont/An, MnO <sub>2</sub> , Model 7:	same as above but with zero-order MnO <sub>2</sub> dissolution.

cell, but all the initial and secondary carbonate (rhodochrosite) phases had completely dissolved. (If additionally the Al-bearing phase had been completely dissolved, the  $pH$  was even lower). This transient remnant of MnO<sub>2</sub> (third row in Table 8.6) occurred in all simulations with a  $CMR$  ratio less than 1.5 ( $5.25 \times 10^{-3}$ ,  $1.05 \times 10^{-2}$  and  $2.1 \times 10^{-2}$  initial carbonate concentrations and  $2 \times 10^{-2}$  initial MnO<sub>2</sub> concentration). Simulations with  $CMR$  less than 1.5 resulted in lower  $pH$  values and more rapid dissolution of carbonates, and therefore, in relatively lower retardation factors for the rhodochrosite and Al-phase dissolution fronts (Tables 8.8 and 8.9; Fig. 8.4a).

In simulations with  $CMR$  ratios near 1.5, the complete dissolution of MnO<sub>2</sub> and rhodochrosite occurred nearly simultaneously, but was preceded by the complete dissolution of calcite (Fig. 8.4b). For most of these simulations, the rhodochrosite dissolution front had a retardation factor ( $R$ ) close to 4.7, the same as the MnO<sub>2</sub> front. Disregarding the Ca and Mg

Table 8.8. Calcite dissolution-front retardation factors. See Table 8.7 caption and notes for explanation of headings and abbreviations. One additional set of simulations reported here used a *CEC* of 1 meq/100 g but no rhodochrosite was allowed to precipitate (low *CEC*, no rhodo).

Reaction model	Initial carbonate mineral concentrations ( $\times 10^{-2}$ )							
	0.525	1.05	2.1	3.0	4.2	8.4	16.8	33.2
Basic reaction model, (1)	1.2	1.5	2.2	2.7	3.4	8.0	22.7	52.0
Dispersivity, (1), PHREEQM	1.0	1.3	2.0	2.5	3.3	8.0	23.0	53.0
Dispersivity, (1), PHREEQC	1.0	1.3	2.0	2.5	3.3			
Low <i>CEC</i> , (1)	1.5	1.9	2.5	3.1	3.8	8.2	22.9	52.3
High <i>CEC</i> , (1)	2.5	3.5	4.9	5.9	6.9	10.7	25.4	54.8
CO <sub>2</sub> , log $p_{\text{CO}_2} = -0.9865$ , (1)	1.1	1.4	2.1	2.6	3.3	7.3	18.4	40.8
CO <sub>2</sub> , log $p_{\text{CO}_2} = -1.33$ , (1)	1.2	1.5	2.2	2.8	3.6	8.8	23.0	51.2
Low <i>CEC</i> , no rhodo., (1)	1.5	2.1	3.0	3.9	5.0	13.8	32.4	69.5
Basic reaction model, (3)	1.2	1.6	2.2	2.7	3.4	8.7	24.7	56.7
Basic reaction model, (4)	1.3	1.6	2.2	2.7	3.5	8.9	25.6	59.1
Low <i>CEC</i> , (3)	1.5	1.9	2.6	3.1	3.8	8.9	25.0	57.0
High <i>CEC</i> , (3)	2.5	3.5	4.9	5.9	7.0	11.4	27.4	59.5
Surf. Comp., (3), no Cu, Zn, Co, Ni		2.1	2.7	3.2	3.9	10.2	26.3	58.4
Surf. Comp., (3), with Cu, Zn, Co, Ni	1.7	2.0	2.6	3.1	3.8	8.9	22.2	48.2
Tremolite, Mod. 2, (1)	1.5	1.9	2.8	3.5	4.5	113.7	353.5	>500
Tremolite, MnO <sub>2</sub> , Model 2, (1)	1.6	2.2	3.3	4.3	5.5	10.0	18.9	36.8
Biotite/K-mont/An, Model 7, (1)	DA	DA	DA	DA	DA	DA	DA	DA
Biotite/K-mont/An, MnO <sub>2</sub> , Model 7, (1)	1.6*	2.2*	3.2*	4.2*	5.4*	9.7*	18.4*	35.7*
Biotite/K-mont/An, Model 7, (3)	DA	DA	DA	DA	DA	DA	DA	DA

\*All simulations referring to Model 7 in Table 8.5 have initial dolomite instead of calcite. DA: no calcite specified and dolomite accumulates.

silicate dissolution simulations, the highest rhodochrosite *R* values were obtained for simulations that specified a high ion-exchange capacity (*CEC*), a surface-complexation model, or equilibrium with a low fixed  $p_{\text{CO}_2}$  ( $10^{-1.33}$ ). In the high *CEC* simulations, however, the retardation factor of the rhodochrosite front was lower than that of the MnO<sub>2</sub> dissolution front ( $R = 9.2$ ), i.e., the rhodochrosite dissolution front preceded the MnO<sub>2</sub> dissolution front.

Finally, in the simulations with a *CMR* ratio greater than 1.5 ( $4.2 \times 10^{-2}$ ,  $8.4 \times 10^{-2}$ ,  $1.68 \times 10^{-1}$  and  $3.32 \times 10^{-1}$  initial carbonate concentrations and  $2 \times 10^{-2}$  initial MnO<sub>2</sub> concentration), complete dissolution of MnO<sub>2</sub> generally occurred before the complete dissolution of secondary rhodochrosite (with the exception of the two high *CEC* simulations). In simulations with an initial carbonate concentration of  $8.4 \times 10^{-2}$  or greater, exhaustion of the initial MnO<sub>2</sub> also occurred before the complete dissolution of the primary calcite (and/or dolomite). The faster movement of the MnO<sub>2</sub> dissolution front relative to the carbonate mineral dissolution fronts resulted in higher *pH* waters contacting the carbonate minerals and Al-phase minerals, and therefore in slower dissolution and higher retardation factors.

#### 8.5.2.7 Influence of the aluminum mineral allowed to precipitate on the evolution of the low-*pH* waters

The choice of Al-bearing phase allowed to precipitate was the third major factor controlling the relative retardation of the rhodochrosite and Al-phase dissolution fronts in the simulations without Ca and Mg silicate dissolution. The simulations that allowed AlOH<sub>2</sub>SO<sub>4</sub> to precipitate, instead of amorphous Al(OH)<sub>3</sub>, exhibited greater *R* values for the rhodochrosite and Al-phase dissolution fronts. Remarkably, the simulations that used the more stable AlOH<sub>2</sub>SO<sub>4</sub> (solubility product  $10^{-3.23}$ ) compared to simulations that used the less stable AlOH<sub>2</sub>SO<sub>4</sub> phase

Table 8.9. Retardation factors for the final aluminum phase dissolution-front. See Table 8.7 caption and notes for explanation of headings and abbreviations. One additional set of simulations reported here used a *CEC* of 1 meq/100 g but no rhodochrosite was allowed to precipitate (low *CEC*, no rhodo.). In some cases, the aluminum phase was not exhausted during the 5000 time steps allowed for a simulation.

Reaction model	Initial carbonate mineral concentrations ( $\times 10^{-2}$ )							
	0.525	1.05	2.1	3.0	4.2	8.4	16.8	33.2
Basic reaction model, (1)	1.4	1.8	2.6	6.5	22.3	69.6	143.3	290.8
Dispersivity, (1), PHREEQM	1.3	1.8	2.7	8.4	25.3	78.9	162.7	330.3
Dispersivity, (1), PHREEQC	1.2	1.7	2.7	7.6	23.3			
Low <i>CEC</i> , (1)	1.7	2.2	3.2	3.9	20.6	68.8	142.6	290.1
High <i>CEC</i> , (1)	2.7	3.7	5.3	6.9	9.1	62.6	136.8	284.5
CO <sub>2</sub> , log <i>p</i> <sub>CO<sub>2</sub></sub> = -0.9865, (1)	1.3	1.9	3.2	5.3	20.8	61.9	113.6	217.3
CO <sub>2</sub> , log <i>p</i> <sub>CO<sub>2</sub></sub> = -1.33, (1)	1.5	2.3	3.9	13.9	39.6	106.4	203.9	399.0
Low <i>CEC</i> , no rhodo., (1)	1.6	2.2	3.3	4.2	8.6	37.7	91.4	198.6
Basic reaction model, (3)	0.0	2.3	3.6	7.9	30.3	89.1	171.3	335.5
Basic reaction model, (4)	1.8	2.7	4.5	>500	>500	>500	>500	>500
Low <i>CEC</i> , (3)	1.6	2.3	3.7	5.0	27.5	87.6	169.9	334.1
High <i>CEC</i> , (3)	0.0	0.0	0.0	6.4	8.8	76.0	158.5	323.3
Surf. Comp., (3), no Cu, Zn, Co, Ni		3.5	7.4	24.7	45.9	96.8	176.6	335.8
Surf. Comp., (3), with Cu, Zn, Co, Ni	2.9	3.5	8.8	31.6	48.1	102.8	172.3	300.8
Tremolite, Model 2, (1)	AA	AA	AA	AA	AA	AA	AA	AA
Tremolite, MnO <sub>2</sub> , Model 2, (1)	8.2	12.5	21.1	28.4	38.2	72.6	141.1	278.4
Biotite/K-mont/An, Model 7, (1)	AA	AA	AA	AA	AA	AA	AA	AA
Biotite/K-mont/An, MnO <sub>2</sub> , Model 7, (1)	AA	AA	AA	AA	AA	AA	AA	AA
Biotite/K-mont/An, Model 7, (3)	9.2	8.0	6.9	6.5	5.0	5.8	6.6	7.3

\*All simulations referring to Model 7 in Table 8.5 have initial dolomite instead of calcite. AA: Al(OH)<sub>3</sub> accumulates!

(solubility product  $10^{-2.2}$ ) resulted in higher *R* values for the AlOH<sub>2</sub>SO<sub>4</sub> dissolution front, but did not result in significantly different *R* values for the rhodochrosite dissolution front. More generally, substantial differences in retardation factors (for a given initial carbonate concentration) between the Al(OH)<sub>3</sub> and the AlOH<sub>2</sub>SO<sub>4</sub> simulations occurred only in simulations with *CMR* ratios above 1.5. The reason for this behavior is not clear, but is probably related to the faster movement of the MnO<sub>2</sub> dissolution front relative to the rhodochrosite dissolution front. In any case, the precipitation of Al(OH)<sub>3</sub> generates three times more protons than AlOH<sub>2</sub>SO<sub>4</sub>, as demonstrated in the following equations:



Precipitation of Al(OH)<sub>3</sub> results in substantially lower *pH* waters and faster carbonate mineral dissolution, which explains the generally smaller retardation factors found in simulations with Al(OH)<sub>3</sub>.

The precipitation of Al(OH)<sub>3</sub> (or AlOH<sub>2</sub>SO<sub>4</sub>) generally occurred because dissolution of carbonate minerals caused an increase in *pH*. Reaction with the more acidic infilling waters eventually caused redissolution of the Al-bearing phases. In the case of the simulations with low initial carbonate concentrations and with either AlOH<sub>2</sub>SO<sub>4</sub> (solubility product:  $10^{-2.2}$ ) or with Al(OH)<sub>3</sub> precipitation allowed, complete consumption of the Al-bearing phase occurred at least twice during each simulation. The retardation factors for the Al-phase dissolution fronts given in Table 8.9 refer to the last dissolution front in each simulation.

### 8.5.2.8 *Effects of the irreversible dissolution of Ca and Mg silicates on the evolution of low-pH Fe(II)-rich waters*

Several simulations were conducted by using reactions specified in the PHREEQC inverse Models 2 and 7 (Table 8.5). In addition to allowing secondary  $\text{Al}(\text{OH})_3$ ,  $\text{Fe}(\text{OH})_3$ , and rhodochrosite to precipitate and specifying initial amounts of calcite (or dolomite) to also react to equilibrium, these simulations forced the dissolution of a fixed number of moles of Ca and Mg-silicate minerals into each cell at each time step, thereby simulating a zero-order kinetic dissolution process that matched (over the 10-cell column) the net amount of Ca- and Mg-silicate minerals dissolved according to PHREEQC inverse Models 2 and 7 in Table 8.5. Irreversible dissolution of tremolite was specified in the simulations based on Model 2 (Fig. 8.5). Irreversible dissolution of biotite and anorthite and removal from solution of K-montmorillonite was specified in the simulations based on Model 7. The silicate dissolution processes would have been more correctly simulated with a *pH*-dependent rate law, but this capability was not present in the PHREEQC code used. An inexhaustible supply of silicate minerals was assumed available to all cells throughout the course of the simulations. Despite the crudeness of these assumptions, it was hoped that these simulations would contribute some insights on the importance of silicate mineral dissolution in the *pH* evolution of acidic contaminated waters.

The Ca- and Mg-silicate dissolution simulations specified an essentially infinite amount of chalcedony that was available to react to equilibrium. Following the results of Models 2 and 7 in Table 8.5, gypsum precipitation was excluded from the simulations. (A few simulations were run allowing gypsum precipitation, but the results were not substantially different and are not presented here.) Although an initial fixed amount of  $\text{MnO}_2$  ( $2 \times 10^{-2}$  mol  $\text{kg}^{-1}$   $\text{H}_2\text{O}$ ) was specified in most simulations, two sets of simulations specified instead a zero-order dissolution process for  $\text{MnO}_2$ , according to the amounts determined by Models 2 and 7 in Table 8.5. Finally, one set of simulations was based on Model 7 (Table 8.5), but allowed  $\text{AlOHSO}_4$  to precipitate instead of  $\text{Al}(\text{OH})_3$ .

All the simulations that specified a fixed initial  $\text{MnO}_2$  concentration resulted in rhodochrosite precipitation and accumulation (Table 8.7, Fig. 8.5a). A rhodochrosite dissolution front never formed; the continuous proton consumption caused by dissolution of the silicate minerals and the high initial Mn and *TDIC* concentrations in the infilling water (were sufficient to ensure that the infilling water never became undersaturated with respect to rhodochrosite. In contrast, the simulations that allowed irreversible zero-order dissolution of  $\text{MnO}_2$  produced rhodochrosite dissolution fronts (Fig. 8.5b) because the oxidation of dissolved Fe(II) caused the precipitation of  $\text{Fe}(\text{OH})_3$  and constantly generated acidity that dissolved rhodochrosite. The *R* values for the rhodochrosite dissolution fronts nearly doubled for each doubling of the initial carbonate concentration if carbonate concentrations were above  $4.2 \times 10^{-2}$  mol  $\text{kg}^{-1}$   $\text{H}_2\text{O}$ ; at lower initial carbonate concentrations, rhodochrosite *R* values increased only by 50% or less for each doubling in initial carbonate concentration.

The two sets of simulations with irreversible tremolite dissolution (with and without fixed initial  $\text{MnO}_2$  concentrations) generated calcite dissolution fronts (Table 8.8, Fig. 8.5). In contrast, of the three sets of simulations based on inverse Model 7 (and irreversible biotite and anorthite dissolution rather than tremolite dissolution), only the simulations that allowed continuous zero-order dissolution of  $\text{MnO}_2$  (and consequent production of acidity) generated calcite dissolution fronts. In the simulations with tremolite dissolution and fixed initial  $\text{MnO}_2$ , the calcite dissolution *R* values jumped by a factor of 25, from 4.5 to 113.7, as the initial calcite concentration used in each simulation increased from  $4.2 \times 10^{-2}$  to  $8.4 \times 10^{-2}$  mol  $\text{kg}^{-1}$   $\text{H}_2\text{O}$  (and then tripled with each further doubling of the initial calcite concentrations above that). The jump by a factor of 25 in the *R* values occurred when, as a result of the higher initial calcite concentration, the calcite dissolution front moved more slowly than the  $\text{MnO}_2$  dissolution front (*R* = 4.7). In simulations that also used a fixed initial  $\text{MnO}_2$  concentration ( $2 \times 10^{-2}$  mol  $\text{kg}^{-1}$   $\text{H}_2\text{O}$ ) but attempted to emulate inverse Model 7, any initial dolomite dissolution was eventually followed by dolomite precipitation and accumulation. Because of the

additional contribution of Fe(II)-containing biotite, the retardation factor was 4.5 for the  $\text{MnO}_2$  dissolution front in these simulations.

Most of the simulations with Ca- and Mg-silicate dissolution did not produce an Al-phase dissolution front (or produced only a temporary one). The proton consumption caused by the silicate dissolution reactions caused the continuous precipitation of  $\text{Al}(\text{OH})_3$  from the infilling water (Table 8.9). The set of simulations with irreversible tremolite dissolution and zero-order  $\text{MnO}_2$  dissolution did generate an  $\text{Al}(\text{OH})_3$  dissolution front because of the acidity generated by the continuous addition of  $\text{MnO}_2$  by zero-order kinetics, its oxidation of dissolved Fe(II), and the consequent precipitation of  $\text{Fe}(\text{OH})_3$ . The set of simulations emulating Model 7, but allowing  $\text{AlOHSO}_4$  to precipitate instead of  $\text{Al}(\text{OH})_3$ , produced a  $\text{AlOHSO}_4$  dissolution front. Surprisingly, the  $R$  value for that front decreased as the initial carbonate concentration increased to  $4.2 \times 10^{-2} \text{ mol kg}^{-1} \text{ H}_2\text{O}$  and then continued to increase with higher initial carbonate concentrations.

The  $pH$  values obtained during the evolution of the well 402 water during the simulations with irreversible Ca- and Mg-silicate dissolution (Fig. 8.5) were close to the  $pH$  values predicted for the various mineral assemblages in Table 8.6, but only when carbonate minerals (rhodochrosite or calcite) were still present and  $\text{MnO}_2$  was either being added or was still present. The first 10 shifts of the simulations show a large increase in the  $pH$  of cell 10 because of the constant dissolution of Ca- and Mg-silicates into the background water that initially filled the column; after 10 shifts the water in the column has been replaced by reacted infilling water.

#### 8.5.2.9 *The effect of not allowing rhodochrosite precipitation*

One set of simulations, without Ca- and Mg-silicate dissolution, used a low cation-exchange capacity (1 meq/100 g), but disallowed rhodochrosite precipitation. For those simulations, the calcite dissolution front was the most important  $pH$  front to consider, because it was either the only, or the slowest (for simulations with initial dolomite and calcite), carbonate mineral dissolution front that needed to be considered. (The rhodochrosite dissolution front was the slowest carbonate mineral dissolution front in all other simulations.) The  $R$  values for the calcite dissolution front were greater in the simulations without rhodochrosite precipitation than in the simulations that allowed rhodochrosite precipitation. However, the calcite  $R$  values in the simulations without rhodochrosite precipitation were up to two times smaller than the rhodochrosite  $R$  values in the runs that allowed rhodochrosite precipitation. The  $pH$  values after complete dissolution of calcite in the simulations without rhodochrosite precipitation match the low- $pH$  values after complete rhodochrosite dissolution in the simulations that allowed precipitation of that mineral (Table 8.6).

In simulations with low initial carbonate ( $2.1 \times 10^{-2} \text{ mol kg}^{-1} \text{ H}_2\text{O}$  and lower), the faster movement of the  $\text{Al}(\text{OH})_3$  dissolution front relative to the rhodochrosite dissolution front meant that the complete dissolution of rhodochrosite led to a large  $pH$  decrease (Fig. 8.4a). In simulations with higher initial carbonate concentrations, the second  $\text{Al}(\text{OH})_3$  dissolution front travelled more slowly than the rhodochrosite front and therefore the disappearance of rhodochrosite resulted in a relatively small decrease in  $pH$  (Figs. 8.4b, 8.4c, 8.4d). The  $R$  values for the  $\text{Al}(\text{OH})_3$  final dissolution-front were smaller (by as much as 1/3 in the runs with high initial carbonate concentrations) in the simulations without rhodochrosite precipitation relative to the  $\text{Al}(\text{OH})_3$   $R$  values obtained in the simulations that allowed rhodochrosite to precipitate. For simulations with the three lowest initial carbonate concentrations ( $5.25 \times 10^{-3}$ ,  $1.05 \times 10^{-2}$  and  $2.1 \times 10^{-2}$ ), however, differences in the  $R$  values between the simulations that did or did not include rhodochrosite precipitation were relatively small.

#### 8.5.2.10 *The $\text{CO}_2$ open system simulations*

A few reactive-transport simulations allowed the 1-dimensional column to equilibrate with an infinite gaseous  $\text{CO}_2$  reservoir at a fixed partial pressure of either  $10^{-1.33}$  (the calculated  $p_{\text{CO}_2}$  for water at well 503, Brown, 1996) or  $10^{-0.9865}$  (the measured  $p_{\text{CO}_2}$  of the unsaturated zone at

site 500 in November 1991). Opening the system up to  $\text{CO}_2$  affected the retardation of the calcite, rhodochrosite and  $\text{Al}(\text{OH})_3$  dissolution fronts, particularly in the simulations with at least  $3 \times 10^{-2} \text{ mol kg}^{-1}$  of initial calcite (i.e., with *CMR* ratios of 1.5 and above). The simulations conducted under the higher fixed  $p_{\text{CO}_2}$  value ( $10^{-0.9865}$ ) generally resulted in lower *R* values for the calcite, rhodochrosite, and  $\text{Al}(\text{OH})_3$  dissolution fronts, compared to the values determined in the BRM simulations. In contrast, the simulations conducted under the lower fixed  $p_{\text{CO}_2}$  value ( $10^{-1.33}$ ) resulted in higher *R* values for all three mineral dissolution fronts, compared to the values determined in the BRM simulations. The relevance of these simulations to the migration of the acidic ground waters at Pinal Creek field site is questionable. It is unlikely that groundwaters at the site maintain contact with the unsaturated zone during their evolution. However, the  $\text{CO}_2$  equilibration simulations have large effects on the movement of the fronts, and further study is needed to confirm that  $\text{CO}_2$  ingassing or outgassing is not significant at the field site.

#### 8.5.2.11 The effect of longitudinal dispersion

When the longitudinal dispersivity ( $\alpha$ ) is increased from 0 to 560 m (which represents 10% of the distance between wells 402 and 503), the retardation of the calcite or rhodochrosite dissolution fronts are not significantly affected, except for the simulations with the lowest initial carbonate concentrations ( $3 \times 10^{-2} \text{ mol kg}^{-1} \text{ H}_2\text{O}$  and lower, corresponding to *CMR* ratios below 1.5). Dispersion typically has little effect on the propagation of sharp fronts caused by simple mineral dissolution reactions, especially if the initial mineral concentrations are sufficient to significantly retard the propagation of the fronts. At the limit, dispersion would have no effect on the retardation of a mineral dissolution front for which an infinite initial mineral concentration had been specified. Of course, using a dispersivity of 560 m has a large effect on the spreading of non-reacting solutes, and is also expected to affect the mineral dissolution fronts that propagate at nearly the same speed as the water. Longitudinal dispersion implies that portions of a tracer or solute of interest move both faster and slower than the average groundwater velocity. The spreading of a conservative solute after a given travel time, or travel distance, can be calculated from the following equation (Appelo and Postma, 1993):

$$\sigma_x = \sqrt{2\alpha vt} = \sqrt{2\alpha x} \quad (8.11)$$

If  $\alpha = 560 \text{ m}$  and  $x = 5600 \text{ m}$ , the distance between wells 402 and 503,  $\sigma_x = 2504 \text{ m}$ .  $\sigma_x$  represents a distance between two specific points in a 1-D homogeneous column. At those two points, a conservative tracer injected continuously at the beginning of the column (i.e., at well 402), with a relative concentration  $c/c_0$  of 1.0, would have achieved relative concentrations of 0.5 and 0.16, respectively. When the relative concentration of a conservative tracer reaches 0.5 at well 503, 5600 m downgradient from well 402, the 0.16 relative concentration level has already moved ahead by 2504 m. In contrast, the 0.84 relative concentration level would be 2504 m upgradient from well 503. The above analysis assumes steady-state flow through a porous medium with homogeneous physical properties and also assumes that there are no “dead-water” zones into which the conservative tracer can diffuse.

The simulations that included longitudinal dispersion were conducted with both the PHREEQM code and with an unpublished version of the PHREEQC v. 2 code obtained in 1996 (David Parkhurst and Tony Appelo, written commun.). Unlike its first 1995 version, PHREEQC v. 2 simulated longitudinal dispersion by using an algorithm similar to the one used in PHREEQM. Efforts were made to ensure that the thermodynamic databases for PHREEQM and PHREEQC were identical, particularly for Al species. Although we are not aware of any differences, some minor differences may have still remained. The database used in the PHREEQC v. 2 runs was identical to that used in all the other PHREEQC runs (the PHREEQC v. 1 runs, without dispersion). Unfortunately, we were unable to make PHREEQC v. 2 converge for the entire set of simulations. Although current versions of

PHREEQC are more stable and have more features than the earlier pre-publication version that was used, modeling comparisons with PHREEQM, and with later versions of PHREEQC v. 2, leave us confident that the results obtained with the earlier version would match those obtained with more recent versions.

#### 8.5.2.12 *The influence of cation exchange and surface-complexation sorption processes*

The reader is referred to Appelo (1996), Appelo and Postma (1993, 2005), Dzombak and Morel (1990) and Davis and Kent (1990) for excellent descriptions of the theories of cation exchange and surface-complexation sorption processes. The cation exchange conventions used in the PHREEQM and PHREEQC codes are described in Appelo and Postma (1993). PHREEQC's simulation of surface complexation sorption processes implements the diffuse double-layer surface-complexation model presented by Dzombak and Morel (1990) and is fully described in Parkhurst (1995) and Parkhurst and Appelo (1999).

Allowing cation exchange with a cation-exchange capacity (*CEC*) of 1 meq/100 g did not substantially affect rhodochrosite and calcite retardation factors (Tables 8.7, 8.8). The ions allowed to exchange were  $\text{Al}^{3+}$ ,  $\text{Fe}^{2+}$ ,  $\text{Mn}^{2+}$ ,  $\text{Ca}^{2+}$ ,  $\text{Mg}^{2+}$ ,  $\text{Sr}^{2+}$ ,  $\text{Ba}^{2+}$ ,  $\text{Na}^{+}$ , and  $\text{K}^{+}$ . Proton exchange was also simulated. The selectivity coefficients used were the default values present in the PHREEQC thermodynamic database (which are nearly identical to values given in Appelo and Postma, 1993). A *CEC* of 1 meq/100 g [equivalent to  $52.2 \text{ meq kg}^{-1} \text{ H}_2\text{O}$  appears to be a reasonable estimate for the Pinal Creek sediments, given the low organic carbon content (less than 1%) and relative coarseness of the sediments]. The empirical formula given by Breeuwsma *et al.* (1986) relating the *CEC* to the  $<2 \mu\text{m}$  clay fraction and to the organic carbon content is assumed applicable (cited in Appelo and Postma, 1993):

$$CEC \text{ (meq/100g)} = 0.7 \text{ (\% clay)} + 3.5 \text{ (\% C)} \quad (8.12)$$

Direct measurements of the *CEC* of Pinal Creek sediments, and of the exchangeable ion composition of the sediments, would be preferable to an empirical formula. The purpose of our simulations, however, was to determine the effect of ion-exchange processes on the evolution of the low-*pH* and high-Fe(II) contaminated groundwaters at the site. Therefore, simulations were also conducted using an unrealistically high *CEC* of 10 meq/100 g, a *CEC* that would be applicable to sediments with more than 10% clay content (and 1% organic carbon). As discussed earlier, these high *CEC* simulations resulted in a doubling of the retardation of the  $\text{MnO}_2$  dissolution front (from 4.7 to 9.2 for an initial  $\text{MnO}_2$  concentration of  $2 \times 10^{-2} \text{ mol kg}^{-1} \text{ H}_2\text{O}$ ). The high *CEC* ion-exchange simulations generally increased the retardation factors for the calcite dissolution front but did not result in a uniform increase in the retardation of the rhodochrosite or of the Al-phase dissolution fronts (as a function of initial carbonate). At the lowest initial carbonate concentrations ( $0.525 \times 10^{-2}$ ), the high *CEC* simulations did not result in rhodochrosite precipitation. At higher initial carbonate concentrations, between  $2.1 \times 10^{-2}$  and  $3.0 \times 10^{-2} \text{ mol kg}^{-1} \text{ H}_2\text{O}$ , the high *CEC* simulations had higher *R* values for the rhodochrosite dissolution front than in the model runs that did not simulate cation exchange (or those that assumed a low *CEC*). At even higher initial carbonate concentrations ( $4.2 \times 10^{-2}$  and above), however, this behavior was reversed: the *R* values for rhodochrosite dissolution for the high *CEC* simulations were lower than the *R* values observed in the simulations with lower or no ion exchange capacity. The retardation factors for the  $\text{Al}(\text{OH})_3$  dissolution front also exhibited complex behavior with increasing initial carbonate concentration.

The PHREEQC simulations that included a diffuse double-layer surface-complexation-sorption model resulted in retardation factors for the rhodochrosite, calcite and  $\text{AlOHSO}_4$  dissolution fronts that were generally higher than the *R* values determined in simulations without sorption. Surface protonation and deprotonation reactions were incorporated into the sorption model, along with surface complexation of Mn, Ca, Mg, Cu, Zn, Co, Ni and  $\text{SO}_4$  at weak and strong surface sites.

The thermodynamic sorption model was based on the compilation of intrinsic constants for hydrous ferric oxide published by Dzombak and Morel (1990) and used by default in PHREEQC. The number of weak and strong sorption sites used ( $1.5 \times 10^{-2}$  and  $3.8 \times 10^{-4}$  respectively) and the amount of surface area per kg of  $\text{H}_2\text{O}$  used ( $4032 \text{ m}^2$ ) were identical to the values used by Brown (1996) in his 1-D simulation of reactive transport at the Pinal Creek site, and also in his PHREEQC-simulation fit of the column experiment conducted by Stollenwerk (1994). Using a higher number of sorption sites in our simulations would probably have resulted in more significant effects on the retardation of the mineral dissolution fronts.

Cu ( $36.2 \text{ mg L}^{-1}$ ), Zn ( $4.97 \text{ mg L}^{-1}$ ), Co ( $4.14 \text{ mg L}^{-1}$ ) and Ni ( $1.57 \text{ mg L}^{-1}$ ) concentrations measured in the well 402 water were added to one set of simulations. Another set of simulations was conducted without those elements. This second set of simulations resulted in higher  $R$  values for the rhodochrosite and calcite fronts, but in slightly lower  $R$  values for the  $\text{AlOHSO}_4$  front except in the simulations with the two highest initial carbonate concentrations.

#### 8.5.2.13 *Other minor effects on the evolution of the low-pH waters*

Several simulations included an initial concentration of dolomite, in addition to calcite, or allowed kaolinite to precipitate (instead of  $\text{Al}(\text{OH})_3$  or  $\text{AlOHSO}_4$ ). The simulations otherwise used the BRM setup, but all specified the same initial carbonate mineral concentration ( $8.4 \times 10^{-2} \text{ mol kg}^{-1} \text{ H}_2\text{O}$ ). The resulting retardation factors for the calcite, dolomite and rhodochrosite dissolution fronts can be found in Glynn and Brown (1996, Table 12). Including or excluding dolomite did not, by itself, affect the retardation of the low-pH fronts. The important variable was the total moles of solid carbonate, whether in the form of calcite or dolomite. Allowing kaolinite to precipitate instead of  $\text{Al}(\text{OH})_3$  resulted in slightly lower retardation factors for the calcite and rhodochrosite dissolution fronts (Table 12 in Glynn and Brown). In contrast, the  $R$  values obtained for the final kaolinite dissolution front were generally much greater than those obtained for the final  $\text{Al}(\text{OH})_3$  dissolution front. These effects were due to the greater stability of kaolinite, relative to  $\text{Al}(\text{OH})_3$ , in the presence of acidic water.

#### 8.5.2.14 *Comparison of the reactive transport simulation results with observations at the Pinal Creek site*

Although groundwater samples at the Pinal Creek site have been collected and analysed by the U.S. Geological Survey since 1984, limited resources, and the large size of the basin and of the contaminant plume, prevented the emplacement of a high number of wells. The sparseness of the available spatial information have made it difficult to determine the location of the low-pH and high-Fe(II) groundwaters (Fig. 8.6) through time. The longitudinal spreading of the fronts (and especially of the Fe(II) front), which might give valuable information on reaction kinetics, has also been difficult to determine.

Nevertheless some estimates of the velocity of the low-pH front can be made, primarily because of the breakthrough of low-pH waters (from a pH of 4.96 in March 1989 to a pH of 4.24 in August 1989) that was observed at well 451 only a few months after its emplacement (December 1988). If the creation of Webster Lake in 1940, approximately 18.5 km upgradient from well 451, provided the principal source of acidic contaminated waters, then an effective velocity of about  $1 \text{ m day}^{-1}$  can be estimated for the low-pH front over that section of the aquifer. This velocity can be compared to an estimated average groundwater velocity of  $8.4 \text{ m day}^{-1}$  between Webster Lake and well 451, giving an estimated retardation factor of about 8.4 for the movement of the low-pH waters. This retardation factor estimate is thought to be a maximum estimate, because the applicable groundwater velocity could be as low as  $5 \text{ m day}^{-1}$ . Eychaner (1991) and Glynn *et al.* (1991) estimated that a lower  $R$  value of 5 would be reasonable for the movement of the pH front from Webster Lake to well 451.

Similarly, a low-pH (4.0 to 4.5) high-Fe(II) water was found to be present during drilling (in February 1995) of a group of wells (LPC wells) emplaced by the Pinal Creek Group (a consortium of copper companies) slightly west of well 503 (on the other side of the

creek bed). Given the distance of the LPC wells from well 451 (1.3 km), the minimum velocity of the low-*pH* front is estimated to be greater than  $0.65 \text{ m day}^{-1}$ . Using this velocity with an estimated average groundwater velocity of about  $5 \text{ m day}^{-1}$  (between 451 and 503) results in a maximum *R* value of about 7.7 for the low-*pH* front. The acidity of the well 451 water in August 1989 was ~2 times lower than that of the well 402 water used in our simulations, although the potential acidity (cf. discussion of Table 7 in Glynn and Brown, 1996) of the well 451 water did increase with time until a maximum acidity, about 70% of that for well 402, was reached in November 1991.

In comparison to this field evidence, results of a column elution experiment conducted by Stollenwerk (1994), using water from well 51 (of composition similar to that presented in Glynn and Brown, 1996, Table 7) and an 80-cm column containing uncontaminated alluvium from the Pinal Creek site, indicated an *R* value for the low-*pH* front of about 2.5. Many factors can explain the lower retardation found in the column experiment relative to the field values. The low-*pH* front *R* values estimated from the field evidence incorporate significant effects of dilution (Fig. 8.3). The Webster Lake waters were more acidic than the well 51 water used in Stollenwerk's column experiment. The potential acidity of the well 51 water was 4.5 times greater than that of the well 402 water used in the Glynn and Brown (1996) simulations shown here. As a result, the retardation factor of 2.5 determined by Stollenwerk (1994) should translate to a retardation factor of approximately 7.8,  $(2.5 - 1) \times 4.5 + 1 = 7.75$ , had well 402 water been used in his column experiments. Equation (8.4) is used to normalize these results, assuming that  $\Delta M$  is proportional to the acidity of the low-*pH* solution and that the field and laboratory experiments both had identical homogeneous mineral concentrations and reactions. Similarly, considering that the water from well 451 in August 1989 was about 2 times less acidic than the water used in the simulations shown here, the *R* value of 7.7 determined between 451 and the LPC site would correspond to an *R* value of 4.35, if normalized to the acidity of the well 402 water ( $89/1/12$ ). These normalized retardation factors (4.4 and 7.8) can be compared with the *R* values obtained in our numerical simulations of the rhodochrosite dissolution front (the best analog for the low-*pH* front observed in the field). The simulation results in Table 8.7, for runs without irreversible dissolution of Ca and Mg-silicates, indicate that initial carbonate mineral concentrations between  $2.1 \times 10^{-2}$  and  $4.2 \times 10^{-2} \text{ mol kg}^{-1} \text{ H}_2\text{O}$  and certainly no lower than  $1.05 \times 10^{-2} \text{ mol kg}^{-1} \text{ H}_2\text{O}$  would give reasonable simulated retardation factors for the low-*pH* waters. This assumes that an  $\text{MnO}_2$  concentration of  $2 \times 10^{-2} \text{ mol kg}^{-1} \text{ H}_2\text{O}$  was also reasonable. If not, two different situations can be considered. A lower initial  $\text{MnO}_2$  concentration would result in a higher *CMR* value and therefore (cf. section 8.5.2.6) could increase the simulated retardation factors for the low-*pH* front. Consequently, initial carbonate concentrations would have to be adjusted slightly downward in order to match the estimated lab and field retardation factors. Alternatively, a higher initial  $\text{MnO}_2$  concentration would probably not have a substantial effect on the simulated low-*pH* front *R* values (for initial carbonate mineral concentrations between  $1.05 \times 10^{-2}$  and  $3.0 \times 10^{-2} \text{ mol kg}^{-1} \text{ H}_2\text{O}$ ).

In the simulations with Ca- and Mg-silicate dissolution, the retardation factors for the rhodochrosite front are so high that an initial carbonate concentration of  $5.25 \times 10^{-3}$  or lower is needed to match the observed retardation of the low-*pH* front in Stollenwerk's experiments and in the field, if we assume that the disappearance of rhodochrosite controls the low-*pH* front. Such a low initial carbonate concentration is not realistic given our knowledge of the alluvial sediments at the site, and we conclude that the simulations with irreversible dissolution of Ca- and Mg-silicate should be conducted by using a finite (as opposed to an inexhaustible) source of these silicates. Further field information on the concentration and rate of dissolution of silicate minerals would however be needed. The calcite *R* values obtained in our forward simulations of inverse Model 2 (Table 8.5) are perhaps reasonable, but only for initial calcite concentrations below  $4.2 \times 10^{-2} \text{ mol kg}^{-1} \text{ H}_2\text{O}$ . The disappearance of calcite did not by itself, however, result in a sufficient *pH* decrease to match the *pH* values of 4.0 to 4.5 that we associate with the low-*pH* front in the field (Fig. 8.6).

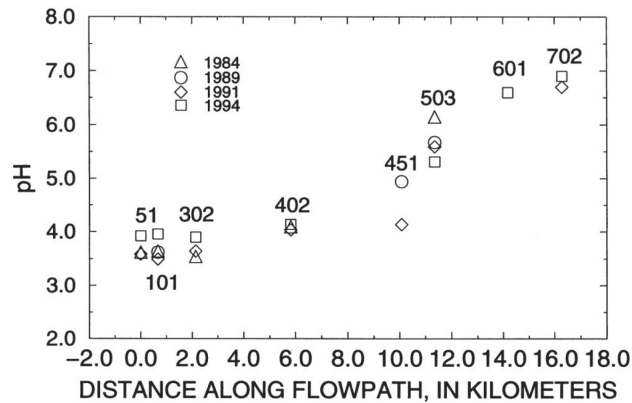


Figure 8.6. *pH* profiles along an aquifer flowpath based on the most contaminated wells in the Pinal Creek alluvial aquifer. Well 451 was drilled in December 1988 and destroyed during the floods of spring 1993. Therefore only January 1989 and November 1991 *pH* data are presented for that well. Water samples taken from 451 show a large *pH* decrease between those dates (most of the decrease occurred between March and August 1989).

The identity of the secondary aluminum phase that precipitates and the rate of redissolution of that phase are also important to consider. Table 8.6 shows that the most acidic waters (below *pH* 5.0) can only be obtained if  $\text{Al}(\text{OH})_3$  is not present: i.e., it either never precipitates out, or if it does, it has completely redissolved, or its rate of dissolution is so slow that it can be considered “unreactive”. If we assume that secondary  $\text{Al}(\text{OH})_3$  does precipitate out and that the Local Equilibrium Assumption controls its precipitation and later dissolution, then our simulations of the  $\text{Al}(\text{OH})_3$  dissolution front show (Table 8.9) that initial carbonate concentrations would have to be lower than  $3.0 \times 10^{-2} \text{ mol kg}^{-1} \text{ H}_2\text{O}$  to match the retardation of the low-*pH* front observed in the field and in Stollenwerk’s laboratory columns.

As of 1996, there had been no direct observation of the breakthrough of the high-Fe(II) waters at the Pinal Creek site. Waters from wells 451 and the LPC site (near well 503) already had high Fe(II) concentrations during the emplacement of those wells (in November 1991 and February 1995 respectively). The fact that dissolved Fe(II) was present at well 451 before the low-*pH* breakthrough suggests that the Fe(II) front moves faster than the low-*pH* front, or at least precedes the low-*pH* front at that point in time. If we use the creation of Webster Lake as an initial condition, retardation factors between 5 and 8.4 can be estimated for the high Fe(II) front as it moved between Webster Lake and well 451. Similarly, the evidence based on data from well 451 and from the LPC wells suggests a maximum retardation factor of 7.7 over that section of the aquifer. The latter factor is equivalent to a maximum retardation factor of about 3.2 in our simulations, after correcting for the three times higher Fe(II) concentration of well 402 relative to that of well 451 (in August 1989).

In his laboratory column experiments, Stollenwerk (1994) observed retardation factors of approximately 2 for the high-Mn(II) spike, and 2.5 for the high-Fe(II) front. The lag in the Fe(II) front suggests that the rate of  $\text{Fe}(\text{OH})_3$  precipitation was delayed relative to the rate of  $\text{MnO}_2$  dissolution. Normalizing those retardation factors to an infilling solution with 4.7 times less dissolved Fe(II) (for well 402) results in an equivalent retardation factor of between 5.7 and 8.1.

After normalization to the infilling water used in our simulations, the field and laboratory determined retardation factors for the high-Fe(II) front encompass a range from 3.2 to 8.1. This range compares favorably with the retardation factor of 4.7 determined for most of the simulations. Furthermore, according to field and laboratory observations the  $\text{MnO}_2$

dissolution front moves slightly faster than the low-*pH* front, but it is not moving much faster, and therefore the *CMR* ratio is probably close to 1.5.

The *pH* values determined for the various *pH*-plateaus in our simulations (Table 8.6, Figs. 8.4 and 8.5) are within the range of the values observed in the field (Fig. 8.6). Therefore the hypothesis that the complete dissolution of secondary rhodochrosite occurs after the dissolution of calcite and is accompanied by a significant decrease in *pH* (in the absence of  $\text{Al}(\text{OH})_3$ ) is consistent with the field evidence.

## 8.6 CONCLUSIONS

The basic theory and assumptions of inverse geochemical modeling were presented. Although much less commonly used than reactive-transport modeling, particularly in investigations of groundwater contamination, inverse geochemical modeling provides a powerful tool to identify the reactions that affect the chemical and isotopic evolution of contaminated groundwaters. The reaction models identified by inverse modeling can be incorporated into a geochemical reactive-transport model to investigate the effects of the various reactions on the transport of reactive contaminants. This approach was demonstrated for the case of acidic groundwater with heavy-metal contamination in the Pinal Creek basin, Arizona.

The interactive inverse geochemical modeling code NETPATH was used to construct a series of inverse models that quantified observed differences in chemical composition between an initial acidic Fe(II)-rich water and an evolutionary, partially-neutralized Fe(II)-poor water, according to a postulated set of reactions. Each inverse model was evaluated according to existing knowledge of the geochemistry of the aquifer and the thermodynamic and kinetic feasibility of the model reactions. Once a plausible set of inverse models was identified, the PHREEQC inverse modeling code was used to further evaluate the set of inverse models. Unlike NETPATH, PHREEQC accounts for uncertainties in the analytical data and, additionally, includes alkalinity-balance, charge-balance and water-balance constraints in solving inverse models.

Inverse modeling with NETPATH and with PHREEQC quantified the reaction processes responsible for the evolution of an acidic Fe(II)-rich groundwater into a partially neutralized Fe(II)-poor water at the Pinal Creek site. The principal reaction processes appear to be the reductive dissolution of solid  $\text{MnO}_2$  by aqueous Fe(II), the consequent precipitation of  $\text{Fe}(\text{OH})_3$ , the dissolution of calcite and/or dolomite, the precipitation of an aluminum phase, probably  $\text{Al}(\text{OH})_3$  (rather than  $\text{AlOHSO}_4$ ), and, possibly, the precipitation of chalcodony. Results of the inverse modeling simulations also led to the following conclusions:

1. Ca- and Mg-silicate dissolution must be an important process during the neutralization of the low-*pH* waters, given that  $\text{CO}_2$  exsolution probably does not occur.
2. Dilution of the acidic groundwaters occurs, and Cl, Na, and  $\text{SO}_4$  can be considered conservative constituents that quantify the extent of the dilution. The PHREEQC models revealed that  $\text{SO}_4$  could be considered a conservative constituent given its associated analytical uncertainty.
3. Rhodochrosite precipitation (or possibly an  $\text{MnO}_2$ - $\text{Mn}(\text{OH})_3$  electron-transfer or  $\text{Mn}^{2+}$  sorption mechanism) is responsible for the lower than expected increase in dissolved Mn(II) concentrations caused by the aqueous Fe(II) reduction of  $\text{MnO}_2$  solids.

After a brief review of previous reactive-transport modeling at the Pinal Creek site, the results of some new forward simulations were presented. These geochemical transport simulations explored the effects of reactions—identified by inverse modeling and cited by other researchers—on the chemical evolution of an acidic Fe(II) rich water from the Pinal Creek site. The purpose of the PHREEQC and PHREEQM transport simulations was to determine the effect of the reactions on the relative rates of movement of the Fe(II)-rich and low-*pH* groundwaters.

The only factors affecting the retardation of the Fe(II)-rich waters and the propagation of the  $\text{MnO}_2$  dissolution front in our simulations were the initial specified concentration of  $\text{MnO}_2$  and the concentration of Fe(II) in the inflowing contaminated water. As demonstrated in the text, the rate of movement of the  $\text{MnO}_2$  front could be easily calculated by hand, but only in the absence of ion-exchange or other processes substantially affecting the Fe(II) concentration.

The propagation of various  $pH$  fronts caused by complete dissolution of carbonate and aluminum minerals, however, could not have been easily predicted. The use of a geochemical transport code such as PHREEQM or PHREEQC is necessary to determine the retardation factors applicable to interacting mineral dissolution fronts. The initial amount of carbonate (calcite and/or dolomite) in each simulation was the primary factor determining the movement of the low- $pH$  waters. Other important factors were the ratio of initial carbonate to initial  $\text{MnO}_2$ , the type of Al phase allowed to precipitate, and whether or not rhodochrosite was allowed to precipitate. High initial carbonate to  $\text{MnO}_2$  ratios, allowing rhodochrosite precipitation, and allowing  $\text{AlOHSO}_4$  precipitation (instead of  $\text{Al(OH)}_3$  precipitation), resulted in higher retardation factors for the movement of the low- $pH$  waters. [As mentioned earlier though, Bigham and Nordstrom's (2000) review of environmental conditions required for the occurrence of  $\text{AlOHSO}_4$  phases reinforces Glynn and Brown's (1996) view that an  $\text{Al(OH)}_3$  phase was probably a more reasonable phase to consider in modeling the evolution of Pinal Creek groundwaters.] Allowing the irreversible dissolution of Ca- and Mg-silicates, so as to match the mass transfers determined in a few inverse models, resulted in unrealistically high retardation factors for the rhodochrosite and  $\text{Al(OH)}_3$  dissolution fronts, although the retardation factors for the calcite dissolution front were reasonable. More field and laboratory information is required on the rates and extents of reaction for these silicate minerals to further constrain reactive-transport simulations.

Inclusion of ion-exchange processes did not substantially affect the retardation of the various  $pH$  fronts when a reasonable low (1 meq/100 g) CEC was used. Because of surface-protonation, allowing surface-complexation reactions resulted in higher retardation factors for the carbonate and  $\text{AlOHSO}_4$  dissolution fronts. Allowing equilibrium with a  $p_{\text{CO}_2}$  of  $10^{-0.9865}$  resulted in lower retardation factors for the carbonate and  $\text{Al(OH)}_3$  dissolution fronts, particularly at initial carbonate concentrations greater than  $3 \times 10^{-2}$  mol  $\text{kg}^{-1}$   $\text{H}_2\text{O}$ . Allowing equilibrium with a lower  $p_{\text{CO}_2}$  of  $10^{-1.33}$  resulted in higher retardation factors for the carbonate and  $\text{Al(OH)}_3$  dissolution fronts. Simulation of longitudinal dispersion was not an important factor controlling the movement of the calcite and rhodochrosite dissolution fronts except at low initial carbonate concentrations. Longitudinal dispersion also did not affect the simulated rate of movement of the Fe(II)-rich waters. Including dolomite in addition to calcite in the background aquifer and allowing kaolinite to precipitate instead of  $\text{Al(OH)}_3$  did not significantly affect the propagation of the low- $pH$  fronts associated with the dissolution of calcite and rhodochrosite.

A comparison of the retardation factors for the low- $pH$  and high-Fe(II) fronts determined in our local equilibrium simulations with retardation factors estimated from field evidence and Stollenwerk's (1994) laboratory column elution tests suggests that an initial carbonate concentration between  $2.1 \times 10^{-2}$  and  $4.2 \times 10^{-2}$  mol  $\text{kg}^{-1}$   $\text{H}_2\text{O}$  and the initial  $\text{MnO}_2$  concentration of  $2 \times 10^{-2}$  mol  $\text{kg}^{-1}$   $\text{H}_2\text{O}$  used in our simulations are reasonable. The  $pH$  values obtained in our local equilibrium simulations are reasonable given the  $pH$  values observed in the field.

The retardation factors determined for the mineral dissolution fronts in various simulations are useful not only in estimating the rate of movement of the low- $pH$  and high-Fe(II) groundwaters at the Pinal Creek site, but also in identifying the most important chemical parameters controlling the movement of these contaminated waters. Our simulation results may also provide information on the rate of movement of acidic, metal-laden waters at other groundwater contamination sites, and our study illustrates how to adjust for  $pH$ , dissolved metal (Al, Fe, Mn) concentrations, and mineralogical characteristics of a given site.

This paper presents and demonstrates an approach for the investigation of the evolution and movement of contaminated groundwaters: the use of inverse geochemical modeling to identify important reaction processes, followed by geochemical reactive-transport simulations that incorporate the inverse-model-derived reactions and account for a range of aquifer characteristics. Such an approach results in an improved understanding of the processes that control the past and future evolution of contaminated groundwaters. This information may then lead to better predictions for the transport of reactive contaminants, which, in turn, may result in more effective remediation of groundwater contamination at sites with sparse spatial information.

### 8.7 THE SENIOR AUTHOR'S FIFTEEN YEAR PERSPECTIVE ON THE GLYNN AND BROWN (1996) PAPER

The geochemical modeling conducted by Glynn and Brown (1996), while confirming and refining knowledge about chemical reactions in the Pinal Creek groundwater system, also highlighted significant knowledge gaps. The Glynn and Brown (1996) study provided a basis for further groundwater geochemical investigations at the Pinal Creek site, including several reactive-transport modeling studies. For example, Brown *et al.* (1998) modified and refined the simulation of groundwater evolution presented in Brown (1996) for 1-D flow (with lateral dilutions as needed) from well 51 to well 701 from 1984 to 1994. Some of the reactions were changed in the modified model as well as the spatial distribution of those reactions. For example, rhodochrosite was allowed to precipitate and  $\text{CO}_2$  was allowed to equilibrate with a  $p_{\text{CO}_2}$  of  $10^{-1.33}$  (typical of the unsaturated zone) in the "neutralized" zone downgradient from well 503. Sensitivity analyses examined, for example, surface complexation and sorption of metals on iron oxyhydroxide. Sorption was relatively less important than initially considered by the authors in controlling  $p\text{H}$  and dissolved metal concentrations relative to other processes (such as redox processes, carbonate dissolution, and dilution). Longitudinal hydrodynamic dispersion was found to be relatively unimportant (a beta version of PHREEQC v.2 was used). Generally, good fits were obtained for the simulation of heavy metals such as Cu, Zn, and Ni. However, the simulation of  $p\text{H}$  and dissolved Fe and Mn still proved problematic, and a simulation of the carbonate and redox reaction kinetics was still needed.

Brown *et al.* (2000), again improving on Brown (1996), found that HYDROGEOCHEM and PHREEQC simulations of the Stollenwerk (1994) column experiments provided similar numerical results, but once again, required accounting for reaction kinetics, if the experimental results were to be matched by the numerical simulations. In the absence of adequate knowledge of reaction rates, the observed experimental results could also have been matched by fitting irreversible mass transfers of water and reactants in PHREEQC. A common result of the Brown *et al.* (2000, 1998) studies was that the numerical simulation results were reasonable only if the number of adsorption sites was reduced to 5% of the initial value considered by Stollenwerk (1994). Stollenwerk simulated, through the use of the geochemical code MINTEQA2, the neutralization and later rinse-out of Pinal Creek acidic groundwater that he observed in a column experiment. Because MINTEQA2 was not a reactive transport code, Stollenwerk used a series of "batch" calculations to simulate transport, and explicitly defined the aqueous and solid-phase chemical inputs for each cell at each time step. As mentioned in Brown *et al.* (2000), "Although output from one time step provided much of the input for the next time step, the aqueous and solid-phase concentrations of selected constituents were manually adjusted to fit measured concentrations in column outflow and measured changes in column mineralogy".

To improve the characterisation of calcite, dolomite, and pyrolusite ( $\text{MnO}_2$ ) dissolution rates at the Pinal Creek site, Brown and Glynn (2003) conducted *in-situ* field experiments that suspended well-characterized commercially-obtained mineral samples in acidic waters at the Pinal Creek site (wells 101 and 301) for various lengths of time (from 96 to 595 days)

starting in April 1998. *In-situ* dissolution rates for calcite and dolomite were determined, and found to be about three orders of magnitude slower than rates determined by Plummer *et al.* (1978) and Busenberg and Plummer (1982) in laboratory experiments. Interestingly, Brown and Glynn (2003) found that the incorporation of the *in-situ* rates, or alternatively, the faster laboratory-determined rates, in PHREEQC v.2 (Parkhurst and Appelo, 1999) reactive-transport simulations did not result in better fits of Stollenwerk's column experiments. Instead, an equilibrium model adequately simulated carbonate dissolution at the shorter and faster (relative to the field situation) spatial and temporal scales of the column experiment. More surprisingly, Brown and Glynn (2003) observed growth in the mass of the pyrolusite material placed in the *in-situ* experiments, despite thermodynamic conditions that, in theory, favored pyrolusite dissolution. They postulated that this result could be related to the result of Villinski *et al.* (2001), who found that the dissolution of  $\text{MnO}_2$  under similar conditions in a laboratory flow-through cell resulted in the precipitation of a mixed oxidation Mn-Fe phase with the structure of jacobsonite ( $\text{MnFe}_2\text{O}_4$ ). Brown and Glynn (2003) then used the rate equations developed by Postma and Appelo (2000) for the reductive dissolution of birnessite ( $\text{MnO}_2$ ) by dissolved Fe(II) to better fit the distribution and evolution of dissolved Mn and Fe concentrations in the transition zone and in the acidic part of the plume (at well 402) from 1984 through 1992. Although the rate constant used in their PHREEQC v.2 simulations was about 3 to 4 orders of magnitude smaller than the range of values used by Postma and Appelo (2000) in their column experiments, Brown and Glynn (2003) did obtain a better fit of the observed Fe, and especially, the observed Mn concentrations in the transition zone. Their simulated *pH* values, however, remained about 1 *pH* unit higher than the observed values.

The field, laboratory and numerical modeling investigations of the Pinal Creek basin provide several lessons that may be useful to other investigations of complex, highly dynamic, systems with a relative paucity of information (and limited funding to obtain information):

1. Constructing, analyzing and interpreting numerical models, regardless of the type of model (hydrologic vs. geochemical; inverse vs. forward), forces the modeler(s), and hopefully the user(s) of the models, to reexamine and revise their conceptual model and perceptions of the available information. The modeling process forces the modelers and users to assemble, structure, transform, and assess a wide variety of information.
2. No model is ever final. As numerical modeling leads to greater understanding of a system, it invariably illuminates knowledge gaps and the need for more information. Frequent iteration is needed among field observation, field experiments, laboratory experiments, and the periodic assembly and interpretation of the available information through numerical modeling.
3. The combination of inverse modeling (including inverse geochemical modeling) and forward or "predictive" modeling is particularly powerful in helping assess available information. Inverse modeling forces the modeler to use basic principles (such as conservation of mass and energy) to *interpret* the available observations in terms of properties of the system (e.g., geochemical mass transfers, possible reactions, other intrinsic system properties). Forward, or predictive modeling, forces the modeler to *test* available information by "extrapolating" forward through time, space or other informational dimensions by using the modeler's preconceptions of system behavior. In the case of the Pinal Creek system, inverse modeling helped Glynn and Brown (1996) identify sets of reactions that could explain the observed geochemical evolution of groundwaters, and helped identify field and laboratory observations/experiments that might improve characterization and quantification of active geochemical processes. Sensitivity analyses conducted through "forward" reactive transport modeling identified which minerals and reaction processes, given knowledge of reaction thermodynamics and stoichiometries, provided reasonable rates of migration of chemical fronts and a reasonable distribution of solution properties (such as *pH* and Fe and Mn concentrations) in space and time. More importantly, the geochemical modeling at the Pinal Creek site helped identify which reactions and processes were *unreasonable*.

4. Determining what is *unreasonable* is generally dependent on limited information and observations (through time, space and process domains) and on an *interpretation* of that limited information. In complex, highly dynamic, systems with limited regularity or steadiness of observations, such as the Pinal Creek groundwater system, the problem of eliminating unreasonable processes is exacerbated: what might seem reasonable, or unreasonable, given available information at some point in time and space could change. The studies conducted at the Pinal Creek site illustrate the fact that nature always keeps surprises in reserve for its observers and interpreters. Humility, and frequent testing of assumptions, are needed in modeling nature's systems.
5. Given our often limited knowledge of natural systems, it behooves us to model these systems by considering *general* system behavior before interpreting, matching, and predicting *specific* system behavior. Curve and point-by-point matching of numerical simulations to the observed chemical evolution at the Pinal Creek site, or laboratory columns, was generally difficult, and provided limited, albeit useful, returns on expended effort. Inverse modeling and sensitivity analyses of general system behavior, however, through relatively unconstrained reactive-transport simulations, provided substantial insights on knowledge gaps and information needs that could improve understanding of the complex, highly dynamic processes at the site. These modeling efforts should have been conducted much earlier in the life of the Pinal Creek project investigations.
6. Finally, the Pinal Creek project taught us the value of spatial and temporal observations. Systems that have a complex suite of active processes and that exhibit dynamic changes in observed properties require extensive (and often costly) adaptive monitoring programs that have sufficient resolution in both time and space. Considering a greater variety of geochemical/hydrological information than might initially be considered in setting up a monitoring program is useful and can sometimes help compensate for a lack of spatial/temporal monitoring: different geochemical or hydrological measurements often reflect different degrees of spatial integration and temporal evolution.

*Other information on the hydrogeochemistry of acidic metal-contaminated waters, geochemical modeling, and on obtaining U.S. Geological Survey computer codes and the PHREEQM code* Further information on the application of geochemical information and geochemical modeling in understanding and dating groundwater systems can be found in Glynn and Plummer (2005), and in a soon to be published IAEA guidebook on dating of old groundwaters and many chapters therein, including Plummer and Glynn (Radiocarbon dating in groundwater systems; in press) and Plummer *et al.* (Characterization and conceptualization of groundwater-flow systems; in press). An excellent discussion of geochemical modeling tools and philosophy is also provided by Nordstrom (2004; updated in 2007). Finally, the reader is directed to the work of Alpers and Nordstrom (1999) and Nordstrom (2000, 2008). These authors have used geochemical modeling and characterization to inform regulatory decision making in the remediation of acid mine waters.

Readers interested in geochemical and hydrological investigations of the acidic and heavy metal contamination in the Pinal Creek basin should also consider the studies conducted on the role of groundwater-surface water interactions. Narrowing of the basin to the north forces groundwater discharge and maintains perennial flow for 7 kilometers along Pinal Creek. Degassing of carbon dioxide raises the *pH* of the stream from about 6.6 to 7.6 (Choi *et al.*, 1998). The return flow of the streamwater to shallow subsurface flowpaths beneath and to the side of the stream (hyporheic zone) brings this higher *pH* water with high concentrations of dissolved  $Mn^{2+}$  back into direct contact with microbes and geochemical coatings in the streambed sediment. Rapid oxidation of  $Mn^{2+}$  in the hyporheic zone sediments is catalyzed by Mn oxidizing bacteria on a timescale of hours, and is accompanied by the sorption of Co, Ni, and Zn onto the biogenic manganese oxides (Bargar *et al.*, 2009). Enhanced oxidation of Mn in the hyporheic zone was found to remove 20% of the dissolved load of Mn reaching the stream, before its flow out of the basin (Harvey and Fuller, 1998). Additionally, sorption

onto the manganese oxides in the streambed sediments accounted for 52%, 27%, and 24% removal of the dissolved Co, Ni, and Zn loads, respectively (Fuller and Harvey, 2000; Kay *et al.*, 2001).

The latest versions of the USGS PHREEQC and NETPATH geochemical codes, and other related codes, can be downloaded directly from the web site: [http://wwwbrr.cr.usgs.gov/projects/GWC\\_coupled/](http://wwwbrr.cr.usgs.gov/projects/GWC_coupled/). Codes available include new versions of NETPATH (NetpathXL; Parkhurst and Charlton, 2008; NETPATH-WIN, El-Kadi *et al.*, 2011) and the 3-dimensional PHREEQC-based reactive transport code PHAST (Parkhurst *et al.*, 2010). USGS codes can also be accessed through the more general USGS National Research Program software web site: <http://water.usgs.gov/nrp/models.html>. PHREEQM is now largely an obsolete code that has been replaced by PHREEQC version 2 (Parkhurst and Appelo, 1999) and by the Windows interactive code PHREEQCi (Charlton and Parkhurst, 1999). Another interactive code, PHREEQC for Windows, can also be downloaded from Vincent Post's web site: <http://pfw.antipodes.nl/index.html>. Additional information on the PHREEQC code can also be obtained from Tony Appelo's web site: <http://www.xs4all.nl/~appt/>, and from the Appelo and Postma (2005) groundwater geochemistry textbook.

## ACKNOWLEDGEMENTS

The original version of this manuscript, Glynn and Brown (1996), received substantial help and reviews from David Parkhurst, Joseph Vrabel, Carl Steefel, Eric Oelkers, Don Thorstenson and Paul Ribbe. Additionally, the current manuscript benefitted greatly from reviews provided by Mark Fuhrman and David Parkhurst, and from additional comments, edits, and discussion provided by Leonard Konikow, Kirk Nordstrom and Kevin Breen. The Senior Author retains full responsibility however for any remaining errors of fact, expression or judgment. The work presented here was funded by the Toxics Substance Hydrology and the Hydrologic Research and Development programs of the US Geological Survey. Finally, any use of trade, product, or firm names is for descriptive purposes only and does not imply endorsement by the U.S. Government.

## REFERENCES

- Alpers, C.N. & Nordstrom, D.K.: Geochemical modelling of water-rock interactions in mining environments. In: G.S. Plumlee & M.J. Logsdon (eds): *Reviews in Economic Geology*, vol. 6A, *The environmental geochemistry of mineral deposits: Part A. Processes, methods and health issues*, Society of Economic Geologists, Littleton, CO, 1999, pp. 289–324.
- Appelo, C.A.J.: Multicomponent ion exchange and chromatography in natural systems. In: C.I. Steefel, P. Lichtner & E. Oelkers (eds): *Reactive transport in porous media: general principles and application to geochemical processes. Reviews in Mineralogy* 34, 1996, pp. 193–227.
- Appelo, C.A.J. & Postma, D.: *Geochemistry, groundwater and pollution*. A.A. Balkema, Rotterdam, The Netherlands, 1993.
- Appelo, C.A.J. & Postma, D.: *Geochemistry, groundwater and pollution*. 2nd ed., A.A. Balkema, Leiden, The Netherlands, 2005.
- Appelo, C.A.J. & Willemssen, A.: Geochemical calculations and observations on salt water intrusions, 1, a combined geochemical/mixing cell model. *J. Hydrology* 94 (1987), pp. 313–330.
- Bargar, J.R., Fuller, C.C., Marcus, M.A., Brearley, A.J., Perez De la Rosa, M., Webb, S.M. & Caldwell, W.A.: Structural characterization of terrestrial bacteriogenic Mn oxides from Pinal Creek, AZ. *Geochim. Cosmochim. Acta* 73 (2009), pp. 889–910.
- Bigham, J.M. & Nordstrom, D.K.: Iron and aluminum hydroxysulfate minerals. In: C.N. Alpers, J.L. Jambor & D.K. Nordstrom (eds): *Sulfate minerals—crystallography, geochemistry and environmental significance, Reviews in Mineralogy and Geochemistry* 40, 2000, pp. 351–403.
- Breeuwsma, A., Wösten, J.H.M., Vleeshouwer, J.J., Van Slobbe, A.M. & Bouma, J.: Derivation of land qualities to assess environmental problems from soil surveys. *Soil Sci. Soc. Amer. J.* 50 (1986), pp. 186–190.

- Brown, J.G.: Movement of metal contaminants in ground water in the Pinal Creek Basin, Arizona: Model assessment and simulation of reactive transport. MSc Thesis, University of Arizona, Tucson, AZ, USA, 1996.
- Brown, J.G. & Glynn, P.D.: Kinetic dissolution of carbonates and Mn oxides in acidic water: measurement of *in situ* rates and reactive transport modeling. *Appl. Geochem.* 18:8 (2003), pp. 1225–1239.
- Brown, J.G. & Harvey, J.W.: Hydrologic and geochemical factors affecting metal-contaminant transport in Pinal Creek Basin near Globe, Arizona. In: D.W. Morganwalp & D.A. Aronson (eds): *U.S. Geological Survey Toxic Substances Hydrology Program—Proceedings of the Technical Meeting*, Colorado Springs, Colorado, 20–24 September, 1993: *U.S. Geological Survey Water-Resources Investigations Report* 94–4015, 1994, pp. 1035–1042.
- Brown, J.G., Bassett, R.L., Glynn, P.D. & Parkhurst, D.L.: Reactive transport of metal contaminants in ground water in Pinal Creek Basin, Arizona. In: A.M. Geddis (ed.): *Water Use in Arizona—Cooperation or Conflict. Proceedings of the 8th Annual Symposium of the Arizona Hydrological Society*, Tucson, Arizona, 14–15 September, 1995, pp. 104–105.
- Brown, J.G., Bassett, R. & Glynn, P.D.: Analysis and simulation of reactive transport of metal contaminants in ground water in Pinal Creek Basin, Arizona. *J. Hydrology* 209 (1998), pp. 225–250.
- Brown, J.G., Bassett, R. & Glynn, P.D.: Reactive transport of metal contaminants in alluvium—model comparison and column simulation. *Appl. Geochem.* 15 (2000), pp. 35–49.
- Busenberg, E. & Plummer, L.N.: The kinetics of dissolution of dolomite in CO<sub>2</sub>-water systems at 1.5 to 65°C and 0.0 to 1.0 atmosphere pCO<sub>2</sub>. *Amer. J. Science* 282 (1982), pp. 45–78.
- Charlton, S.R., Macklin, C.L. & Parkhurst, D.L.: PhreeqcI—A graphical user interface for the geochemical computer program PHREEQC. *U.S. Geological Survey Water-Resources Investigations Report* 97–4222, 1997.
- Charlton, S.R. & Parkhurst, D.L.: PhreeqcI—A graphical user interface to the geochemical model PHREEQC. *U.S. Geological Survey Fact Sheet* FS-031–02, 2002.
- Choi, J., Hulseapple, S.M., Conklin, M.H. & Harvey, J.W.: Modeling CO<sub>2</sub> degassing and pH in a stream-aquifer system. *J. Hydrology* 209 (1998), pp. 297–310.
- Davis, J.A. & Kent, D.B.: Surface complexation modeling in aqueous geochemistry. In: M.F. Hochella Jr & A.F. White (eds): *Mineral-Water Interface Geochemistry. Reviews in Mineralogy* 23, 1990, pp. 177–260.
- Dria, M.A., Bryant, S.L., Schechter, R.S. & Lake, L.W.: Interacting precipitation dissolution waves: the movement of inorganic contaminants in groundwater. *Water Resour. Res.* 23 (1987), pp. 2076–2090.
- Dzombak, D.A. & Morel, F.M.M.: *Surface complexation modeling: Hydrous ferric oxide*. Wiley & Sons, New York, 1990.
- El-Kadi, A.I., Plummer, L.N. & Aggarwal, P.: NETPATH-WIN: An interactive user version of the mass-balance model, NETPATH. *Ground Water* 49:4 (2011), pp. 593–599.
- Engesgaard, P. & Kipp, K.L.: A geochemical transport model for redox-controlled movement of mineral fronts in groundwater flow systems: a case of nitrate removal by oxidation of pyrite. *Water Resour. Res.* 28 (1992), pp. 2829–2843.
- Eychaner, J.H.: Movement of inorganic contaminants in acidic water near Globe, Arizona. In: G.E. Mallard & S.E. Ragone (eds): *U.S. Geological Survey Toxic Substances Hydrology Program—Proceedings of the Technical Meeting*, Phoenix, Arizona, 26–30 September, 1989: *U.S. Geological Survey Water-Resources Investigations Report* 89–4220, 1989, pp. 567–575.
- Eychaner, J.H.: The Globe, Arizona, research site—Contaminants related to copper mining in a hydrologically integrated environment. In: G.E. Mallard & D.A. Aronson (eds): *U.S. Geological Survey Toxic Substances Hydrology Program—Proceedings of the Technical Meeting*, Monterey, California, 11–15 March, 1991: *U.S. Geological Survey Water-Resources Investigations Report* 91–4034, 1991, pp. 475–480.
- Eychaner, J.H. & Stollenwerk, K.G.: Neutralization of acidic ground water near Globe, Arizona. In: K.D. Schmidt (ed): *Groundwater contamination and reclamation*. Proceedings of a Symposium, Tucson, Arizona, 14–15 August, 1985, Bethesda, Maryland. American Water Resources Association, 1985, pp. 141–148.
- Ficklin, W.H., Love, A.S. & Papp, C.S.E.: Solid-phase variations in an aquifer as the aqueous solution changes, Globe, Arizona. In: G.E. Mallard & D.A. Aronson (eds): *U.S. Geological Survey Toxic Substances Hydrology Program—Proceedings of the Technical Meeting*, Monterey, California, 11–15 March, 1991: *U.S. Geological Survey Water-Resources Investigations Report* 91–4034, 1991, pp. 475–480.

- Fuller, C.C. & Harvey, J.W.: Reactive uptake of trace metals in the hyporheic zone of a mining-contaminated stream, Pinal Creek, Arizona. *Environ. Sci. Technol.* 34 (2000), pp. 1150–1156.
- Glynn, P.D.: MBSSAS: A code for the computation of Margules parameters and equilibrium relations in binary solid-solution aqueous-solution systems. *Comput. Geosci.* 17 (1991a), pp. 907–966.
- Glynn, P.D.: Effect of impurities in gypsum on contaminant transport at Pinal Creek, Arizona. In: G.E. Mallard & D.A. Aronson (eds): *U.S. Geological Survey Toxic Substances Hydrology Program—Proceedings of the Technical Meeting*, Monterey, California, 11–15 March, 1991: *U.S. Geological Survey Water-Resources Investigations Report* 91–4034, 1991b, pp. 466–474.
- Glynn, P.D.: Solid-solution solubilities and thermodynamics: sulfates, carbonate and halides. In: C.N. Alpers, J.L. Jambor & D.K. Nordstrom (eds): *Sulfate minerals-crystallography, geochemistry and environmental significance. Reviews in Mineralogy and Geochemistry* 40, 2000, pp. 481–511.
- Glynn, P.D. & Brown, J.G.: Reactive transport modeling of acidic metal-contaminated ground water at a site with sparse spatial information. In: C.I. Steefel, P. Lichtner & E. Oelkers (eds): *Reactive transport in porous media: general principles and application to geochemical processes. Reviews in Mineralogy* 34, 1996, pp. 377–438.
- Glynn, P.D. & Busenberg, E.: Dissolved gas and chlorofluorocarbon content of ground waters in the Pinal Creek Basin, Arizona. In: D.W. Morganwalp & D.A. Aronson (eds): *U.S. Geological Survey Toxic Substances Hydrology Program—Proceedings of the Technical Meeting*. Colorado Springs, CO, 20–24 September, 1993: *U.S. Geological Survey Water-Resources Investigations Report* 94–4015, 1994a, pp. 1043–1054.
- Glynn, P.D. & Busenberg, E.: Unsaturated zone diffusion of carbon dioxide and oxygen in the Pinal Creek Basin, Arizona. In: D.W. Morganwalp & D.A. Aronson (eds): *U.S. Geological Survey Toxic Substances Hydrology Program—Proceedings of the Technical Meeting*. Colorado Springs, CO, 20–24 September, 1993: *U.S. Geological Survey Water-Resources Investigations Report* 94–4015, 1994b, pp. 1055–1064.
- Glynn, P.D. & Plummer, L.N.: Geochemistry and the understanding of ground-water systems. *Hydrogeology J.* 13 (2005), pp. 263–287.
- Glynn, P.D., Engesgaard, P. & Kipp, K.L.: Use and limitations of two computer codes for simulating geochemical mass transport at the Pinal Creek toxic-waste site. In: G.E. Mallard & D.A. Aronson (eds): *U.S. Geological Survey Toxic Substances Hydrology Program—Proceedings of the Technical Meeting*, Monterey, California, 11–15 March, 1991: *U.S. Geological Survey Water-Resources Investigations Report* 91–4034, 1991, pp. 454–460.
- Glynn, P.D., Busenberg, E. & Brown, J.G.: Use of chlorofluorocarbons, dissolved gases and water isotopes to characterize ground-water recharge in an aquifer contaminated by acidic, metal-laden wastewater. *U.S. Geological Survey Toxic Substances Hydrology Program—Proceedings of the Technical Meeting*, Charleston, South Carolina, 8–12 March, 1999—Volume 1 of 3—Contamination from Hardrock Mining: *U.S. Geological Survey Water-Resources Investigations Report* 99–4018A, 1999, pp. 155–162.
- Harvey, J.W. & Fuller, C.C.: Effect of enhanced manganese oxidation in the hyporheic zone on basin-scale geochemical mass balance. *Water Resour. Res.* 34:4 (1998), pp. 623–636.
- Herzer, J. & Kinzelbach, W.: Coupling of transport and chemical processes in numerical transport models. *Geoderma* 44 (1989), pp. 115–127.
- Hydro Geo Chem Inc.: Investigation of acid water contamination along Miami Wash and Pinal Creek, Gila County, Arizona. Cyprus Miami Mining Corporation, Claypool, AZ, 1989.
- Kay, J.T., Conklin, M.H., Fuller, C.C. & O'Day, P.E.: Processes of nickel and cobalt uptake by Mn-oxide forming sediment in Pinal Creek. *Environ. Sci. Technol.* 35: 24 (2001), pp. 4719–4725.
- LeBlanc, D.R.: Sewage plume in a sand and gravel aquifer, Cape Cod, Massachusetts. *U.S. Geological Survey Water-Supply Paper* 2218, 1984.
- Lichtner, P.C.: Continuum model for simultaneous chemical reactions and mass transport in hydrothermal systems. *Geochim. Cosmochim. Acta* 49 (1985), pp. 779–800.
- Lichtner, P.C.: The quasi-stationary state approximation to coupled mass transport and fluid-rock interaction in a porous medium. *Geochim. Cosmochim. Acta* 52 (1988), pp. 143–165.
- Lind, C.J. & Stollenwerk, K.G.: Alteration of alluvium of Pinal Creek, Arizona by acidic ground water resulting from copper mining. In: D.W. Morganwalp & D.A. Aronson (eds): *U.S. Geological Survey Toxic Substances Hydrology Program—Proceedings of the Technical Meeting*. Colorado Springs, CO, 20–24 September, 1993: *U.S. Geological Survey Water-Resources Investigations Report* 94-4015, 1994, pp. 1089–1094.

- Mackay, O.M., Freyberg D.L., Roberts, P.V. & Cheny, J.A.: A natural gradient experiment on solute transport in a sand aquifer I: Approach and overview of plume movement. *Water Resour. Res.* 22 (1986), pp. 2017–2029.
- Neaville, C.C. & Brown, J.G.: Hydrogeology and hydrologic system of Pinal Creek Basin, Gila County, Arizona. *U.S. Geological Survey Water-Resources Investigations Report* 93–4212, 1993.
- Nordstrom, D.K.: Advances in the hydrogeochemistry and microbiology of acid mine waters. *Int. Geology Review* 42 (2000), pp. 499–515.
- Nordstrom, D.K.: Modeling low-temperature geochemical processes. In: J.I. Drever (ed): *Treatise on geochemistry*, v. 5, *Surface and ground water, weathering, and soils*. Amsterdam, Elsevier, 2004 (updated in 2007), pp. 37–72.
- Nordstrom, D.K.: Questa baseline and pre-mining ground-water quality investigation. 25. Summary of results and baseline and pre-mining ground-water geochemistry, Red River Valley, Taos County, New Mexico, 2001–2005. *U.S. Geological Survey Professional Paper* 1728, 2008.
- Nordstrom, D.K., Plummer, L.N., Langmuir, D., Busenberg, E., May, H.M., Jones, B.F. & Parkhurst, D.L.: Revised chemical equilibrium data for major water-mineral reactions and their limitations. In: D.C. Melchior & R.L. Bassett (eds): *Chemical modeling in aqueous system II*, American Chemical Society Symposium Series 416, 1990, pp. 398–413.
- Ortoleva, P., Auchmuty, G., Chadam, J., Hettmer, J., Merino, E., Moore, C.H. & Ripley, E.: Redox front propagation and banding molalities. *Physica* 19D (1986), pp. 334–354.
- Parkhurst, D.L.: User's guide to PHREEQC--A computer program for speciation, reaction-path, advective-transport, and inverse geochemical calculations. *U.S. Geological Survey Water-Resources Investigations Report* 95–4227, 1995.
- Parkhurst, D.L.: Geochemical mole-balance modeling with uncertain data. *Water Resour. Res.* 33:8 (1997), pp. 1957–1970.
- Parkhurst, D.L. & Appelo, C.A.J.: User's guide to PHREEQC (Version2)—A computer program for speciation, batch-reaction, one-dimensional transport, and inverse geochemical calculations. *U.S. Geological Survey Water-Resources Investigations Report* 99–4259, 1999.
- Parkhurst, D.L. & Charlton, S.R.: NetpathXL—An Excel® interface to the program NETPATH. *U.S. Geological Survey Techniques and Methods* 6-A26, 2008.
- Parkhurst, D.L., Plummer, L.N. & Thorstenson, D.C.: PHREEQE—A computer program for geochemical calculations. *U.S. Geological Survey Water-Resources Investigations Report* 80–96, 1980.
- Parkhurst, D.L., Plummer, L.N. & Thorstenson, D.C.: BALANCE—A computer program for geochemical calculations. *U.S. Geological Survey Water-Resources Investigations Report* 82–14, 1982.
- Parkhurst, D.L., Kipp, K.L. & Charlton, S.R.: PHAST Version 2—A program for simulating groundwater flow, solute transport, and multicomponent geochemical reactions. *U.S. Geological Survey Techniques and Methods* 6–A35, 2010.
- Petersen, N.P.: Geology and ore deposits of the Globe-Miami district, Arizona. *U.S. Geological Survey Professional Paper* 342, 1962.
- Plummer, L.N. & Glynn, P.D.: Radiocarbon dating in groundwater systems. *Guidebook on dating of old groundwaters*, Chapter 4. International Atomic Energy Agency, in press.
- Plummer, L.N., Wigley, T.M.L. & Parkhurst, D.L.: The kinetics of calcite dissolution in CO<sub>2</sub>-water systems at 5 to 60°C and 0.0 to 1.0 atm CO<sub>2</sub>. *Amer. J. Sci.* 278 (1978), pp. 179–216.
- Plummer, L.N., Parkhurst, D.L. & Thorstenson, D.C.: Development of reaction models for groundwater systems. *Geochim. Cosmochim. Acta* 47 (1983), pp. 665–686.
- Plummer, L.N., Prestemon, E.C. & Parkhurst, D.L.: An interactive code (NETPATH) for modeling net geochemical reactions along a flow path. *U.S. Geological Survey Water-Resources Investigations Report* 91–4078, 1991.
- Plummer, L.N., Prestemon, E.C. & Parkhurst, D.L.: An interactive code (NETPATH) for modeling NET geochemical reactions along a flow PATH. Version 2.0. *U.S. Geological Survey Water-Resources Investigations Report* 94–4169, 1994.
- Plummer, L.N., Sanford, W.E. & Glynn, P.D.: Characterization and conceptualization of groundwater-flow systems. *Guidebook on dating of old groundwaters*, Chapter 2. International Atomic Energy Agency, in press.
- Postma, D. & Appelo, C.A.J.: Reduction of Mn oxides by ferrous iron in a flow system: column experiment and reactive transport modeling. *Geochim. Cosmochim. Acta* 64 (2000), pp. 1237–1247.
- Revesz, K., Coplen, T.B., Baedeker, M.J., Glynn, P.D. & Hult, M.: Methane production and consumption monitored by stable H and C isotope ratios at a crude oil spill site, Bemidji, Minnesota. *Appl. Geochem.* 10 (1995), pp. 505–516.

- Robertson, F.N.: Geochemistry of ground water in alluvial basins of Arizona and adjacent parts of Nevada, New Mexico, and California. Regional Aquifer-System Analysis—Southwest Alluvial Basins, Arizona and Adjacent States. *U.S. Geological Survey Professional Paper* 1406-C, 1991.
- Steefel, C.I. & MacQuarrie, K.T.B.: Approaches to modeling of reactive transport in porous media. In: C.I. Steefel, P. Lichtner & E. Oelkers (eds): Reactive transport in porous media: General principles and application to geochemical processes. *Reviews in Mineralogy* 34, 1996, pp. 85–129.
- Stollenwerk, K.G.: Geochemical interactions between constituents in acidic groundwater and alluvium in an aquifer near Globe, Arizona. *Appl. Geochem.* 9 (1994), pp. 353–369.
- Stollenwerk, K.G. & Eychaner, J.H.: Acidic ground water contamination from copper mining near Globe, Arizona. In: B.J. Franks (ed): *U.S. Geological Survey Toxic Substances Hydrology Program—Proceedings of the Technical Meeting*, Pensacola, Florida, 23–27 March, 1987: *U.S. Geological Survey Open-File Report* 87–109, 1987, pp. D19–D24.
- Tolle, S. & Arthur, G.V.: Aquifer restoration under the clean water act. In: G.E. Mallard & D.A. Aronson (eds): *U.S. Geological Survey Toxic Substances Hydrology Program—Proceedings of the Technical Meeting*, Monterey, California, 11–15 March, 1991: *U.S. Geological Survey Water-Resources Investigations Report* 91–4034, 1991, pp. 520–523.
- Van Cappellen, P. & Gaillard, J.F.: Biogeochemical dynamics in aquatic sediments. In: C.I. Steefel, P. Lichtner & E. Oelkers (eds): Reactive transport in porous media: General principles and application to geochemical processes. *Reviews in Mineralogy* 34, 1996, pp. 335–376.
- Villinski, J.E., O’Day, P.A., Corley, T.L. & Conklin, M.H.: *In situ* spectroscopic and solution analyses of the reductive dissolution of  $\text{MnO}_2$  by Fe(II). *Environ. Sci. Technol.* 35 (2001), pp. 1157–1163.
- Winograd, I.J. & Robertson, F.N.: Deep oxygenated ground water: anomaly or common occurrence? *Science* 216 (1982), pp. 1227–1230.

